

DESIGNING NATURAL HAPTIC INTERFACES AND SIGNALS

by

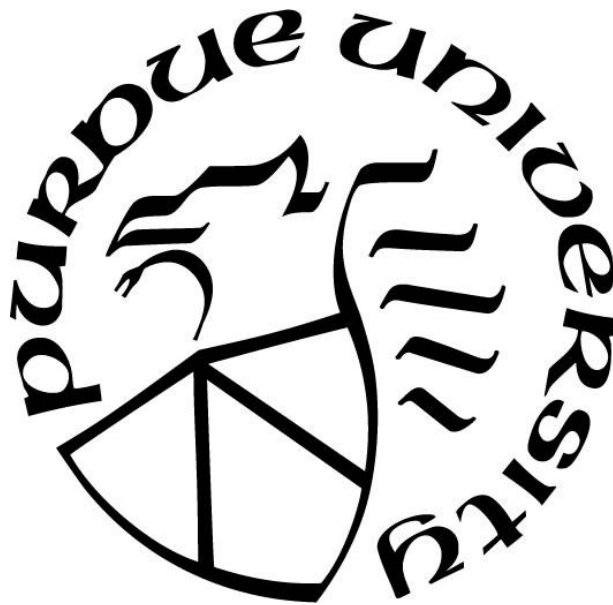
Sang-Won Shim

A Thesis

Submitted to the Faculty of Purdue University

In Partial Fulfillment of the Requirements for the degree of

Master of Science in Electrical and Computer Engineering



School of Electrical & Computer Engineering

West Lafayette, Indiana

May 2019

**THE PURDUE UNIVERSITY GRADUATE SCHOOL
STATEMENT OF COMMITTEE APPROVAL**

Dr. Hong Z. Tan, Chair

School of Electrical and Computer Engineering

Dr. Alexander J. Quinn

School of Electrical and Computer Engineering

Dr. Thomas M. Talavage

School of Electrical and Computer Engineering

Approved by:

Dr. Pedro Irazoqui

Head (interim) of Electrical and Computer Engineering

Father God, Jesus Christ, and Holy Spirit

Hyeyoung, and Haram

Family

Haptic Interface Research Lab., Purdue, and Dr. Hong Z. Tan

Samsung Electronics, Design, Sound Lab.

Soh-Myeong Methodist Church

Korean Presbyterian Church of Purdue

모든 것을 하나님께서 하셨습니다.

주님께 바칩니다.

*"I am the way and the truth and the life. No one comes to the
Father except through me."*

- John 14:6 -

ACKNOWLEDGMENTS

God leads me always to engage His own history, and I give thanks to the Lord for the miracle journey for my family and me. I am also grateful to my beloved families, Hyeyoung and Haram who have been accompanying us on this journey.

I am sincerely thankful to Professor Hong Z. Tan for her advice and mentoring throughout my graduate research at Purdue. As a leader, she has the most crucial aspect of the growth strategies and long-term research plans that maximize the abilities and backgrounds of each student with sincere caring. I would also like to thank Professor Alexander J. Quinn and Thomas M. Talavage for serving on my thesis committee and lending a helping hand throughout the master's research and the coursework.

I appreciate the Samsung Electronics, especially Corporate Design Center and Mobile UX Center. I thank our leaders and members that picked me out send me College of Engineering at Purdue University through Design Power Program, even though it was not an easy decision to send an engineering college from the design team and to give the haptic user experience designer an opportunity for a master's degree.

I appreciate the support the Dot braille module and valuable opinions by Dot Incorporation who change the world for the visually impaired people through beautiful braille technology that I would like to cooperate with them for the same purpose in personal.

I thank Korea University of Technology and Education (KOREATECH) for supporting the electroactive polymer actuator and meaningful discussions on the engineering aspect.

Many thanks to the Yaodong, Sean, and Jacob for their sincere assistance and endeavor with hardware and software prototyping.

I want to express my sincere gratitude to all the Haptic Interface Research Laboratory colleagues and all the church members especially, the pastor Taekryong Kim in Korean Presbyterian Church of Purdue, and the pastor Inhwa Park in Soh-Myeong Methodist Church in Korea.

All this would not have been possible without your prayers and support.

TABLE OF CONTENTS

LIST OF TABLES	7
LIST OF FIGURES	8
ABSTRACT.....	13
1. INTRODUCTION	15
2. BACKGROUND	19
2.1 Human Haptic Perception	19
2.1.1 Receptor Mechanisms (Mechanoreceptors)	21
2.1.2 Related Factors to Tactile Responses	24
2.1.3 Psychophysical Methods	25
2.2 Haptics Technology	29
2.2.1 ERM, LRA.....	30
2.2.2 VCA, Piezoelectric	32
2.2.3 Contactless, Surface, EAP, Microfluidics	35
2.3 Haptic User Experience	40
2.3.1 Emotional Aspects and Interfaces	41
2.3.2 Affect Detection Methods (Measuring Emotion)	42
2.3.3 Related Affective Studies	47
3. PROTOTYPING.....	52
3.1 Introduction.....	52
3.2 Circular Array Braille Display	54
3.2.1 Design and Layout.....	54
3.2.2 Control Circuit.....	58
3.2.3 Concepts and Effects	62
3.3 Braille Stick	65
3.3.1 Design and Layout.....	65
3.3.2 Wireless Serial Communication Module.....	66
3.3.3 Module Ceiling Case	67
3.4 Electroactive Polymer Tactile Display	69

3.4.1	Module Structure Analysis	69
3.4.2	Control Circuit	70
3.5	Summary and Discussion.....	73
4.	PALMSCAPE: CALM AND PLEASANT VIBROTACTILE SIGNALS	76
4.1	Introduction.....	76
4.2	A New Tactile Display: <i>palmScape</i>	78
4.3	Design Approach	79
4.3.1	Design Principles	80
4.3.2	Design Guidelines.....	80
4.4	Affective Rating Experiment	84
4.4.1	Participants	84
4.4.2	Calibration and Equalization of Intensity	84
4.4.3	Stimuli.....	85
4.4.4	Procedure	86
4.5	Results.....	87
4.6	Summary and Design Thinking Revisited	93
5.	CONCLUSIONS AND FUTURE WORK.....	105
	REFERENCES	107
	APPENDIX A: INDIVIDUAL RESULT OF THE AFFECTIVE RATINGS STUDY.....	111
	APPENDIX B: 4-CHANNEL SIGNAL WAVEFORM	125
	VITA.....	139

LIST OF TABLES

Table 2.1 Major factors that affect to sense of touch [1, 2].	20
Table 2.2 Mechanoreceptors: Response characteristics, feature sensitivity and associated function [1].	22
Table 2.3 Response sequences and groupings for transformed up-down procedure [6].	28
Table 2.4 Correlations for SAM ratings and semantic differential factor score with each of the six adjective pairs [15].	45
Table 2.5 Comparisons of affect detection methods [19].	46
Table 2.6 Vibrotactile parameter used in Yoo et al.'s study [20].	47
Table 2.7 Stimulus sets tested in Yoo et al.'s study [20].	47
Table 4.1 The 20 stimuli used in the present study.	85
Table 4.2 V-A rating mean values, range and standard deviation for each signal.	89
Table 5.1 Individual result of affective rating study: P01.	111
Table 5.2 Individual result of affective rating study: P02.	112
Table 5.3 Individual result of affective rating study: P03.	113
Table 5.4 Individual result of affective rating study: P04.	114
Table 5.5 Individual result of affective rating study: P05.	115
Table 5.6 Individual result of affective rating study: P06.	116
Table 5.7 Individual result of affective rating study: P07.	117
Table 5.8 Individual result of affective rating study: P08.	118
Table 5.9 Individual result of affective rating study: P09.	119
Table 5.10 Individual result of affective rating study: P10.	120
Table 5.11 Individual result of affective rating study: P11.	121
Table 5.12 Individual result of affective rating study: P12.	122
Table 5.13 Individual result of affective rating study: P13.	123
Table 5.14 Individual result of affective rating study: P14.	124
Table 5.15 Signal parameter details and applied design approaches.	125

LIST OF FIGURES

Fig. 2.1 Demonstrating the locations of the four types of mechanoreceptors [1].....	21
Fig. 2.2 Minimally detectable (threshold) displacement of the skin produced by a vibrating stimulator, as a function of vibration frequency [1].	23
Fig. 2.3 A muscle spindle embedded in main (extrafusal) muscle fibers contains inner (intrafusal) fibers [1].....	23
Fig. 2.4 Vibrotactile thresholds for contactor sizes as a function of vibration frequency [4].	24
Fig. 2.5 Sensitivity to pressure at different sites on the body [1].	25
Fig. 2.6 Typical data for the simple up-down procedure [6].	27
Fig. 2.7 Haptics technologies, markets, and players (IDTechEx Research).....	29
Fig. 2.8 Structure of an eccentric rotating mass (ERM) motor.....	30
Fig. 2.9 Structure of a linear resonant actuator.	31
Fig. 2.10 Voice-coil haptic actuators and products.....	33
Fig. 2.11 Structure and actuation mechanism of a piezo actuator.	34
Fig. 2.12 Piezoelectric actuator and energy consumption comparison of haptic actuators: piezoelectric, LRA, ERM.	34
Fig. 2.13 Ultra-thin piezoelectric actuator (PiezoHapt™).....	35
Fig. 2.14 Ultrasound: Concepts, prototypes, development kit, and the actuation mechanism.	36
Fig. 2.15 Electrostatic friction: Concepts, prototypes, and the actuation mechanism.	37
Fig. 2.16 Structure of piezoelectric friction haptic display.....	37
Fig. 2.17 Concept image of bending wave haptic.....	38
Fig. 2.18 Electroactive polymer actuator (Novasentis).	38
Fig. 2.19 Haptic actuators and operations using microfluidics (left) and pneumatic (right).	39
Fig. 2.20 Haptic UX design added to Dan Saffer's UX Venn diagram (blue colored oval).	41
Fig. 2.21 The State of User Experience (by Jesse Garrett, UX Week 2009).....	42
Fig. 2.22 Direct circular scaling coordinates for 28 affect words [14].	43
Fig. 2.23 The Self-Assessment Manikin (SAM) used to rate the affective dimensions (valence, arousal, dominance) [15].	44
Fig. 2.24 Experimental results of the tactile icon set of Yoo et al.'s study [20].....	48
Fig. 2.25 Emotional responses of the tactile icons in the valence-arousal space [20].....	48

Fig. 2.26 Distribution of the picture and sound stimuli in the 2-dimensional space (pleasure, arousal) [21].	49
Fig. 2.27 Vibrotactile motors layout and the wristband device used in the experiment [22].	50
Fig. 2.28 Illustration of the three types of vibrotactile patterns and an example of a continuous type pattern [22].	50
Fig. 2.29 Distribution of valences for 258 affect-related life events [23].	51
Fig. 3.1 Dot module with 16 braille cells and control board.	54
Fig. 3.2 Measuring the dimension of a braille module cell.	54
Fig. 3.3 Illustration of the generalized layout of a circular array-type tactile display.	55
Fig. 3.4 Applying a circular tactile display to a smartwatch form factor.	56
Fig. 3.5 Configurations of braille module cells for circular array tactile display.	56
Fig. 3.6 Illustration of the braille circuit board (PCB1 and 2) and wired connection to Dot control board.	57
Fig. 3.7 Illustration of the customized control board for wireless standalone circular braille display.	58
Fig. 3.8 Testing the I/O latency of Arduino.	59
Fig. 3.9 DRV8835 Dual Motor Driver Breakout board and wiring diagram for connecting two DC motors in phase-enable mode.	60
Fig. 3.10 Connection schematic - Arduino, a driver circuit (DRV8835), and a braille motor.	60
Fig. 3.11 Braille module breakout board and connections based on the schematic in Fig. 3.10.	60
Fig. 3.12 Arduino code for switching the up-down state of two braille pins.	61
Fig. 3.13 Controlling up-state and down-state of a pin in the braille cell.	61
Fig. 3.14 Schematic and PCB layout of the customized control board.	62
Fig. 3.15 Ideal layout of the circular tactile display (for concept description).	63
Fig. 3.16 Illustration of ‘clock’ concept in the circular tactile display.	63
Fig. 3.17 Illustration of ‘direction’ concept in the circular tactile display (the temporal sequence is depicted as the transparency in each black dot: lower transparency stands for an earlier sequence).	64
Fig. 3.18 Illustration of ‘metaphor and effects’ concept in the circular tactile display.	65
Fig. 3.19 Illustration of braille stick prototype.	65
Fig. 3.20 Connection schematic for wireless serial communication module (standalone braille stick).	66
Fig. 3.21 Assembled Bluetooth serial control module.	67

Fig. 3.22 Serial communication packet to control the braille module (underlined 16 hexadecimal values with the red color corresponding to the pin state of 16 braille cells).	67
Fig. 3.23 Drawing of the top plate for the ‘braille stick’ for 3D printing.	68
Fig. 3.24 3D printed top plate for ‘braille stick.’	69
Fig. 3.25 3-by-3 electroactive polymer tactile display.	69
Fig. 3.26 Structure of the electroactive polymer actuator.....	70
Fig. 3.27 High voltage control circuit of electroactive polymer actuator (from KOREATECH). 70	
Fig. 3.28 High voltage DC converter (EMCO E50), MOSFET transistor (IXBH2N250-ND), NPN transistor (2N2222) used in the high voltage control circuit.	71
Fig. 3.29 Voltage divider circuit for measuring a high voltage output.	71
Fig. 3.30 Input and output signals of the control circuit.	72
Fig. 3.31 Schematic of PCB for polymer actuator control board (left) and assembled result (right).	73
Fig. 4.1 Illustration of <i>palmScape</i>	78
Fig. 4.2 palmScape (left) and palmScape-II (right, wireless prototype).....	78
Fig. 4.3 Audio interface and amplifier connected to voice-coil actuators of palmScape display. 79	
Fig. 4.4 Expanding the spatial richness of a tactile display from a single-point vibration to a truly 3D experience.	81
Fig. 4.5 (Top) Illustration of the use of lower frequencies for designing vibrotactile icons in the present research. (Bottom) Waveforms for “breathing” that evokes the sensation of holding a small puppy in the palm (left), and “earthquake” that conveys a gradual build-up and dissipation of rough, rumbling sensation under the skin (right).	81
Fig. 4.6 Illustration of the “heartbeat’ signal. Shown are the main events making up a heartbeat and the tactors used to represent each event. See the upper-right corner for tactor numbering. ..	82
Fig. 4.7 Illustration of the “cicadas” signal.....	83
Fig. 4.8 Illustration of the “raindrop” signal.	83
Fig. 4.9 Experimental setup: (left) noise-reduction headset, the tactor array display, elbow support, computer monitor and mouse; (right) the participant in the middle of the affective rating experiment.....	87
Fig. 4.10 A screenshot of the computer screen for the affective rating experiment.	87
Fig. 4.11 Experimental results. The filled dots and squares show results from the present study. See Table 4.2 for the V-A rating values and standard deviations for each signal.	88
Fig. 4.12 Boxplot of valence (left panel) and arousal (right panel) ratings averaged over the 20 signals for each participant.	90

Fig. 4.13 Three types of rating distribution patterns in the V-A space: General, reversed, and neutral.	91
Fig. 4.14 Grand mean for all ratings (red cross) and mean values averaged over the 20 signals for each participant (triangles).....	91
Fig. 4.15 Experimental results. The filled dots and squares show results from the present study. The red downward triangle is redrawn from [20]. See text for details.	92
Fig. 4.16 Increase in valence ratings for stimuli #1-16 as compared to the reference stimulus (#17-20) at similar arousal ratings, calculated from the blue line in Fig. 4.15.	93
Fig. 5.1 Individual result of affective rating study: P01.	111
Fig. 5.2 Individual result of affective rating study: P02.	112
Fig. 5.3 Individual result of affective rating study: P03.	113
Fig. 5.4 Individual result of affective rating study: P04.	114
Fig. 5.5 Individual result of affective rating study: P05.	115
Fig. 5.6 Individual result of affective rating study: P06.	116
Fig. 5.7 Individual result of affective rating study: P07.	117
Fig. 5.8 Individual result of affective rating study: P08.	118
Fig. 5.9 Individual result of affective rating study: P09.	119
Fig. 5.10 Individual result of affective rating study: P10.	120
Fig. 5.11 Individual result of affective rating study: P11.	121
Fig. 5.12 Individual result of affective rating study: P12.	122
Fig. 5.13 Individual result of affective rating study: P13.	123
Fig. 5.14 Individual result of affective rating study: P14.	124
Fig. 5.15 “Breathing” signal (#1).....	126
Fig. 5.16 “Earthquake” signal (#2).	126
Fig. 5.17 “Heartbeat” signal (#3).....	127
Fig. 5.18 “Raindrop” signal (#4).....	127
Fig. 5.19 “Elephant trod” signal (#5).....	128
Fig. 5.20 “Tapping” signal (#6).	128
Fig. 5.21 “Thunder” signal (#7).....	129
Fig. 5.22 “Twinkle” signal (#8).	129
Fig. 5.23 “Bubbles” signal (#9).	130

Fig. 5.24 “Water drop & ripple” signal (#10).....	130
Fig. 5.25 “Cicadas” signal (#11).....	131
Fig. 5.26 “Bathtub water jet” signal (#12).....	131
Fig. 5.27 “Frog” signal (#13).....	132
Fig. 5.28 “(Horse) galloping” signal (#14).....	132
Fig. 5.29 “Knock” signal (#15).....	133
Fig. 5.30 “Bubbles popping” signal (#16).....	133
Fig. 5.31 Reference signal - “alarm” (#17).....	134
Fig. 5.32 Reference signal - “notification 1” (#18).	134
Fig. 5.33 Reference signal - “notification 2” (#19).	135
Fig. 5.34 Reference signal - “notification 3” (#20).	135
Fig. 5.35 Example signal - “sawtooth.”	136
Fig. 5.36 Example signal - “pulsation.”	136
Fig. 5.37 Peak amplitude of each signal used in the affective rating experiment.....	137
Fig. 5.38 Total duration of each signal used in the affective rating experiment.....	138

ABSTRACT

Author: Shim, Sang-Won. MSECE
Institution: Purdue University
Degree Received: May 2019
Title: Designing Natural Haptic Interfaces and Signals
Committee Chair: Hong Z. Tan

This thesis research is concerned with the exploration, design, and validation of novel haptic technologies and signals that feel natural and meaningful in a calm and pleasant way. Our ultimate goal is to expand the possibilities of human-machine interaction by developing a single tactile display and a set of signals through a systematic design approach. It is generally a challenge to evoke a broad range of emotions with vibrotactile stimulation, especially at low signal intensities. During the first part of this thesis research, three types of prototypes were developed and explored using novel haptic technologies. The first was a circular array braille display consisting of eight small six-pin braille modules. The forty-eight pins were arranged in a circular shape to deliver circular tactile information such as time and direction. The second was a braille stick consisting of sixteen six-pin braille modules arranged in a row. The entire display could be easily grasped in the hand so that tactile information can be easily accessible. The third was a 3-by-3 electroactive polymer actuator array driven at high voltages that gives a subtle “tapping” feel on the skin. However, each of the three prototypes suffered from a limited range of expression and was not pursued further.

After the initial prototyping efforts, a 2-by-2 vibrotactile display, the palmScape, was conceived and developed. Custom-designed stimulation patterns based on natural phenomena that feel calm and pleasant were designed and implemented with the palmScape. We use text labels to set the context for the vibrotactile icons that attempt to capture and expresses natural metaphors through variations in signal amplitude, frequency, duration, rhythm, modulation, spatial extent, as well as slow movements. Fourteen participants evaluated twenty vibrotactile icons by rating the perceived valence and arousal levels. The twenty stimuli included sixteen custom-designed vibrotactile icons from this thesis research and four reference patterns from two published studies. The results show that our custom-designed patterns were rated at higher valence levels than the corresponding reference signals at similar arousal ratings. Five of the

sixteen vibrotactile icons from this research occupied the fourth quadrant of the valence-arousal space that corresponds to calm and pleasant signals. These findings support the validity of the palmScape display and our signal design approach for achieving a calm and pleasant experience and the possibility of reaching a broader range of expressiveness with vibrotactile signals.

Future studies will continue with the design of signals that can express a broader range of metaphors and emotions through the palmScape, and build an emotional evaluation database that can be combined with other modalities. Our work can be further expanded to support an immersive experience with naturalistic-feeling vibrotactile effects and broaden the expressiveness of human-computer interfaces in media consumption, gaming, and other communicative application domains.

1. INTRODUCTION

The purpose of this thesis research is to explore the characteristics of the tactile sense and haptics technologies to design a more natural and meaningful haptic interface for the user. While working as a haptic user experience designer, the author has become interested in finding a new technological solution for mobile devices that can deliver natural tactile feedback with a broader range of expressions than the existing vibrotactile patterns and exploring haptic technology capable of providing private notifications without shaking the entire device. In addition, the emotional aspects of the user's experience are also important in this research because every day, humans not only get information through tactile interactions with objects and people but also use the sense of touch for expressing and exchanging emotions. Furthermore, haptic interaction with devices affects the user's overall experience, including emotional, perceptual, and cognitive processes.

Through this thesis research, we tried to overcome the limitations of existing haptic technology that seems to have become stagnant and to open a new chapter of tactile interfaces. Therefore, the main direction of this research can be termed "Sensory Innovation," which aims at introducing new and effective tactile transmission mechanisms beyond currently-available vibrotactile technology and conveying expanded expressions and precise meaning and metaphors in terms of expressiveness and information transfer. We propose prototypes of new haptic interfaces to achieve the above goals and introduce a crafted vibrotactile signal design approach towards a more realistic and lively feeling. This thesis document describes the author's journey to find the next haptic interface through trial and error, from prototyping to identifying new possibilities through a new haptic interface called the *palmScape*. It embodies the potential to achieving a more extended expression range and representing familiar metaphors based on our daily lives through vibrotactile signals.

At the beginning of setting up the research objectives, it was necessary to understand the characteristics of the tactile sense and to explore the technical aspects that can be applied in the near future. Accordingly, Sec. "2.1 Human Haptic Perception" summarizes the basic knowledge needed to explore the perceptual and cognitive characteristics of the tactile sense. We review the factors that affect tactile perception and cognition, receptor mechanisms that lead to touch sensations, factors affecting responses to tactile stimulation, and psychophysical methods to

measure the sensation of tactile stimulation. Sec. “2.2 Haptics Technology” introduces the haptic technologies available at the present along with examples and concepts that have been applied to consumer products. In addition, since haptics has been applied to various products for the past ten years, it has been providing convenience and value to users, and it is necessary to consider user's experience in haptic interface design and research. Therefore, Sec. “2.3 Haptic User Experience” describes methods for evaluating emotions and reviews past studies on emotional responses to vibrotactile stimuli.

The thesis research began with prototyping of new haptic interfaces based on the characteristics of the tactile sense, existing and emerging haptic technologies, and the quest for improved haptic user experience. Chapter 3 of this thesis presents the design and implementation of new haptic interface prototypes and the development of new concepts using the prototypes. Three types of prototypes were covered in this chapter: two braille-technology based tactile displays and one electroactive polymer haptic display. Using a miniature braille module driven with electromagnetic actuators, we devised a circular-array type braille display (Sec. “3.2 Circular Array Braille Display”) and a stick type mobile wireless braille display (Sec. “3.3 Braille Stick”) consisting of a linear array of sixteen 6-pin braille cells. Creating a hardware and software platform that could control actuators using electroactive polymer membranes was also attempted. The prototype delivered deformations at high voltages with a 3-by-3 electroactive polymer tactor array (Sec. “3.4 Electroactive Polymer Tactile Display”).

The major effort of this thesis research is presented in Chapter 4. The efforts to create new tactile interfaces and effects focused on expanding the emotional expressiveness of existing vibrotactile technologies. Past research has shown that the emotional responses to vibrotactile stimuli tend to be neutral, especially when the signal amplitude is low. We set out to develop calm and pleasant vibrotactile signals that are low in stimulus intensity but can lead to positive valence, i.e., pleasant sensations. A key insight from this thesis research is that extremely slow stimuli or phenomenon such as "breathing" are expected to be calmer and more pleasant. When we explored vibrotactile patterns with a carrier frequency below 1 Hz, a calm and relaxing sensation was achieved. This may very well be due to the fact that this very low frequency corresponds to the respiration or heart rate of an adult in a calm and resting state. We pursued such signals with the hope that this type of signals can serve as quiet yet effective notification signals on mobile devices like smartphones.

We concentrated on a haptic technology and hardware platform that are readily available and have the potential for broader expressiveness. Voice-coil actuators were chosen for its relatively wide frequency bandwidth than other types of commodity vibrators. We also sought to experiment with a 2-by-2 tactor array in order to use the spatial extent for increased expressiveness of vibrotactile signals. The result was the *palmScape* prototype that can fit comfortably under the palm of a hand (Sec. “4.2 A New Tactile Display: *palmScape*”).

In Sec. “4.3 Design Approach and Signal Design,” we introduce the design approach consisting of three design principles and five guidelines. These design principles outline strategies for designing tactile displays and signals to enhance the expressiveness, pleasantness, and distinctiveness of tactile feedback. The five guidelines are described in practical terms that provide insights and directions for designing the new tactile display, *palmScape*, and for designing signals based on the principles. Detailed examples and figures of custom-designed signals are provided to illustrate each guideline in detail.

As mentioned earlier, frequencies lower than 1 Hz tend to be associated with aliveness. Therefore we used a 0.8-Hz carrier frequency to represent “breathing.” The tactors were able to deliver a peak-to-peak displacement of 2 mm at this very low frequency, giving the impression of a small puppy resting in the palm. This design thinking opened up new possibilities for vibrotactile expressions. By combining low-frequency movements with high-frequency vibrations and distributing signals across the four tactors in a deliberate way, it was possible to achieve a three-dimensional tactile experience with the *palmScape* by capturing the essence of many natural phenomena.

The evaluation of the designed vibrotactile patterns is presented in Sec. “4.4 Affective Rating Experiment.” A total of sixteen signals were designed to represent natural metaphors. Most of the signals utilized low frequencies (< 3 Hz) to convey a sense of calmness, relaxation, pleasantness, and delight. The sixteen designed vibrotactile signals contain metaphors that have not been commonly used in previous vibrotactile icons. They include sensations inspired by “breathing,” “earthquake,” “heartbeat,” “raindrop,” “bubbles,” “cicadas,” “bathtub water jet,” and other metaphors that are represented in the sixteen custom-designed vibrotactile signals. An additional four reference vibrotactile signals were added to the stimulus set to form a total of twenty vibrotactile signals. Users were invited to experience these signals and rate them on valence (unpleasant vs. pleasant) and arousal (calm vs. exciting). The results from the affective

ratings of the sixteen natural-metaphor inspired signals delivered through *palmScape* are presented and compared to other data in the literature.

In Sec. “4.5 Summary and Design Thinking Revisited”, we summarize the major findings of the rating experiment and reflect on how the five design guidelines have been applied to the design of the sixteen custom vibrotactile signals. The detailed design story of all sixteen custom-designed signals are described in this section including the design approaches, insights, and description of physical parameters used. We share the considerations that are unique to the design of a particular signal or common to multiple signals. We compare and contrast signals that share similar physical parameters but result in drastically different affective ratings, or vice versa. We hope that the contents will spark new ideas and approaches to designing vibrotactile signals.

The thesis concludes with Chapter 5 on Conclusions and Future Work. It is our sincere hope that this thesis research becomes a useful reference for future haptic designers and inspires more research towards designing more comfortable and enjoyable haptic user experience. Finally, the appendices of the thesis contain further details. Results of the affective rating experiment for each participant is enclosed in Appendix A. The details of the twenty vibrotactile signals used in the affective rating experiment are shown in Appendix B, within the figures of the 4-channel waveforms for each signal.

2. BACKGROUND

This chapter provides the background information pertinent to this thesis research. After covering the fundamentals of human haptic perception, a review of haptics technologies is provided. The last part of this chapter covers the topic of haptic user experience, which is at the core of this thesis research.

2.1 Human Haptic Perception

Human beings acquire information, learn, judge, interact with things and people through sensing and perception in the real world. Through the eyes, ears, nose, tongue, and skin, a person feels five main senses: sight, hearing, smell, taste, and touch, respectively. In a given environment, the sensory nerve or receptors are activated by some form of energy, which can be referred to collectively as stimuli that are transmitted to specific regions of the brain corresponding to the receptors to interpret the information. Among the five primary senses, haptic sensing is accomplished by the somatosensory system. It encompasses the interpretation of mechanical displacement in contact with the skin (also termed tactile sense), temperature (thermoception), kinesthetic sense (proprioception), pain (nociception), and vibration (mechanoreception). In addition, tactile senses are accommodated by the skin covering the entire body, while the receptors for the other four senses are concentrated in dedicated locations [Wikipedia, 'sense,' 'somatosensory system'] [1].

Since tactile perception occurs through contact with people or objects, it plays an active role in how we judge the properties and quality of the object in contact. It is especially important to consider the part of tactile feedback in human-computer interaction. While vision dominates in most scenarios, it is sometimes unavailable due to sensory impairments or situational blindness (e.g., in the dark or during driving). To complement this, hearing and tactile information are often needed in addition to visual information. In recent years, there have been attempts to provide user convenience and added value through tactile-based interface design, and efforts have been made to provide a more immersive and realistic user experience through a combination of multiple senses.

Understanding the haptic cognitive properties is essential in haptic interface design. The book "Tactile Aids for the Hearing Impaired" serves as a guide for designing a tactile information delivery system and use the sense of touch a communication channel and tool for the hearing impaired. The first chapter of the book, "Perception via the Sense of Touch," introduces the basic research results on the perception characteristics of touch sense [2]. Research findings on haptic perception provide information for designing tactile systems for people with hearing impairments and the general public whose sense of touch may be compromised temporarily due to various scenarios. For this purpose, major factors needed to understand the tactile cognitive characteristics are summarized in Table 2.1. The most important and relevant factors are emphasized in the table, including frequency as the main factor for the temporal characteristics of a tactile stimulus, and contactor size and body site as the main factors for the spatial characteristics.

Table 2.1 Major factors that affect to sense of touch [1, 2].

<i>Receptor Mechanisms</i>	<i>Tactile receptors (Mechanoreceptors)</i> <i>Kinesthetic receptors</i> Thermoreceptors Nociceptors
<i>Temporal Domain</i>	<i>Frequency</i> Frequency discrimination Stimulus duration Gap detection Amplitude modulation Temporal order
<i>Spatial Domain</i>	<i>Contactor size</i> <i>Body site</i>
Intensity Effects	Subjective magnitude Intensity discrimination Effects of multiple stimulations Adaption

Table 2.1 continued

Complex Stimuli	Patterns
	Spatiotemporal relationships
Subject Variables	Gender
	Age
	Handedness

2.1.1 Receptor Mechanisms (Mechanoreceptors)

Tactile Receptors. Analyzing the mechanisms of the sensory organs and receptors distributed within the skin for tactile stimulation and understanding their role is a fundamental asset in designing any tactile interface. Though there may be differences in the thickness and softness of the layers that make up the skin depending on the body site, most skins consist of basic substructures as shown in Fig. 2.1. The skin is divided into the outermost layer called dermis, the middle layer epidermis, and the inner layer subcutis. There are four types of mechanoreceptors responsible for the sense of touch. Mechanoreceptors respond to mechanical stimuli or pressure. Depending on the size of the receptive field and the rate of adaptation, there are four types of mechanoreceptors: Meissner corpuscles (FA I fast-adapting and small receptive field), Merkel cell-neurite complex (SA I – slowly-adapting and small receptive field), Pacinian corpuscle (FA II – fast-adapting and large receptive field) and Ruffini ending (SA II – slowly-adapting and large receptive field) [1, 3].

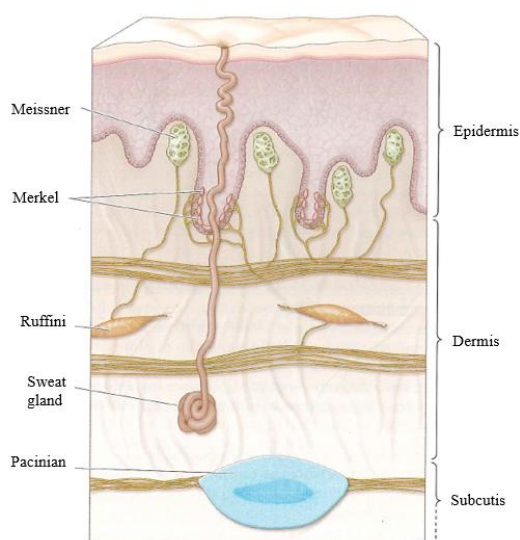


Fig. 2.1 Demonstrating the locations of the four types of mechanoreceptors [1].

In this thesis research, we incorporate slow kinesthetic motion or deformation at very low frequencies below 3 Hz, in addition to high-frequency vibrations that are typically used in mobile devices, etc. The Merkel cells (SA I) are responsible for the perception of spatial deformations at the low-frequency range of 0.4 - 3 Hz and for detecting spatial patterns and forms. We also use the frequency range of 3 - 40 Hz to induce a gentle, temporal change in skin deformation through the Meissner corpuscles (FA I). The reason for focusing on very low frequencies in this thesis is to pursue a differentiation from the frequency range 40 to 500 Hz that are commonly used. Vibrations in this frequency range are mainly detected by the Pacinian (FA II). In other words, it implies a strategic direction of research that expands the range of stimulation by engaging more receptor types and thereby evoking additional distinct sensations, which differentiates this thesis research from the existing approach of employing only vibrational stimulation patterns.

Table 2.2 Mechanoreceptors: Response characteristics, feature sensitivity and associated function [1].

<i>Mechano-receptor</i>	<i>Size of Receptive Field</i>	<i>Adaption Rate</i>	<i>Maximum Feature Sensitivity</i>	<i>Primary Functions</i>
<i>SA-I (Merkel)</i>	<i>Small</i>	<i>Slow</i>	<i>Sustained pressure, very low frequency (0.4-3 Hz) Spatial deformation</i>	<i>Texture perception Pattern/form detection</i>
<i>FA-I (Meissner)</i>	<i>Small</i>	<i>Fast</i>	<i>Temporal changes in skin deformation (3-40 Hz)</i>	<i>Low-frequency vibration detection</i>
<i>FA-II (Pacinian)</i>	<i>Large</i>	<i>Fast</i>	<i>Temporal changes in skin deformation (40 to >500 Hz)</i>	<i>High-frequency vibration detection</i>
<i>SA-II (Ruffini)</i>	<i>Large</i>	<i>Slow</i>	<i>Sustained downward pressure, lateral skin stretches, skin slip (low sensitivity to vibration across frequencies) (100 to >500 Hz)</i>	<i>Finger position, stable grasp</i>

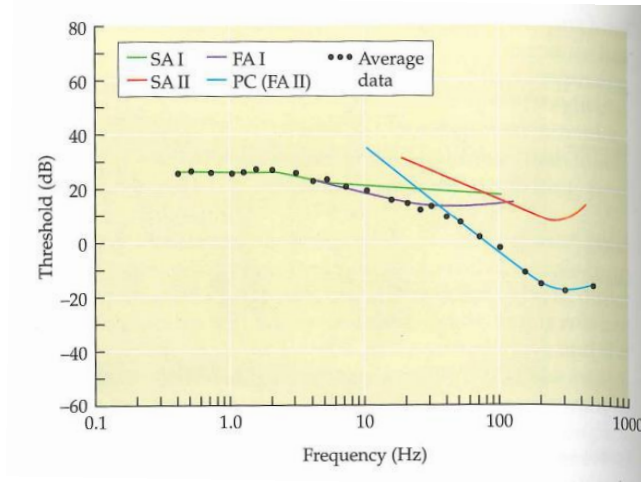


Fig. 2.2 Minimally detectable (threshold) displacement of the skin produced by a vibrating stimulator, as a function of vibration frequency [1].

Kinesthetic Receptors. In addition to the mechanoreceptors distributed in the skin, there are kinesthetic receptors in the muscles, tendons, and joints, which play an important role in recognizing the position and motion of our extremities as well as force. In particular, sensors in muscle spindles can estimate the rate of change of the muscle fibers and transmit the information to the central nervous system. As shown in Fig. 2.3, muscle fibers are divided into main (extrafusal) muscle fibers and inner (intrafusal) muscle fibers. When the inner muscle fibers contract, the response from the spindle is transmitted to the central nervous system, which in turn estimates the length and tension of the muscle. In this thesis research, we employ very low-frequency stimuli with sufficient force to impart a slow variation of pressure on the palm. Compared with the conventional high-frequency vibrotactile stimulation, our display incorporates stimuli that approach those typical of a kinesthetic display [1].

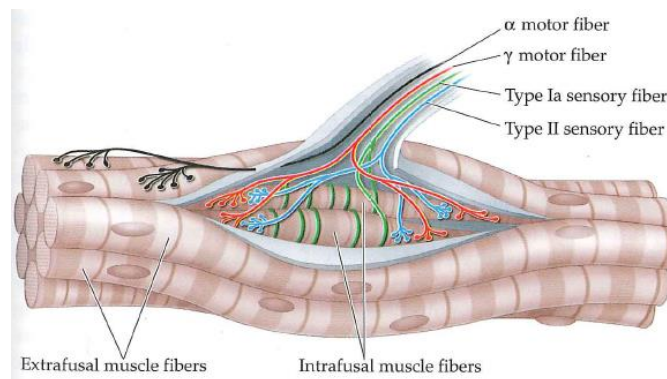


Fig. 2.3 A muscle spindle embedded in main (extrafusal) muscle fibers contains inner (intrafusal) fibers [1].

2.1.2 Related Factors to Tactile Responses

Frequency and Contactor Size. Tactile sensitivity varies with stimulation frequency and contact area for individual participants and should be measured for each participant to ensure that similar perceived intensities are achieved for all participants. Sensitivity is the inverse of the detection threshold, defined as the smallest amplitude that is reliably detected by the participant. There are several factors that affect the absolute or detection thresholds: signal duration, frequency, contact area, body site, and so on [4]. Verrillo's efforts have clarified the relationship of absolute thresholds with frequency and contact area [5]. The relationship of the threshold is derived as shown in Fig. 2.4 by changing the contact area and the frequency with the palm raised on a circular-shaped vibration stimulator protruding on the plane and contacting the prominence on the palm side of the base of the thumb (called thenar eminence). If the contact area is 0.2 cm^2 or less, the threshold is high and constant across all frequencies. If the area is larger than 0.2 cm^2 , the detection threshold is a U-Shaped function of frequency. The skin is most sensitive at around 250 Hz, has a decreasing linear relationship below 250 Hz, and an increasing linear relationship above 250 Hz. As the contact area increases, the threshold response curve is lowered (i.e., the skin becomes more sensitive) while maintaining the U-shape. These results demonstrate the spatial summation property of the tactile sense. For contact areas greater than 2.9 cm^2 , the effect of spatial summation ceases, and the detection thresholds no longer decrease further. In addition, spatial summation does not occur at vibratory frequencies below about 40 Hz.

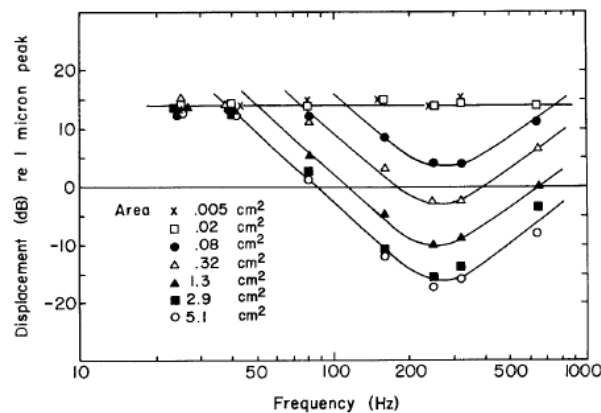


Fig. 2.4 Vibrotactile thresholds for contactor sizes as a function of vibration frequency [4].

In this thesis research, we use a very low frequency of $< 3 \text{ Hz}$ slow kinesthetic motion and a mid-frequency stimulation ($< 40 \text{ Hz}$) in addition to the common high-frequency vibrations

(100-300 Hz) to enrich the sensations that can be evoked. Given the large differences in detection thresholds across frequencies, it is imperative to adjust the signal amplitudes so that the perceived intensities at different frequencies (typically defined as dB above the detection thresholds at the respective frequencies) are balanced.

Body Site. The aim of this thesis research is to explore the possibility of inducing more calm and pleasant stimuli that were difficult to achieve using the existing (high-frequency) vibrotactile stimulus and widening the range of emotions that can be evoked. Therefore, it is preferable to engage a body site that is relatively sensitive to vibrotactile stimulation and is convenient to access. For the purpose of this thesis research, the palm was selected for its high sensitivity and user's acceptance of using the palm for active tactile exploration and interaction with objects. Shown below are the results of a study by Weinstein that indicates the sensitivity of body sites to pressure. The palm is shown to have a relatively high sensitivity (below the hallux and the sole, which are not convenient to use in an interface).

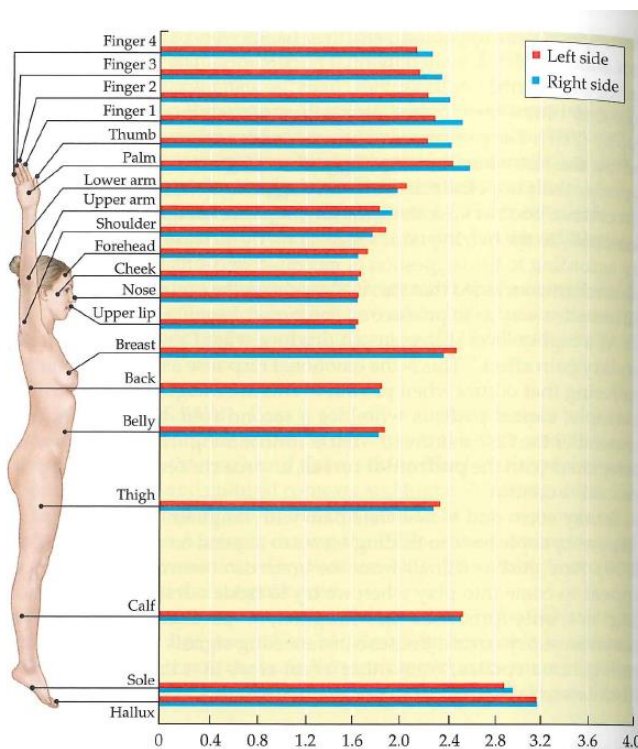


Fig. 2.5 Sensitivity to pressure at different sites on the body [1].

2.1.3 Psychophysical Methods

Gustav Fechner (1801 - 1887), a versatile scientist-philosopher from Britain, is often regarded as the founder of experimental psychology (Boring, 1950). His research goal was to

identify the relationship between the sensation (mind) and the energy (matter) that caused the sensation and to suggest a methodology. As a physicist, he thought that he could explain the relationship between mind and body through mathematics, and his theory is called psychophysics (psycho for the mind, and physics for the matter) [1]. Fechner proposed a method for measuring what people see, hear, and feel, and these methods are still used today. To make it easier to understand psychophysics methods, we use an example of measuring the absolute or detection threshold (AL: *absolute limen*), the minimum energy at which a stimulus can be barely or reliably detected. For example, a beep sound heard through an audio headphone during a hearing test which is barely detectable is the detection threshold for sound decibel. We can also estimate the difference threshold (DL: *difference limen*) to quantify the minimum difference between two stimuli that can be reliably detected. For example, when you grab a reference weight in one hand and gradually increase the weight to the other hand, the difference in weight is the difference threshold when you can reliably detect it [1, 4].

Method of Constant Stimuli. Among the methods for measuring human sensations, the method of constant stimuli uses stimuli of various intensities to find the smallest intensity that can be detected (for AL) or the smallest difference in intensity that can be detected (for DL). Here we use a detection experiment as an example. Each time a test stimulus is given, the participant replies whether the stimulus has been detected or not. In addition, the intensity of the stimulus can be randomly selected from 5 to 9 values, and each intensity is presented multiple times. The number of times a stimulus is detected increases monotonically as the intensity increases, and such a relation is typically modeled with a cumulative Gaussian curve. In general, the stimulus level corresponding to 50% of “detected” responses is selected as the detection threshold [4, 6].

Method of Limit. The method of limits progresses with increasing or decreasing intensity until the participant reverses the response from, for example, detected to not detected. For example, an experiment can start from an upper-limit intensity that is sufficiently larger than the detection threshold. The intensity is gradually decreased as long as the stimulus is detectable, and the experiment stops when the stimulus can no longer be detected. Conversely, the experiment can start from the lower-limit intensity that is not detectable. The intensity is gradually increased until the stimulus can be detected. The detection threshold is estimated as the median of the crossover points of the 'detected' and 'not detected' responses of each descending or ascending

series. The average of the estimates from the equal number of ascending and descending series is the detection threshold corresponding to the 50% point on the psychometric function [4, 6].

Simple Up-down Adaptive Procedure. As a modification of the method of limits, Cornsweet (1962) proposed an up-down or staircase method. If the participant's response changes from 'detected' to 'not detected' or vice versa, record the value and reverse the direction of increasing or decreasing the intensity. Estimated threshold values are calculated as the mean values at the reversal points. This method results in a detection threshold level that is at the 50% point on the psychometric function [4, 6]. To estimate thresholds at other percentile levels, the transformed adaptive procedures can be employed (discussed next).

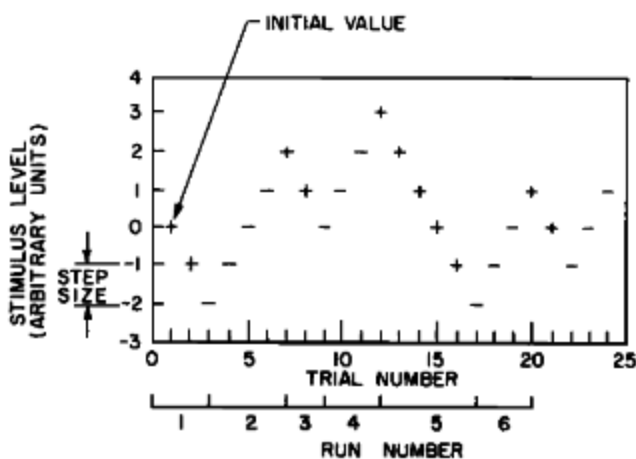


Fig. 2.6 Typical data for the simple up-down procedure [6].

In the simple up-down adaptive procedure, the step size needs to be selected carefully. In general, it is better to set the initial step size larger than the optimal step size. If the initial step size is larger than the optimal step size, the efficiency is reduced by 25%. If the smaller initial step size used, then the efficiency is reduced by nearly 100%. In addition, it is theoretically advantageous to reduce the step size for each trial for a better resolution of the final estimates. In this thesis research, we used a relatively large initial step size for faster convergence and a smaller step size after the first four reversals for better resolution of the threshold estimates.

Transformed Adaptive Procedure. In order to estimate thresholds at points other than the 50-percentile point, Levitt proposed many transformed up-down procedures [6]. The procedures can be characterized by the rules for increasing stimulus intensity and decreasing intensity. For example, the one-up two-down method (entry 2 in Table 2.3) means that a stimulus intensity is increased after one incorrect response and decreased after two consecutive correct answers. The

threshold so-obtained corresponds to the 70.7% point on the psychometric function. It now follows that the experimenter can select the up-down rules according to the desired “probability of positive response at convergence” (see Table 2.3). In this thesis research, we used the one-up two down adaptive procedure (second entry in Table 2.3) to measure the detection threshold corresponding to a probability of 70.7%.

Table 2.3 Response sequences and groupings for transformed up-down procedure [6].

Entry	Response sequences		Response groupings	
	UP group increase level after:	DOWN group decrease level after:	Probability of a sequence from DOWN group = $P[\text{DOWN}]$	Probability of positive response at convergence
1	—	+	$P(X)$	$P(X) = 0.5$
2	+ — or —	++	$[P(X)]^2$	$P(X) = 0.707$
3	— —	— + or +	$[1 - P(X)]P(X) + P(X)$	$P(X) = 0.293$
4	+ + — or + — or —	+++	$[P(X)]^3$	$P(X) = 0.794$
5	+ + + — or + + — or + — or —	++++	$[P(X)]^4$	$P(X) = 0.841$
6	— — — —	— — — + or — — + or — + or +	$1 - [1 - P(X)]^4$	$P(X) = 0.159$
7	Any group of 4 responses with 1 or more nega- tive responses	++++	$[P(X)]^4$	$P(X) = 0.841$
8	— — — + — + — —	+ + + — + — + +	$[P(X)]^2[3 - 2P(X)]$	$P(X) = 0.5$

2.2 Haptics Technology

According to a recent report by IDTechEx Research titled “Haptics 2018-2028: Technologies, Markets and Players”, the market for haptics technology is predicted to grow in the next decade. Fig. 2.7 is a schematic representation of the haptic technology mapped to two axes: mass production possibility (horizontal axis) and production volume (vertical axis) (from the initial research stage to ubiquitous adoption). (For reference, this chart is a partial change from the sample page of Haptics 2018-2028 provided by IDTechEx Research.) Electromagnetic haptic actuators have been the most used in the industry for decades because they are inexpensive, reliable, and efficient. Although ERMs and LRAs continue to dominate the market, piezoceramic and voice-coil actuators, which secured the mass production and reliability of mounting on devices, constituted the first alternative sector. The chart also categorizes contactless, surface, electroactive polymers, and microfluidics as the second alternative option, although not quite ready for mass production and product application yet. Shape memory actuators. Are categorized as an emerging proof-of-concept option. In this chapter, we will cover the haptic technologies applicable to interface design by focusing on the dominant and alternative sectors, based on the need for designing new natural haptic interfaces.

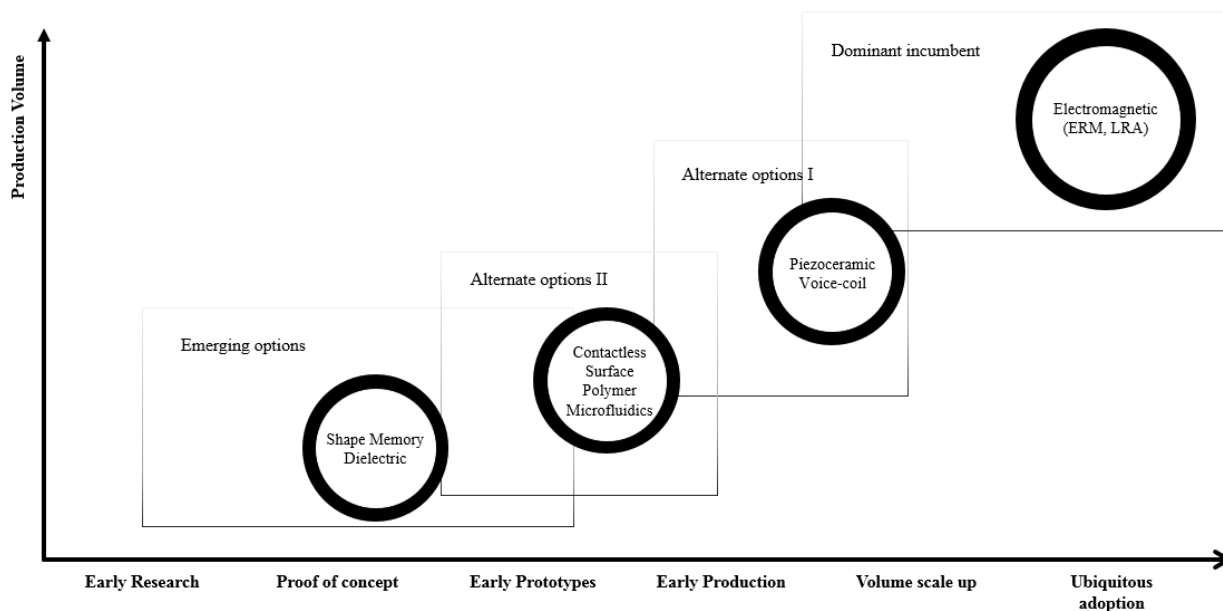


Fig. 2.7 Haptics technologies, markets, and players (IDTechEx Research).

(<https://www.idtechex.com/research/reports/haptics-2018-2028-technologies-markets-and-players-000596.asp>)

2.2.1 ERM, LRA

Eccentric Rotating Mass (ERM) Motor. ERM motor is the most widely used vibrotactile actuator in devices such as mobiles and wearables. It has the same structure as a general DC motor but generates vibrations by rotation of the eccentric mass attached to the end of the motor shaft. When a direct current is applied to the motor, the eccentric mass rotates continuously and produces a centrifugal force proportional to the square value of the angular velocity of the mass [7]. ERM can be made small, and it is used universally for consumer products such as mobile and wearable devices and gaming and VR controllers because it generates strong vibrations compared to its size. Typical examples include a DualShock controller that produces different shocks with two motors with different eccentric masses and a small fitness band such as a Fitbit. In DualShock, the two ERM motors located on the left and right of the controller deliver two types of shocks to the user, one for a massive shock and the other for a light shock. ERMs are typically attached directly to a device, and the rotation of the eccentric mass causes the entire device to vibrate, delivering vibrations to the skin in contact with the device. There is a relatively long delay before the ERM reaches its peak acceleration and the same before the ERM reaches a full stop. Therefore, it is difficult to utilize ERM when fast response such as text input feedback is required in the touch interface.

When it is required to miniaturize the vibration actuator due to the small mounting space available, such as the Fitness Band, the ERM has a significant advantage when it is viewed as a vibration force relative to the mounting space. In general, the smaller the size of the actuator, the higher the frequency of rotation and hence vibration. The higher vibration frequency tends to lead to the perception of a penetrating vibration and audible noise, which degrades the overall perceived vibration quality.

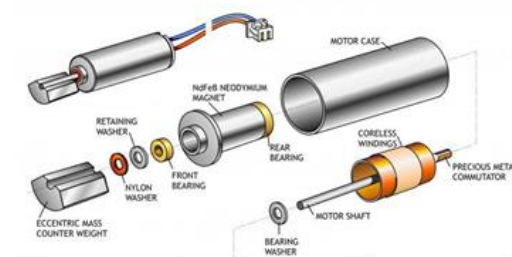


Fig. 2.8 Structure of an eccentric rotating mass (ERM) motor.

The sensations that can be delivered by vibrations using ERMs are limited to a duration of about 20 - 30 ms, a weak impact, a shock at about 50 - 100 ms, and a long "buzz" vibration at over 100 ms. When a driver IC is used to improve the response time by over-driving and active-breaking, click-like feedback at a duration of about 20 ms can be achieved. Thus, ERMs are limited in expressing emotions and metaphors due to the rough (rattling) feeling of the vibrations of the rotating body, the narrow frequency range, and the slow response. There is a possibility that when accompanied by (audio) rhythm or synchronized with visual information, the overall experience may be slightly improved.

Linear Resonant Actuator (LRA). The Linear Resonance Actuator (LRA) is a widely used vibrotactile actuator with ERM, commonly referred to as a Linear Actuator. It uses the same electromagnetic force as ERM but generates vibration through unidirectional spring motion of the mass attached to the spring. The design of LRAs can be optimized in terms of resonant frequency and viscosity [7]. LRA is also an actuator that is used in general purpose such as mobile, wearable device, game controller, etc. LRAs have faster response, higher energy efficiency, and stronger force characteristics than ERMs. They are suitable for providing not only feedback of notifications, feedback to deliver a sense of impact in gaming and VR environments, but also physical interaction feedback in combination with a touch interface that requires a faster response.

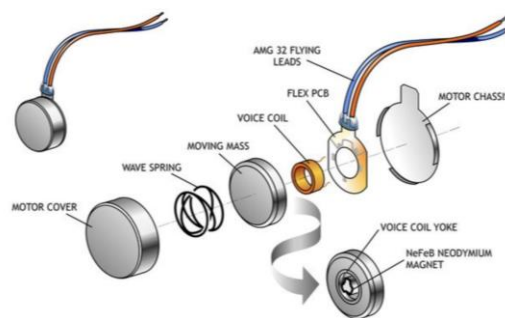


Fig. 2.9 Structure of a linear resonant actuator.

There are cases where the LRA is applied to consumer products by taking advantage of their more rapid response. In the mid-2000s, Samsung combined LRAs with a touch-based feature phone device. In particular, they created tactile feedback in a variety of use cases, including tactile feedback to the touch input for typing, and tactile feedback combined with graphical controller interactions. At the time, they used the brand name 'Haptic' on their mobile

phone, a term that had been used mainly in academia until then and was somewhat controversial. But over time, as wearable devices became popular, Apple began actively applying LRAs to merchandising devices, starting with the Apple Watch. Initially, Apple Watch did not change the previous mechanism of LRA but took advantage of more space and ergonomics to take the existing LRA a step further. Because it is a wearable device that touches the body directly, Apple seems to be deeply concerned with the quality of transmitted vibrations in terms of the most suitable feeling for the wrist considering human factors for a wearable smartwatch. To realize a more natural feel on the wrist and skin, a new linear actuator was designed, and the actuator technology itself was branded as "Taptic Engine." The linear actuator with relatively large size, which accounts for more than one-third of the Apple Watch's mounting space, delivers the feeling of knocking at low frequencies and is a trade-off of power consumption and battery life – the most critical feature in Smartwatch. In recent years, Samsung has introduced wide-band linear actuators to enlarge the range of expressiveness of vibrotactile feedback on a smartphone which accommodates lowering the frequency for notification signals, optimizing the frequency for several use-cases, and generating multi-frequency vibration patterns. Taken together, the recent 10-year trend shows that haptic technology has become popular in consumer products.

However, once again looking at the range of expressiveness through the LRA, its ability to express emotions and metaphors is still very limited like the ERM. Although the LRA has a faster response than the ERM, its resonant frequency is decreased, or the length of vibration is reduced to minimize exposure time, it still delivers a monotonic feeling compared to the rich sense of touch we experience every day.

2.2.2 VCA, Piezoelectric

Voice-coil Actuator (VCA). Voice-coil actuators are not commonly used in popular devices such as smartphones and smartwatches but are often applied in niche products. A voice-coil actuator consists of a permanent magnet and a coil winding connected to the compliant suspension in a structure very similar to the speaker. These two components give forces in opposite directions proportional to the current applied to the coil. One of the two components is usually attached to the casing, and the other is movable [8]. Because a voice-coil actuator is almost the same structure as a speaker, it can produce audible output if placed close to the ear or attached to the surface. Also, when the actuator touches the skin, the bone-conduction of sound

can occur [9]. As a result, it is not only used as a tactile actuator but also as an exciter and a bone-conduction speaker that attaches to a surface to be used as a speaker, and a bone-conduction headset that is placed near the jaw joint on the face. In addition, voice-coil actuators can deliver realistic vibrotactile signals to the hands as many researchers have noted, and there are many applications such as telerobotic systems, haptic recreation of virtual textures, contact vibrations, and tactile enhancement of hand tools. These actuators have an extensive range of frequency response, like speakers, compared to the frequency-limited eccentric rotational mass motors or linear resonant actuators. Therefore it acts as a wide-band high-definition haptic actuator. In designing a vibrotactile signal, voice-coil actuators have the advantage of being able to express richer and more nuanced sensations compared to ERMs and LRAs that are commonly used in existing devices. The ability to generate vibrotactile signals through sound design methods also extends the range of tactile expressions that can be achieved with voice-coil actuators.



Fig. 2.10 Voice-coil haptic actuators and products.

In a phonemic-based tactile display for speech communication study, 24 voice-coil actuators are arranged in 4-by-6 form. The tactile display is implemented in a sleeve form factor worn on the forearm. Haptic codes for the 39 English phonemes have been designed and delivered to the user via the tactile sleeve [10]. The haptic codes employ a carrier frequency of 300 Hz in some cases, similar to the vibrotactile feeling of the conventional vibration felt on most mobile devices. The codes also employ a lower carrier frequency of 60 Hz for a “heavier” feel and use amplitude modulation for roughness perception.

In this study, the same voice-coil actuator as the tactile speech project is arranged in a 2-by-2 form and the palm is placed on the array to receive tactile feedback. We found that these voice-coil actuators respond to very low frequencies, such as under 3 Hz, and can move a few

mm in the out-of-plane direction. This has led us to design vibrotactile displays and signals that are distinctly different from conventional high-frequency vibrations.

Piezoelectric Actuator. Piezoelectric actuators generate vibrations by utilizing the deformation property of piezo layers when a voltage is applied. By placing different polarities at the top and bottom of the thin piezo layer, the surface of the anode is shrunk, and on the contrary, the surface of the cathode is expanded, causing the piezo and attached metal plate to bend up and down, and therefore provides haptic feedback. They have the advantages of broader frequency bandwidth and faster response as compared to ERMs and LRAs. It is possible to express heavy vibrations at low frequencies and fine vibrations like small particles at high frequencies. It seems to be suitable for button click feedback because of the quick response and instantaneous power transfer. On the other hand, piezo actuators require much higher driving voltage (40 - 200 V) as compared to ERMs and LRAs, and consequently, need voltage boost circuits. In terms of energy efficiency, it is better than LRA and ERM in short vibration of about 10 - 20 ms which is used in click feedback. However, the longer the duration, the lower the efficiency as described in Fig. 2.12. In addition, the high price of piezo actuators acts as a barrier, and it is imperative to define the additional user value that outweighs these disadvantages. In summary, piezo have the advantage of expanding the limited expressiveness of ERMs and LRAs to a richer range, can be utilized for various purposes such as force interface, and can be mass produced and mounted on any device.

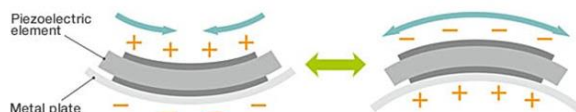


Fig. 2.11 Structure and actuation mechanism of a piezo actuator.

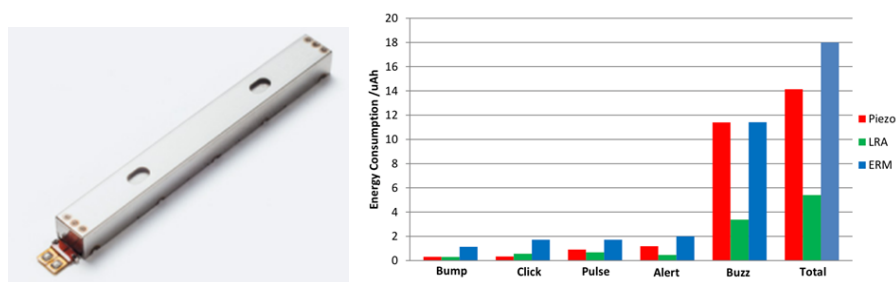


Fig. 2.12 Piezoelectric actuator and energy consumption comparison of haptic actuators: piezoelectric, LRA, ERM.

(<http://www.ti.com/lit/an/sloa194/sloa194.pdf>)

Piezoelectric - Ultra-thin Actuator: PiezoHapt™. PiezoHapt™ is a very thin (0.35mm) piezoelectric actuator with a low driving voltage (less than 24 V) compared to conventional piezo actuators. It operates at a lower frequency than expected (200 Hz) and has a fast response (4 ms). TDK introduced PiezoHapt™ to enable a variety of haptic patterns and provide a typical displacement of 55 μm when a sine wave of 24 V (peak) at 200 Hz (carrier frequency) is applied. It is expected that controlling shorter durations of vibrotactile stimulation (e.g., ≤ 10 ms on the piezo actuator is possible due to the quick response. Therefore, piezo is suitable to produce repeated click feedback that requires shorter duration and fast rising and falling time to ensure adequate interstimulus interval for repeated stimuli perception.

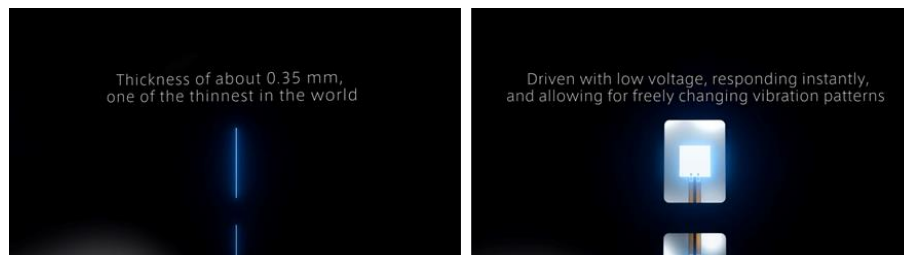


Fig. 2.13 Ultra-thin piezoelectric actuator (PiezoHapt™).

2.2.3 Contactless, Surface, EAP, Microfluidics

Contactless - Ultrasound: Ultrahaptics. Ultrasound haptics technology creates a haptic sensation in the air (mid-air) by concentrating the sound energy delivered through the air from the ultrasonic speaker array. In order to concentrate the sound energy at a specific spatial focal point as shown in Fig. 2.14, the phase delays for the speakers are carefully controlled so that the pressure waves overlap at a certain point. The superimposed sound pressure energy coalesces to create a sensation by pressure in mid-air on the bare skin, without any contact. This allows one to feel the presence of a virtual object in space in a tactile sense. The technology facilitates mid-air interactions with virtual objects. This haptic technology was developed by Hiroyuki Shinoda at the University of Tokyo, and also by the Bristol University. In addition, the company UltraHaptics was launched by researchers at Bristol University, and it has appeared as a concept and exhibition demo in HMI and kitchen appliances, and it targets automotive, medical, public interfaces, smart home, marketing, and advertising. The company provides a development hardware kit that combines a spatial motion-sensing controller, leap motion, and an ultrasound transducer array. It also provides a software development environment and graphic-aided

computer design tools for haptic feedback. It is expected that it could be widely used to provide haptic feedback in space without wearing any haptic equipment in the VR and AR fields in the future. However, the relatively weak sensation achievable by such displays may be a barrier to the wide adoption of this technology.

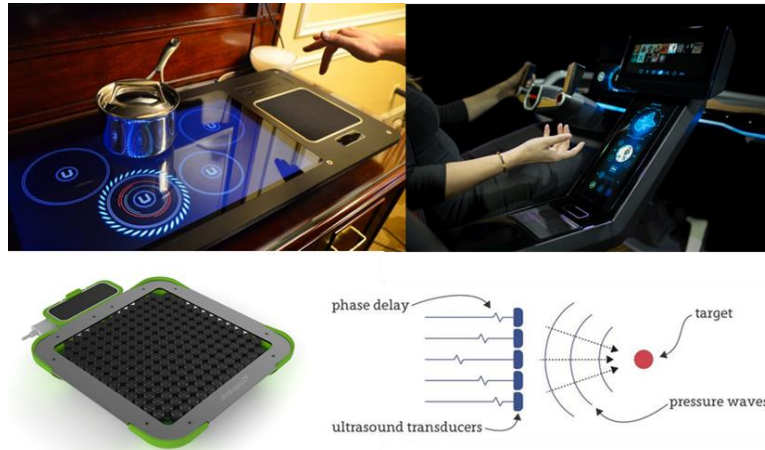


Fig. 2.14 Ultrasound: Concepts, prototypes, development kit, and the actuation mechanism.

Surface - Electrostatic Friction (ESF): Senseg (acquired by O-Film, 2016. 2), Tanvas. Electrostatic friction technology uses electrostatic attraction forces to increase the friction force on a finger sliding across the surface [11]. With this haptic technology, we can experience the texture of the surface, such as the roughness of sand and rubber on an otherwise smooth touch screen. The Senseg dev kit allows the programming of two types of sensations. The first is the perception of a rough *area* felt on the fingertip due to electrostatic friction during the swipe interaction on the surface. The other one is the perception of a rough border. The combination of these two types of textures creates tactile feedback by electrostatic friction on a flat, smooth touch screen, which is different from feeling a real rough surface and therefore has a limited range of expression to represent real textures. Presently, there are prototypes on touch-screen-based tablets and car infotainment systems, but there are no foreseeable applications for mass production yet.

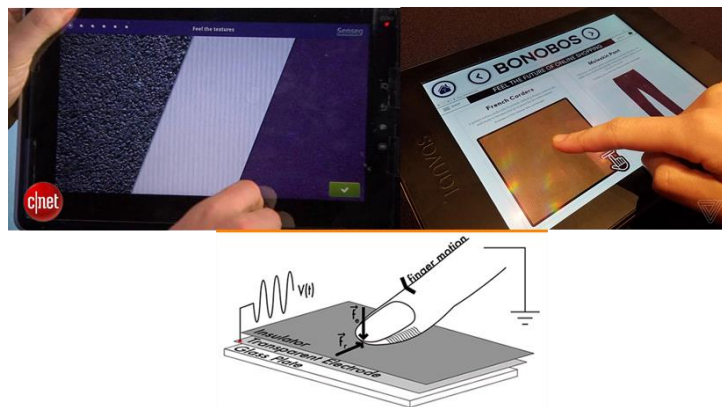


Fig. 2.15 Electrostatic friction: Concepts, prototypes, and the actuation mechanism.

Surface - Piezoelectric Friction (Ultrasonic Vibration): hap2U. Piezoelectric friction is another method of modulating surface friction. Unlike electronic friction displays that can only increase the perceived friction coefficient of a surface, piezo-based displays can only decrease the perceived friction coefficient of a surface. An array of piezoelectric ceramic actuators are arranged along the edges of the glass. The ultrasonic vibrations generated by the piezo actuators on the glass surface generate standing waves that subsequently trap air when a finger moves across the surface. A more extensive range of surface friction modulation can be achieved by combining piezoelectric friction and electrostatic friction techniques.



Fig. 2.16 Structure of piezoelectric friction haptic display.

Surface - Bending Wave Haptic: Redux ST (acquired by Google, 2017.8). Unlike the surface haptic technologies that utilize the electronic friction mentioned above, the Redux bending wave technology produces a haptic effect by generating and controlling sound waves on the surface of a screen precisely. It is a technology that enables haptic feedback on the screen surface as well as surround sound reproduction on the surface without a speaker. The bending wave technology is used to create a haptic effect or play a sound at a specific location on the screen, and accurately control the sound waves on a plane or surface. Redux ST introduces

haptics for border detection, realistic mechanical buttons, and switches, and can be used in a variety of applications including mobile and consumer electronics, automotive and aerospace.

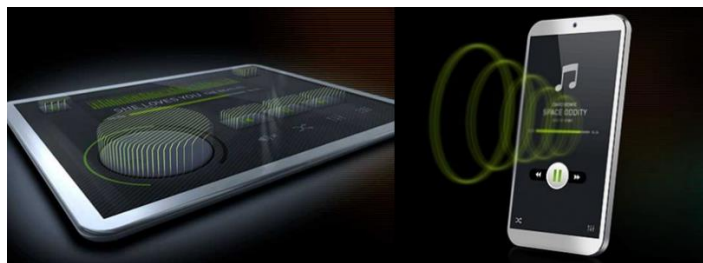


Fig. 2.17 Concept image of bending wave haptic.

Electroactive Polymer. Electroactive polymer type actuators are characterized by thin, lightweight, flexible and fast response. Similar to a piezoelectric actuator, an electroactive polymer actuator requires high operating voltages over 100 volts to deform. It also has the advantage of responding to audio signals similar to loudspeakers and thus delivering haptic and audio feedback at the same time. Novasentis is a representative company that developed the actuator with electroactive polymer and introduced it as the electro-mechanical polymer (EMP) technology. The small square-shaped actuator has two sizes that measure 10×10 mm and 12×12 mm respectively with a thickness of 120 microns, and lightweight of 0.001 g, and a fast response time of less than 5 ms. One application is to minimize the thickness of a mobile keyboard by removing all moving parts and replacing them with a thin electroactive polymer actuator. In addition to providing tactile feedback to touch input, the actuator itself can also act as a sensor or an input, which replaces the need for a physical key. The EMP is capable of generating a long continuous vibration of the 'buzz' type, and slow deformation effect at low frequencies. The flexible, thin and light form factor of the EMP actuator enable its applications in flexible structures such as the strap of a wearable device. However, it is challenging to house the EMP actuators in a mechanical structure without impeding its freedom to move, and the need for high operating voltages and boost circuits is another barrier.



Fig. 2.18 Electroactive polymer actuator (Novasentis).

Microfluidics and Pneumatic - Tactus Technology, HaptX. Microfluidics technology takes advantage of the ability of a small volume of fluid (microfluid) to expand or contract in response to an electrical signal. This allows a transparent membrane placed on a display to rise or flatten again. Therefore, it can act as a physical button that appears and disappears with proper click feedback. However, it suffers from limited durability, limited stiffness and slow dissipation (unless the fluid is actively removed from the display surface).

The right panel of Fig. 2.19 shows the expansion and contraction of the membrane by a change of medium pressure similar to microfluidics technology. The pneumatic actuator cell developed by HaptX is controlled by regulating air flow and pressure. HaptX has embedded a pneumatic actuator module in a glove and used a 130 pneumatic cell array in the area of the palm. It is expected that the actuator cells expand and contract due to the air so that it delivers a delicate yet soft feel. In addition, localized motion feedback through 130 cells placed on the palm provides a rich tactile experience compared to a global vibration in a glove interface. However, the hardware for controlling 130 pneumatic cells with air pressure is complex and cumbersome, making it difficult to apply such technology in wearable devices.



Fig. 2.19 Haptic actuators and operations using microfluidics (left) and pneumatic (right).

2.3 Haptic User Experience

Based on Law et al.'s study that gathered the views from researchers and practitioners from academia and industry through a survey, user experience (UX) is to be scoped to products, systems, services, and objects that a person interacts with through a user interface [12].

According to Hekkert, user experience is “The entire set of affects that is elicited by the interaction between a user and a product, including the degree to which all our senses are gratified (aesthetic experience), the meanings we attach to the product (experience of meaning), and the feelings and emotions that are elicited (emotional experience) [13].” To design a compelling experience with haptic displays, we need to have a holistic approach to all of the relevant aspects of a user's experience with products, interfaces, systems, and services.

Furthermore, it is not just about making a task easier to perform, but also about the pleasure associated with the use, aesthetic and emotional factors, and meaningful experience. Fig. 2.20 is the User Experience Venn Diagram presented by Dan Saffer and illustrates the overlapping areas associated with user experience design. In the diagram, the field located at the core is interaction design, which overlaps with visual design, sound design, industrial design, human-computer interaction, and human factors. Although there is no mention of haptic design in this diagram, in the product domain for the past decade, active use of haptic technology has been observed in smartwatches, smartphones, virtual reality, and gaming. In learning, medical, and automotive infotainment systems, we can discover concepts and prototypes that utilize haptic technology in interfaces and interactions. While haptics is not a common area of design, haptic technology, and its interfaces and interactions are considered human factors, human-computer interaction, and overlap with visual and sound design in multimodality. Accordingly, we considered haptic as a field of design and added a haptic (user experience) design area as a blue ellipse to Dan Saffer's Venn diagram. In other words, the tactile sense and the systems and interfaces that make use of it are considered to be an element of user experience design.

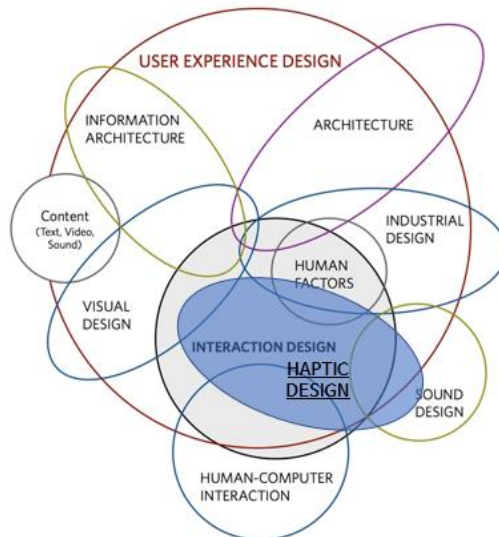


Fig. 2.20 Haptic UX design added to Dan Saffer's UX Venn diagram (blue colored oval).

2.3.1 Emotional Aspects and Interfaces

In recent years, many consumer products that incorporate haptics technology have been developed. Samsung's Haptic phones were introduced in the mid-2000s. Since the mid-2010s, Apple's smartwatch, smartphone, laptop, and other products incorporated haptic technologies into their functionalities. Thus, nowadays haptic technology has been experienced by and become popular with many users. While the earlier products appealed to the user with functionality such as reacting to tactile feedback on the Haptic phone, more recent products take into consideration more holistic factors such as improving the haptic feedback quality, designing the interface using haptic technology, and combining with emotional scenarios. In particular, the quality of vibration feedback has become very important because the smartwatch has direct and constant contact with the skin that is exposed to numerous notifications throughout the day. Users have also become more sophisticated in perceiving and judging the quality of vibration feedback, evidenced by user feedback and product reviews. Despite the small number of users expressing opinions about the quality of haptic feedback, keywords such as "tapping," "pulse," "buzz" and other distinctions have been used to describe the haptics in products. The qualitative aspect of haptic feedback can be seen as touching the emotional part of users who are exposed to frequent feedback. Therefore, it is important to provide feedback that feels pleasant and calm to lower the stress levels and to ensure a pleasant experience with frequent exposure to haptic feedback. Another example of a haptic interface is the overall quality of a simulated key click,

including both quantitative and emotional aspects, such as the quick reactivity of the click feedback, and an appropriate force profile that mimics a physical button. All these aspects contribute to the overall user satisfaction with the simulated clicks. In Jesse Garrett's "The State of User Experience" (Fig. 2.21), he defines human engagement for four factors - perception, action, cognition, and emotion - and expresses in a Venn diagram how the design fields contribute to each other. In designing the haptic interface, we also need to consider the four factors proposed by Garrett. For example, a rotational interface of a smartwatch such as a bezel or crown provides haptic interaction feedback that mimics the mechanical wheel feedback. It may engage four factors: action – rotation for some task, perception – proper angle rotated, cognition – what task accomplished, and emotion – feeling of haptic wheel feedback.

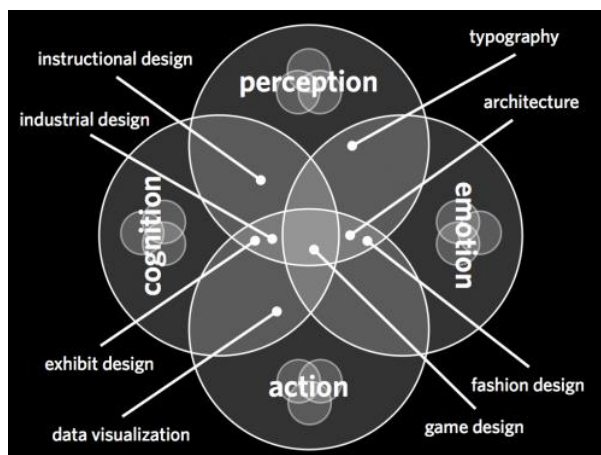


Fig. 2.21 The State of User Experience (by Jesse Garrett, UX Week 2009).

2.3.2 Affect Detection Methods (Measuring Emotion)

A Circumplex Model of Affect. Psychologists would lean against a set of dimensions by a verbal expression of emotion that changes or is evaluated independently of each other to account for emotions. However, the dimensions representing these emotions are systematically related to each other rather than being independent, and the relationship of these verbal expressions of emotion can represent a circular relationship in a two-dimensional space. James A. Russell's study has shown that 28 affect words are placed on a circular coordinate based on the three scaling methods: Ross' (1938) technique developed for variables falling in a circular ordering, multidimensional scaling, and unidimensional scaling of pleasure-displeasure and degree-of-arousal dimensions [14] (see Fig. 2.22). Typical affect words are listed in order of 45 degrees, starting with pleasure (0 degrees), followed by excitement, arousal, distress, displeasure,

depression, sleepiness and relaxation (315 degrees). This model is used by psychologists to evaluate emotions and express cognitive structures through self-reports. In addition, among the 28 affect words that constitute the circumplex model, the pleasure (0 degrees) -displeasure (180 degrees) for the valence axis and the arousal (90 degrees)-the sleepiness (270 degrees) for the arousal axis are used as two independent affect dimensions that are important for evaluating or expressing emotions.

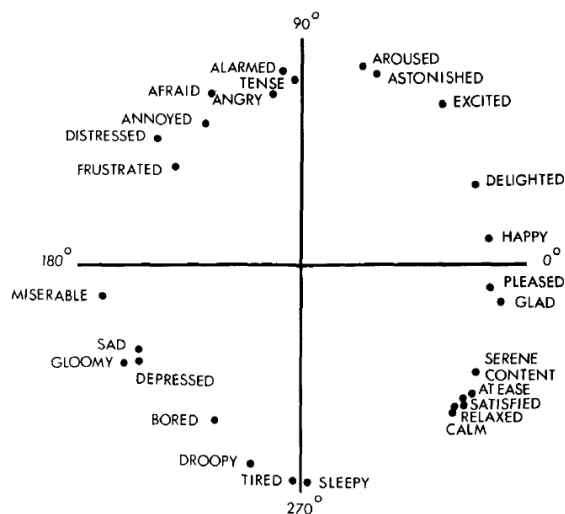


Fig. 2.22 Direct circular scaling coordinates for 28 affect words [14].

Self-Assessment Manikin (SAM). The semantic differential for emotional reactions using multiple adjectives or dimensions based on the adjective pairs in evaluating emotions (e.g., unpleasant-pleasant for valence, calm-excited for arousal) has several disadvantages, such as the ambiguity of the many affect words, and the time and effort involved in evaluating those dimensions. Also, the affect expressed in a specific language may not translate well to a different language. To overcome this problem, Bradley and Lang devised a self-assessment manikin (SAM), a picture-based assessment tool rather than a language-based affect detection method [15] (see Fig. 2.23). SAM represented each range of three major affect dimensions in a step-by-step pictorial manner. The three independent emotional dimensions to describe a state of feeling are valence, arousal, and dominance. Valence represents how pleasant an emotion could be, arousal is how stimulated emotion is, and dominance represents the controlling and dominant nature of emotion, and valence and arousal correspond to the horizontal and vertical axes in two independent emotional dimensions of the aforementioned “circumplex model of affect [14, 16, 17].”

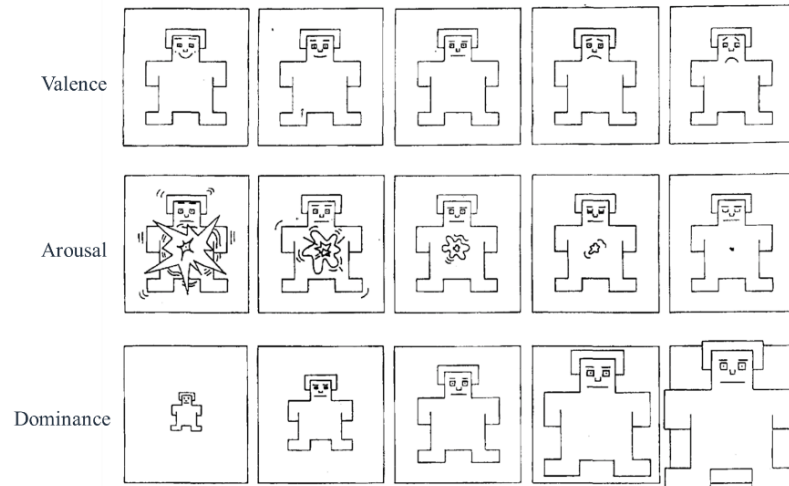


Fig. 2.23 The Self-Assessment Manikin (SAM) used to rate the affective dimensions (valence, arousal, dominance) [15].

Bradley and Lang compared the results and correlations between the two affect assessment methods: The first method is semantic differential scale devised by Mehrabian and Russel for assessing the 3-dimensions of pleasure, arousal, and dominance which resulting from 18 bipolar adjective pairs [16]. The second method is the image-based SAM regarding the affective ratings of 21 pictures from the International Affective Picture System (IAPS, [18]). The results of comparing the correlations between the results of assessing the 3-dimensions (pleasure, arousal, and dominance) from these methods show that dominance is not highly correlated between the two models, but they are highly correlated with valence and arousal. In addition, adjective pairs that are highly correlated with valence are 'Unhappy-Happy' and 'Annoyed-Pleased,' while with arousal are 'Relaxed-Stimulated' and 'Calm-Excited.' In this study, we also evaluated the two affect dimensions of valence and arousal using SAM in order to evaluate the vibrotactile signals we have designed.

Table 2.4 Correlations for SAM ratings and semantic differential factor score with each of the six adjective pairs [15].

	SemDiff	PP SAM	CS SAM
Pleasure			
Unhappy–Happy	.99	.99	.98
Annoyed–Pleased	.98	.99	.99
Unsatisfied–Satisfied	.99	.97	.96
Melancholic–Contented	.98	.97	.96
Despairing–Hopeful	.98	.98	.97
Bored–Relaxed	.82	.68	.68
Arousal			
Relaxed–Stimulated	.97	.92	.91
Calm–Excited	.96	.90	.92
Sluggish–Frenzied	.96	.91	.88
Dull–Jittery	.97	.94	.88
Sleepy–Wideawake	.97	.92	.93
Unaroused–Aroused	.95	.90	.93
Dominance			
Controlled–Controlling	.81	.56	.44
Influenced–Influential	.70	.54	.64
Cared for–In control	.65	–.37	–.53
Awed–Important	.64	.35	.41
Submissive–Dominant	.39	.08	.00
Guided–Autonomous	.12	.32	.39

Comparisons of Affect Detection Methods. Evaluating users' emotions in a modern society where people are exposed to various stimuli is an important consideration in designing a user experience. Recently, researchers have used various methods to assess emotions, and to combined them or developed new methods. These methods can be classified into self-report (for a dimensional framework), autonomic measures (e.g., electrodermal gland and cardiovascular for a dimensional framework), startle response magnitude (e.g., eye blink, EMG), brain states (e.g., EEG, fMRI), and behavior measures (e.g., vocal characteristics, facial expressions). Their advantages and disadvantages are summarized in Table 2.5 below [19]. The affect assessment method to be used in this study considers the intrusiveness and accuracy, the time efficiency over the short study period, and the efficiency compared to the complexity of the apparatus. While sensor-based measurements may be numerically precise, they may also suffer from environmental noise that takes time and experience to detect and remove. Therefore, in this study, we decided to use the self-report affect assessment method for its simplicity, efficiency, high accuracy, and non-intrusiveness.

Table 2.5 Comparisons of affect detection methods [19].

	Intrusiveness	Accuracy	Robustness	Continuity (time resolution)	Cost
Self-report	No	Very good	No	No (pre- post test)	No
Heart rate/ respiration rate	Intrusive	Good	Robust	Yes	Low
EEG/fMRI	Very intrusive	Not good	Not robust	Yes	Very high
Facial expression	No	Very good	Very robust	Yes	Develop- mental cost
Speech recognition	No	Very good	Very robust	Yes	Develop- mental cost
Body posture/ motion	No	Not good	Not robust	Yes	Develop- mental cost

2.3.3 Related Affective Studies

Emotional Responses of Tactile Icons. This thesis research evaluates affective ratings of vibrotactile signals that express metaphors or natural phenomena by combining various signal design parameters. The signals are then delivered through four tactors in contact with the palm. In a previous study, Yoo et al. estimated the emotional responses to vibrotactile signals whose physical parameters were systematically varied [20]. The participants in Yoo et al.'s study held a smartphone with a vibration actuator attached that delivered the signals. The results show the pattern and distribution of emotional responses in response to systematic changes in amplitude, frequency, duration, and envelope that span most of the parameter ranges available for vibrotactile actuators. The parameters used for the tactile icon are shown in Table 2.6 below, and the three experimental sets of parameters reconstruction are shown in Table 2.7. The first experiment showed the emotional response in the valence-arousal space by changing all five frequencies and five amplitudes (top left corner in Fig. 2.24). The second experiment consisted of combining three primary carrier frequencies and all six durations (top and bottom right in Fig. 2.24). The third experiment tested all six envelope frequencies for two carrier frequencies and two amplitudes (bottom left in Fig. 2.24).

Table 2.6 Vibrotactile parameter used in Yoo et al.'s study [20].

Parameter	Values
Amplitude	A1, A2, A3, A4, A5
Carrier Frequency (Hz)	60, 100, 150, 200, 300
Duration (ms)	50, 100, 300, 500, 1000, 2000
Envelope Frequency (Hz)	0*, 1, 2, 4, 8, 16

* Envelope frequency 0 Hz represents no modulation, i.e., $E(t) = A$.

Table 2.7 Stimulus sets tested in Yoo et al.'s study [20].

Set	F_c (Hz)	A	F_e (Hz)	D (ms)	# of Icons
FA	All	All	0	1000	25
D	60, 100, 200	A2, A5	0	All	36
E	100, 200	A2, A5	All	1000	24

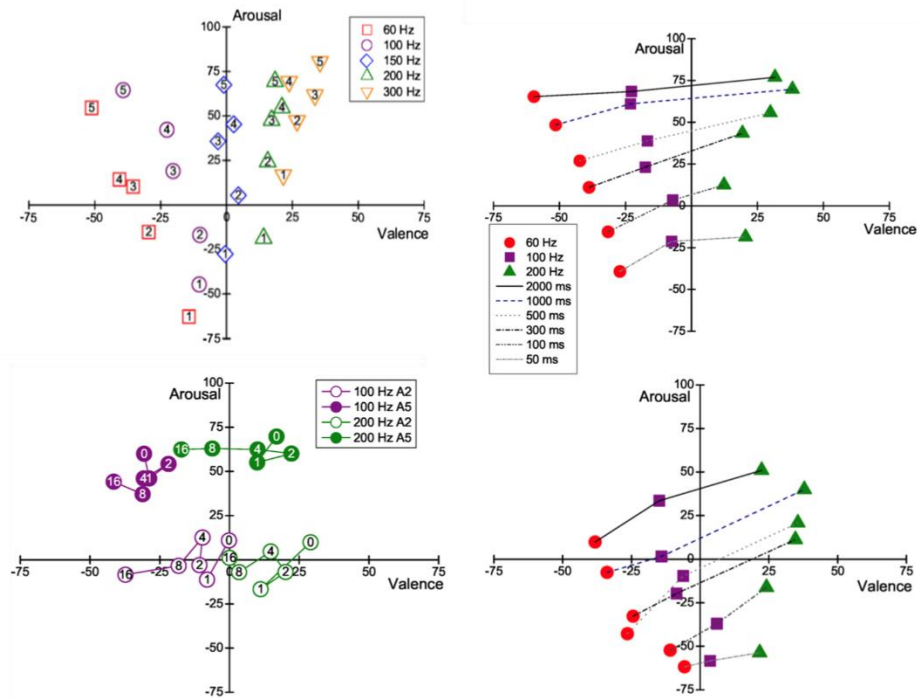


Fig. 2.24 Experimental results of the tactile icon set of Yoo et al.'s study [20].

(FA: upper left, D: top and bottom right, E: bottom left)

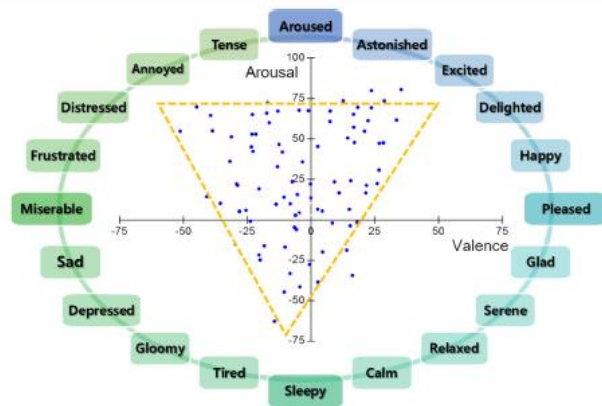


Fig. 2.25 Emotional responses of the tactile icons in the valence-arousal space [20].

As a result, affective ratings of vibrotactile icons with systematically changing design parameters has a distribution that fits into an inverted triangle centered on the valence-arousal space. The emotional labels on the circular plot (Fig. 2.25) were taken from the circumplex model of affect [14]. Comparing the results of previous studies of affective ratings for images (IAPS, 2005 in Fig. 2.26) and sounds (IADS, 1999 in Fig. 2.26) with the Yoo et al.'s study of valence responses of vibration, the range of valence (pleasure) for images and sounds is around 1

- 9, on the other hand, the valence range of vibration is around 3 - 6.5. In other words, the emotion distribution for the vibrotactile signal is relatively narrow and somewhat neutral compared to the emotion evaluation results from image and sound databases. It should be noted that the vibrotactile signals in Yoo et al.'s study were generated by systematically changing the signal parameters and thereby do not carry any contextual meaning with them. This is very different from the images and sounds in IAPS and IADS that have explicit contextual cues. Therefore, care should be taken when comparing the emotional responses to images/sounds and vibrations.

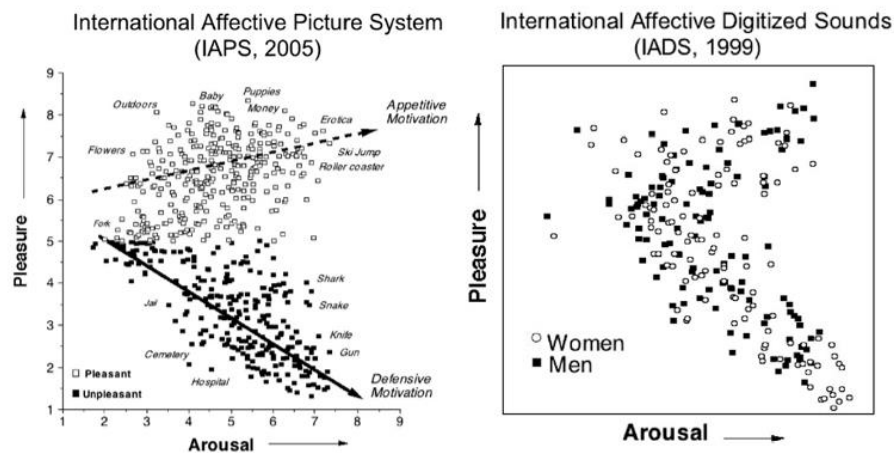


Fig. 2.26 Distribution of the picture and sound stimuli in the 2-dimensional space (pleasure, arousal) [21].

Another observation from Yoo & Choi's study shown in Fig. 2.25 is that the higher the arousal, the wider the range of valence from the affective ratings of vibrotactile icons. In contrast, the range of valence is narrow and neutral in the very low arousal area, which means that it is difficult to express and induce positive or negative emotions with the low-intensity vibrotactile stimuli. This tendency appears to be the same in the affective ratings of images and sounds as shown in Fig. 2.26, although a relatively wider range of positive and negative emotions is expressed at a lower arousal state. In summary, given the limited ranges of emotional response that have been achieved in the past with vibrotactile signals, we have set a challenging goal for this thesis research to design a new vibrotactile system that can achieve a broader range of emotions and expressiveness.

A Vibrotactile Alarm System for Pleasant Awakening. Korres et al.'s study share similar goals with our research in that it is an attempt to design a new vibrotactile display to provide pleasant feelings and experiences for alarms [22]. Six ERM actuators were attached to a wrist band with equal distances (Fig. 2.27). Through the tactile display placed on the wrist, they evaluated three types of vibrotactile stimulation patterns: simultaneous (all actuators vibrate at the same time), continuous (stimulation created from overlapping activation of successive actuators), and successive (actuators activated one after another with no overlap) stimulation (Fig. 2.28). Based on these types, they developed eight different patterns that differed in intensity, velocity, and direction.

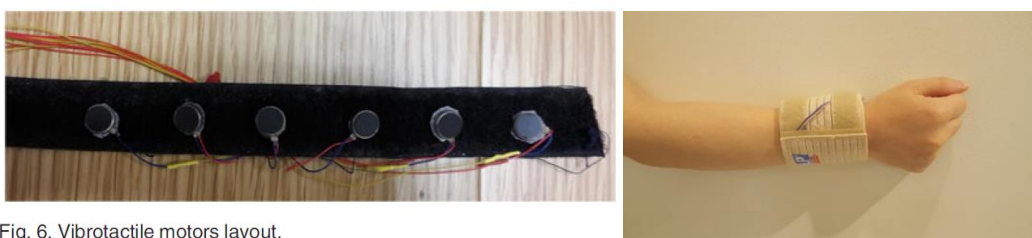


Fig. 6. Vibrotactile motors layout.

Fig. 2.27 Vibrotactile motors layout and the wristband device used in the experiment [22].

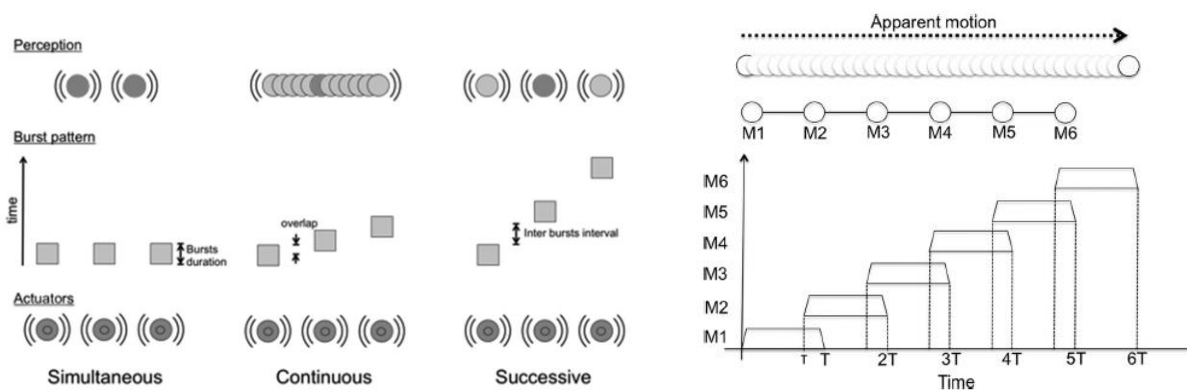


Fig. 2.28 Illustration of the three types of vibrotactile patterns and an example of a continuous type pattern [22].

Note that Korres et al.'s study introduces the user to a particular context (alarm clock) for the emotional evaluation of the vibrotactile patterns. The goal was to design vibrotactile alarm signals that were arousing enough to wake up sleeping individuals but still feel pleasant. The results indicate that among the three stimulation patterns, the continuous type has a relatively high valence score compare to successive (next best) and simultaneous (least pleasant) types. Within the continuous type, pattern No. 5 in which the factors were arranged in a circle on the wrist and sequentially changed their intensity and direction, resulted in the highest valence.

Affect Related Life-Events. Cohen et al.'s research focused on emotion assessment using a database of phrases that contained contexts of everyday life events, in addition to previous studies on affective ratings based on affect words [23]. This is a way to overcome the problem that affect words can be evaluated differently when measuring semantic differential through affect words. Cohen et al.'s study consists of two experiments. The first is to develop a standardized affect-related life event corresponding to 171 positive, negative, and neutral values. The second is to evaluate the relationship between the strengths of affect and significance of the event. Fig. 2.29 shows the result of the valence rating for 258 life events. There is a discarded events area for ensuring that the negative, neutral, and positive events are more clearly defined, resulting in a total of 171 events. The 171 events are divided into three equal groups of 57 each, corresponding to positive, negative, and neutral life events, respectively. Additionally, the BDI (Beck's Depression Inventory [24]) score was measured to assess whether there was a biased relationship between the assessor's level of depression and valence assessment of life events. To be specific, if depressive individuals (high BDI scores) rated positive events as less positive than non-depressive participants, then a negative correlation between the affective ratings and BDI scores could be predicted. However, the results in Cohen et al.'s study showed that there was no significant relationship between the mean valence ratings and the depression levels based on the BDI scores. In this thesis research, we attempt to express natural metaphors explicitly and therefore provide a clear context by assigning explicit labels for the signals designed for each metaphor. This was achieved by the author carefully designing each vibrotactile pattern to match the characteristics of natural events.

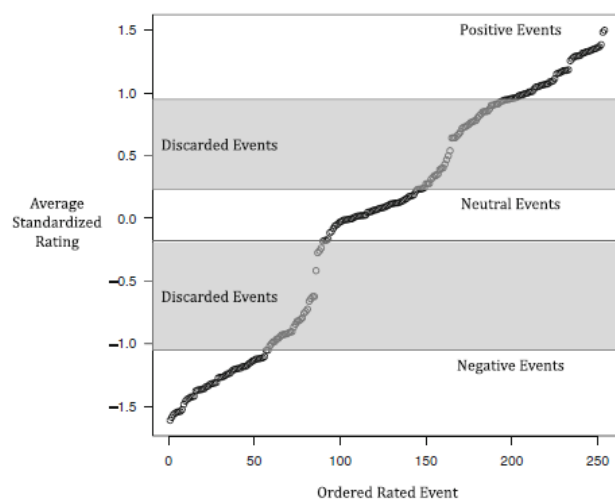


Fig. 2.29 Distribution of valences for 258 affect-related life events [23].

3. PROTOTYPING

This chapter provides an overview of three prototypes developed to explore new configuration and signal design for novel tactile interfaces.

3.1 Introduction

Braille Display – “finding a new tactile transmission method.” It is meaningful to think about more efficient notification delivery methods other than vibrotactile feedback, which shake the entire device. This is because the notification method through the vibration may not recognize the notification depending on the degree of movement or the contact, and there is a somewhat monotonic aspect compared with the rich tactile sensation experienced in daily life or nature. In particular, wearable devices are always in contact with, or close to the skin, it is also possible to imagine various ways to transmit tactile feedback in addition to the method of shaking the terminal. For example, directly stimulate by pushing the local area, indirectly delivering tactile feedback by generating static electricity to make the hair move, making momentary pressure by pneumatic or ultrasonic, and so on. In this thesis research, we also found an efficient braille module while considering the new tactile transmission method applicable to mobile devices and tried to make the tactile feedback and notifications recognizable by the subtle pressure force through the movement of the braille pin. In addition, we consider the enhance the expressiveness and delivering meaningful information through a tactile display using the motion of tactile array as well, and finally, we decided to use recent braille technology and develop braille displays.

The electromagnetic-based small stepper-motor type braille module used in Dot Watch (<https://www.dotincorp.com/>) operates with battery power. Due to the efficiency of the operation, it can be utilized in mobile devices, thereby making it widely available to people with severe visual impairments and technology enthusiasts. Taking advantage of this latest development of a braille module made by Dot Incorporation, two types of mobile tactile displays using the Dot braille module were prototyped. First, we designed a circular array braille-tactile display which delivers time, direction, progress, and other metaphoric information in an active (actively feel the tactile by contacting the fixed braille) or passive (passively feel the tactile from

the motion of moving braille pin or its sequence) braille fashion in a watch form factor with a circular array of braille cells (see Sec. “3.2 Circular Array Braille Display”). Secondly, we devised a stick-type braille display that acts as a mobile medium for easy access to information about devices and objects through a linear array of 16 braille cells in the form factor of a bar or stick. (see Sec. “3.3 Circular Array Braille Display”)

Electroactive Polymer Display – “exploring the deformation.” The haptic technology and actuator, which change shape or generate torque-accompanied movements, make sense in that they try a new sense of touch. In the conventional electromechanical method, a vibration of the mass due to high-frequency rotation or spring motion shakes the medium or the entire device, making it difficult to transmit pleasant feeling. Although vibrotactile actuators such as ERM, LRA, which are used in most mobile and wearable devices, are effective mediators of notifications, there is still a slight lack of sense of touch mechanism to satisfy human factors and qualitative and emotional aspects. As a result, a more natural vibration or tactile delivery method has been contemplated, and attempts have been made from two points of view, namely, improvement of existing electromechanical methods and attempts at new technologies. On the other hand, efforts have been made to apply new technologies to devices such as piezoelectric, solenoid resonate, and an electroactive polymer.

Electroactive polymers produce torque and movement through the deformation of the actuator. There have been attempts to apply it to flat keyboards or wristband for tactile feedback. Deformation effect creates a more natural sensation, although the need for high voltage drive circuit presents a barrier to commercialization, it is still worth exploring in a research setting. The 3-by-3 electroactive polymer actuator array used in this study made by Korea University of Technology and Education and the actuator transmits a gentle tapping feeling through small vertical displacement of each actuator pin. In this subsection, we present the circuit development process for driving the 3-by-3 electroactive polymer actuator array (see Sec. “3.4 Electroactive Polymer Tactile Display”).

Taken together, we hope that the prototypes we introduced through this thesis research using a braille module and an electroactive polymer actuator will be utilized as a research platform for presenting new tactile sensations and as a new way of information transmission.

3.2 Circular Array Braille Display

Dot braille modules consist of a control board and a set of 16 cells each with six braille pins. Each module is connected via FPCB with a 12-pin narrow pitch connector on the control board, and the 16 braille modules can be connected to the control board in a row (Fig. 3.1).

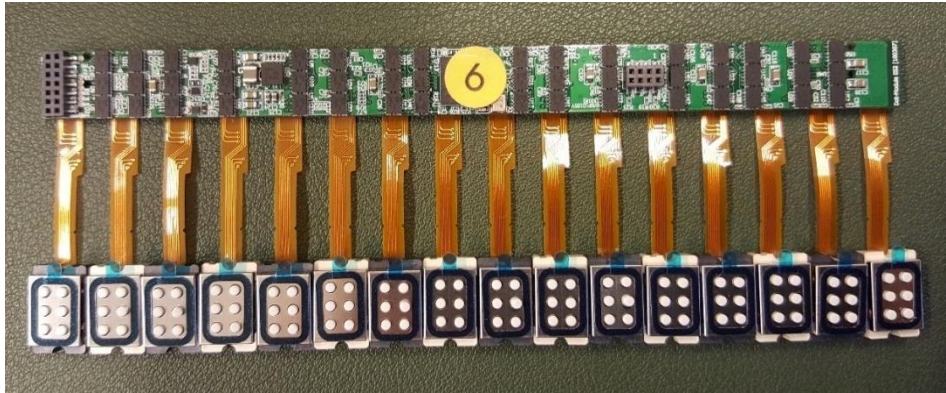


Fig. 3.1 Dot module with 16 braille cells and control board.

Dot braille module can be combined with 3.7V lithium-ion battery to operate stably and efficiently, so it is possible to design a smartwatch form factor with mobility as shown in Fig. 3.4 below. First of all, we thought about the placement of a braille cell to implement a circular braille array in the form of a smartwatch. When we measure the size of one braille cell with six pins, the width was 11 mm, the height is 6 mm, and the height is 3 mm, which is considerably smaller and thinner.

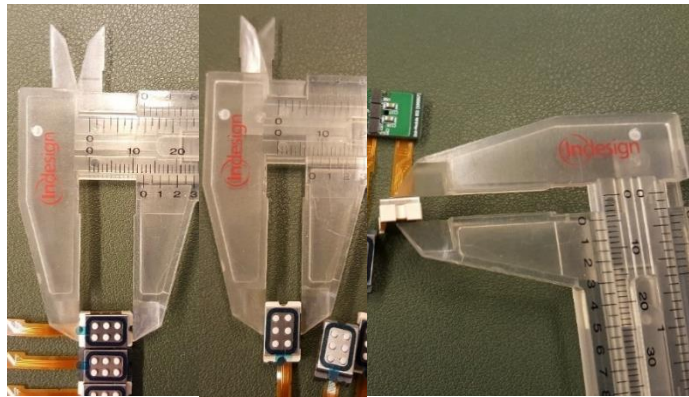


Fig. 3.2 Measuring the dimension of a braille module cell.

3.2.1 Design and Layout

We devised a platform in which braille cells are placed in a circle to deliver tactile information and effects corresponding to the circular arrangement of the prototype in an active or

passive manner (active manner: actively feel tactile by contacting the fixed braille, passive manner: passively feel tactile from the motion of moving braille pin or its sequence). A circular tactile display system aims to enhance the expressiveness of tactile signals suitable for the arrangement such as rotation, direction, physical phenomenon and movement (e.g., ripple effect). Fig. 3.3 shows a generalization of a braille pin arranged in a circular array and each dot represents one braille pin. A braille pin is placed at the center of the circle, and the number of M pins are placed around the smallest inner circle at the same angular distance, and finally, the same number of M braille pins are located on the number of N circles, and those braille pins are arranged with the same angle.

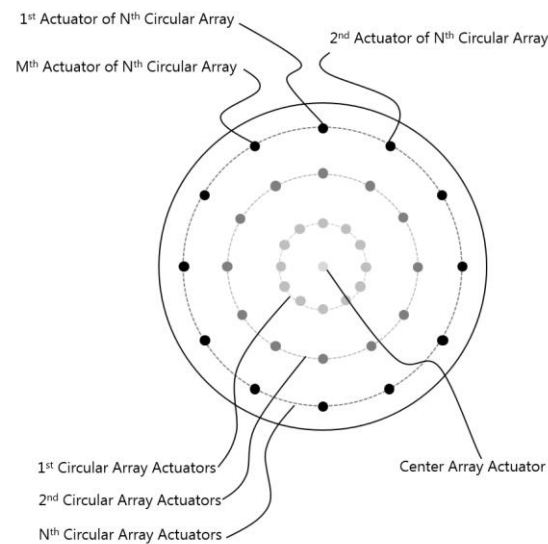


Fig. 3.3 Illustration of the generalized layout of a circular array-type tactile display.

Fig. 3.4 shows the idea of applying the circular tactile display to a smartwatch, with the circular display on the upper side of the smartwatch (left panel in Fig. 3.4) or the lower side (right panel in Fig. 3.4). When the braille display is on top of the watch, the user can actively explore the up-down state of the braille pins, typically forming circular static patterns, with the fingertip. When the braille display is at the bottom of the watch, the up-down patterns of Braille pins can be passively perceived through the skin in contact. In this case, the pins can move up and down to deliver movement and sequential information.

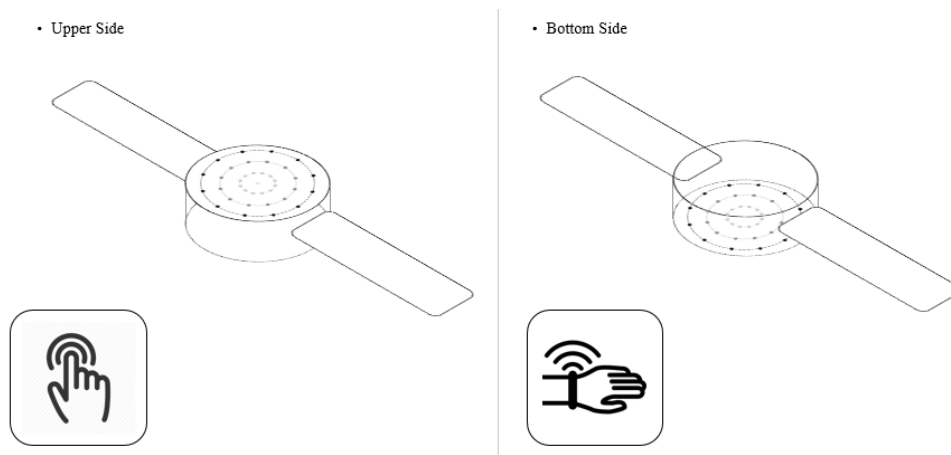


Fig. 3.4 Applying a circular tactile display to a smartwatch form factor.

Based on the measured cell size, we designed the configuration of the module cells to place the braille pin in a circle. The first configuration on the left side of Fig. 3.5 (Configuration I) composed of multiple circles through the arrangement of multiple 6-pin cells without disassembling the existing braille cells. This configuration has the effect of obtaining three circular arrays by arranging eight modules every 45 degrees. Although, the disadvantages include a different number of pins in each circle, and minor misalignment along a circle, the advantage is that 6-pin braille cells can be used as it is. Also, when we place the module at 45-degree intervals, the prototype width is expected to be about 40 - 45 mm, which is about the size of a typical man's watch. Configuration II on the right side of Fig. 3.5 shows an alternative way of arranging braille arrays to form multiple circles, with each 6-pin cell cut into two 3-pin cells. Three layout schemes are proposed for Configuration II, which aim to reduce the overall size of the layout, thus reducing the size of the prototype. We decided to implement Configuration I since it does not require dismantling the 6-pin Braille cells.

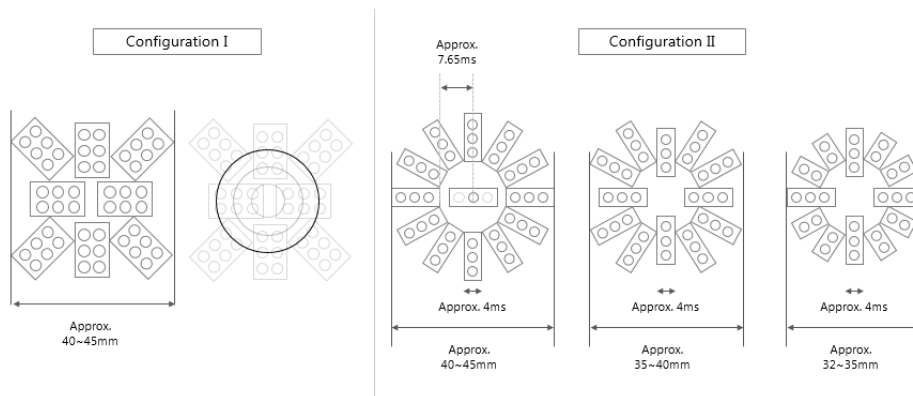


Fig. 3.5 Configurations of braille module cells for circular array tactile display.

One issue that needs to be resolved is the connection of Braille modules to the control board. To apply a circular tactile display to a smartwatch form factor, we designed a circular type PCB (PCB 1 in Fig. 3.6). This circuit board is equipped with a module to be placed in a circular shape, connected to the narrow pitch connector of the module's FPCB and the braille control board through an extension cable. The top panel of Fig. 3.6 is an illustration of the cover, front and back of the board. On the top side, an expansion connector to the control board consisting of 100-pin and 12-pin narrow pitch connectors to the braille module cells are arranged. Additionally, we placed a guide space at the border of the circuit where the FPCB passes through since the front mounted module is connected to the rear connector. The extension connector of the prototype is connected to the Dot braille control board (PCB2 in Fig. 3.6) and requires an adapter board PCB 2 to connect the expansion connector to the control board. The control board is connected to a serial communication port and controls the 16 dot module cells according to custom-defined packets.

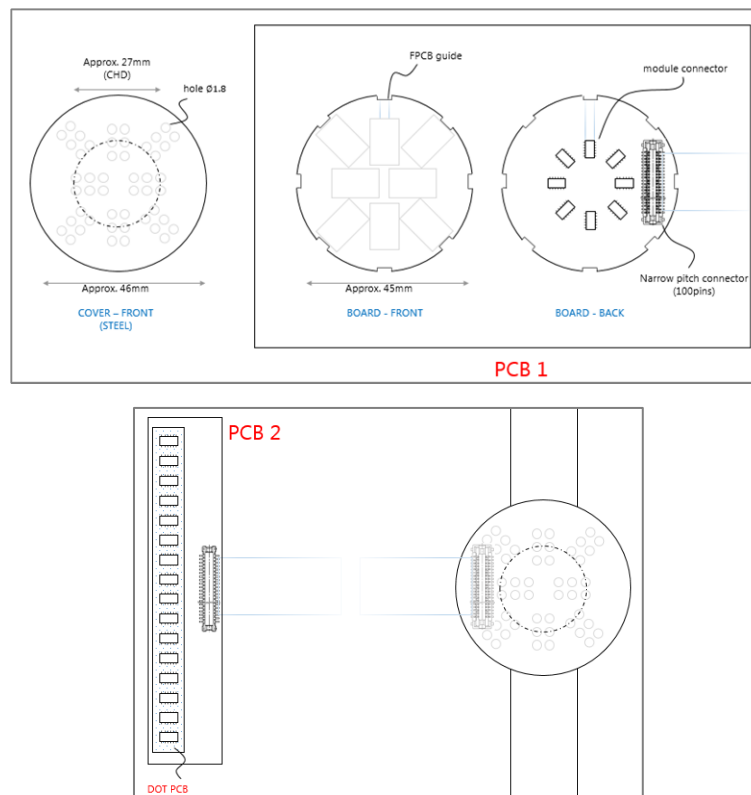


Fig. 3.6 Illustration of the braille circuit board (PCB1 and 2) and wired connection to Dot control board.

For configuring a customized circuit without connecting to an external control board, we need a customized control circuit board, a Bluetooth module for serial communication, a battery,

and a charging circuit as shown in Fig. 3.7. To set up a wireless standalone prototype, the control board needs to be designed into a customized circuit by combining various parts such as DC motor drivers (DRV8835) for each pair of braille pins, step up converter and buffer-line driver.

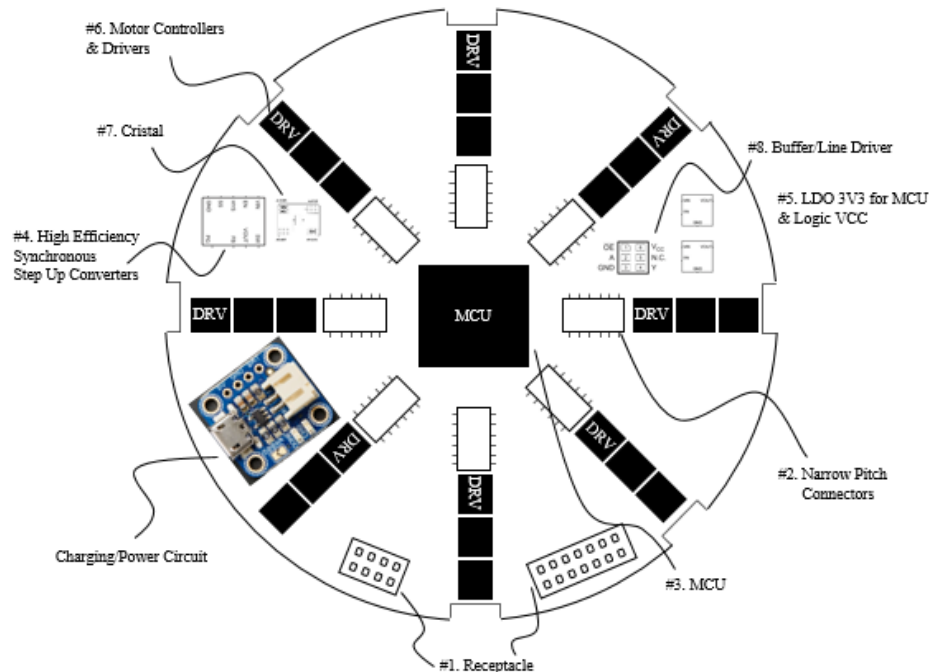


Fig. 3.7 Illustration of the customized control board for wireless standalone circular braille display.

3.2.2 Control Circuit

To implement the desired tactile sequence in the circular array tactile display, it would take too long to control the 16 braille modules in sequence through the control board provided. The dev kit provided by Dot Incorporation controls the sixteen six-pin cells sequentially from the first to the sixteenth cell with one packet unit signal. The up-down state of each Braille pin is then changed from the first pin of the first module cell to the last pin of module sixteenth, with a total time of about 120 ms. For reference, the operation time of the braille module according to the packet signal was videotaped at 60-fps video, and the operation time of the entire pin was checked. Therefore, there may be an error of up to 16.7 ms corresponding to 1 frame of the recorded video clip. Therefore, it can be concluded that sequential control by serial communication on a packet basis makes it difficult to produce desired effects and sequences. For example, to create a ripple effect that moves from the center of a circular tactile array to the outside, the pins need to be activated in an arbitrary order, which is not possible through the

sequential control mechanism. In addition, the 120 ms that it takes to “scan” all the pins are too long for refreshing a new pattern sequence. Therefore, it is necessary to develop a custom control circuit that can raise/lower individual pins in an arbitrary sequence.

To implement a circular braille display, eight of the sixteen module cells and the total number of 48 braille pins need to be controlled independently. To achieve this, we used an Arduino Mega that supports 52 I/O channels and measured the latency that occurs when controlling all I/O channels simultaneously. The latency is measured by connecting two LEDs to the lowest number (#2) and the highest number (#53) of I/O channels and switch each pin to on-state sequentially from the lowest number to the highest number of I/O. The time difference between the onset of the two LEDs was measured through a 60-fps video recording. The Arduino code is shown on the left of Fig. 3.8. The right side of the figure shows the connection of the two LEDs at the lowest and highest I/O channels. The measured latency was about 16.7 ms or less occurs considering that the two LEDs were turned on within one frame of the 60-fps video clip. The result confirms that the channel output latency is acceptable for implementing 48-pin motion sequences using the Arduino.

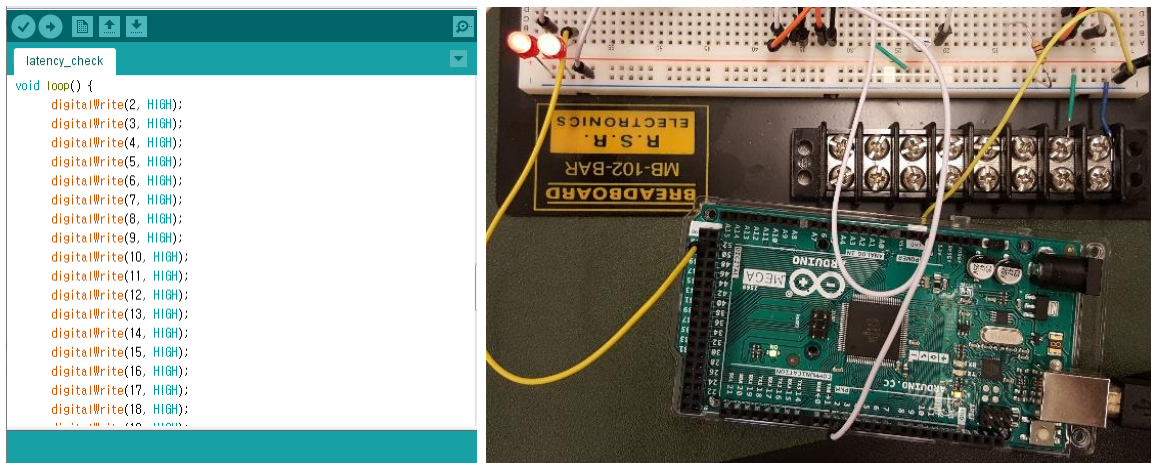


Fig. 3.8 Testing the I/O latency of Arduino.

A DC stepper motor moves each braille pin, and a driver IC (DRV8835) is required to operate it. A DRV8835 motor driver breakout board can be used as shown in Fig. 3.9, and two pins (motors) can be driven by one driver chip or breakout board.

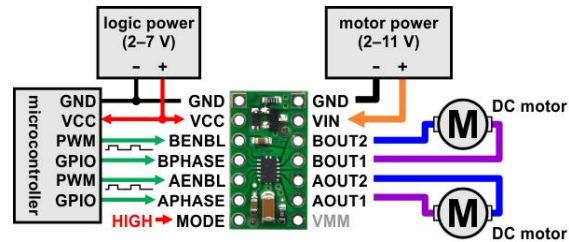


Fig. 3.9 DRV8835 Dual Motor Driver Breakout board and wiring diagram for connecting two DC motors in phase-enable mode.

(<https://www.pololu.com/product/2135>)

The schematic in Fig. 3.10 represent the connections of Arduino, DRV8835, and Braille module connections and I/O assignments to drive two braille pins. To connect the braille module cell to the breakout board, we use a connector header of 0.4-mm pitch connected to the FPCB of the module. Therefore, a breakout board with a narrow pitch connector (left panel in Fig. 3.11) is required for connection to each pin of the module, and a pitch connector receptacle is mounted. The right panel in Fig. 3.11 shows the Arduino, driver board, and braille cell breakout board connected to two braille pins according to the schematic in Fig. 3.10.

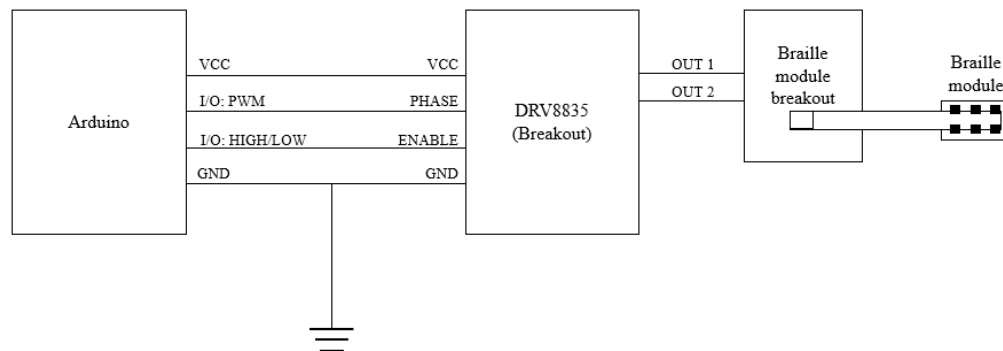


Fig. 3.10 Connection schematic - Arduino, a driver circuit (DRV8835), and a braille motor.

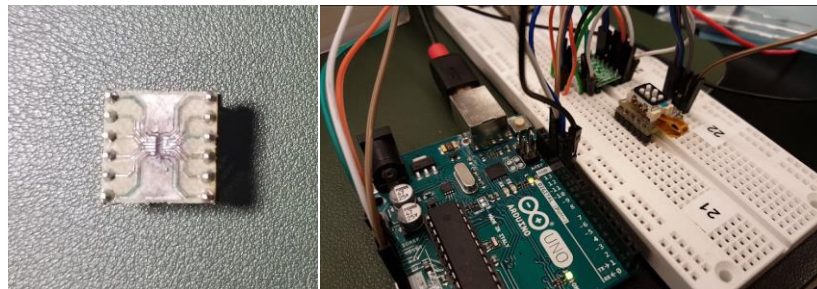


Fig. 3.11 Braille module breakout board and connections based on the schematic in Fig. 3.10.

Fig. 3.12 below is Arduino code that repeats switching up-down state between two pins at 50 ms interval, and PWM frequency used for the PHASE signal is set to 245.10 Hz. For reference, the PWM operates at 980 Hz as a default in Arduino, and it can be adjusted to 30.64 Hz as the minimum depending on the register settings.

```

braille_independent$

void setup() {

  pinMode(PHASE, OUTPUT);
  pinMode(IN1, OUTPUT);
  pinMode(IN2, OUTPUT);
  TCCR2B = TCCR2B & B11111000 | B00000101; // for PWM frequency of 245.10 Hz
}

void loop() {
  analogWrite(PHASE, 128);
  digitalWrite(IN1, HIGH);
  digitalWrite(IN2, LOW);
  delay(50);
  digitalWrite(IN2, HIGH);
  digitalWrite(IN1, LOW);
  delay(50);
}
Done Saving.

```

Fig. 3.12 Arduino code for switching the up-down state of two braille pins.

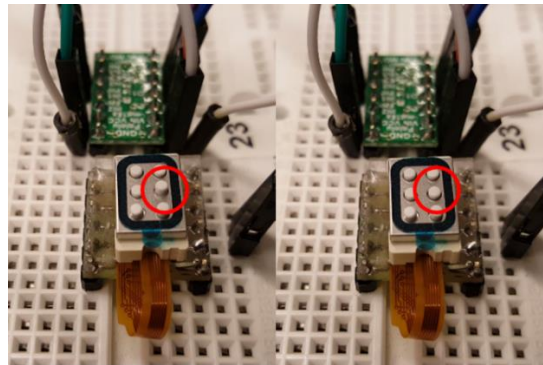


Fig. 3.13 Controlling up-state and down-state of a pin in the braille cell.

After connecting the Arduino and DRV8835 to the braille cell to check whether the two pins are controllable, we designed a custom circuit to control a circular array tactile display consisting of eight module cells and a total of 48 pins. The following diagram is a circuit schematic and PCB layout for individually controlling the 48 pins with 24 driver circuit, and it was designed to be fully connected to the top of the connection terminal of the Arduino Mega.

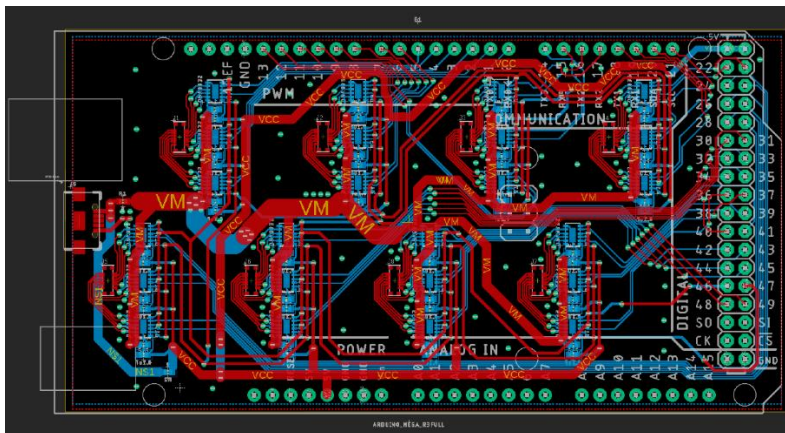
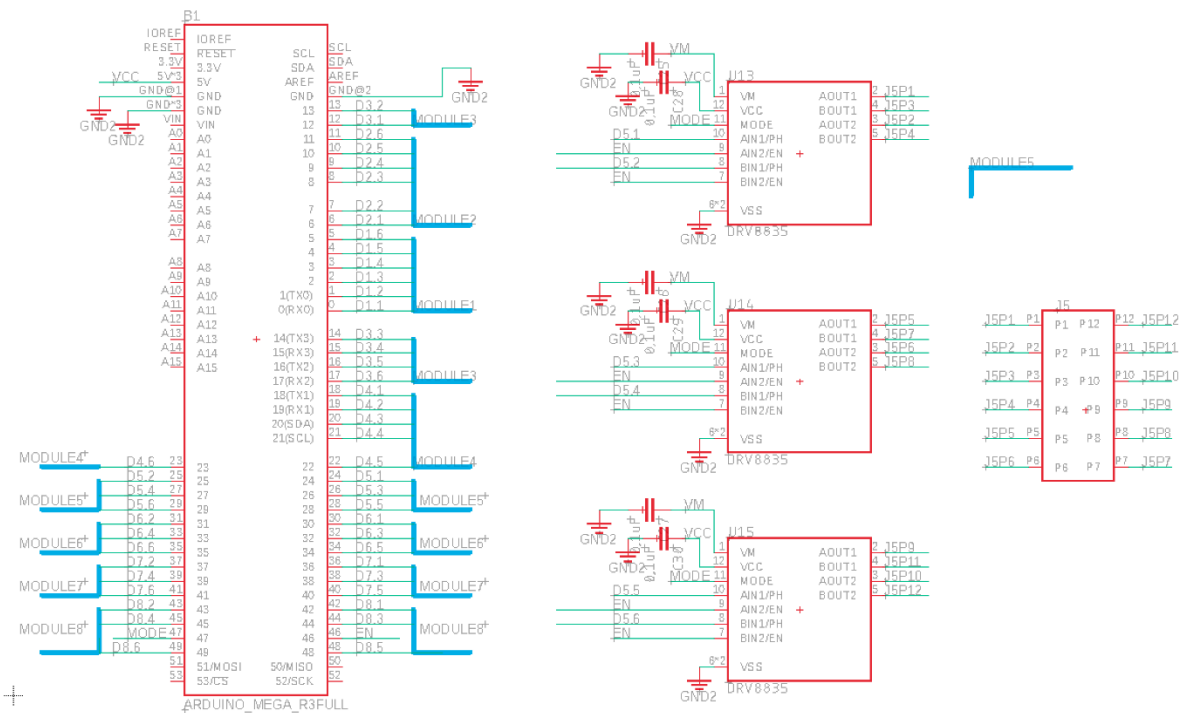


Fig. 3.14 Schematic and PCB layout of the customized control board.

3.2.3 Concepts and Effects

New concepts and tactile effects were developed based on the ideal layout of the circular tactile display shown in Fig. 3.15. This chapter introduces some representative examples of the concepts developed.

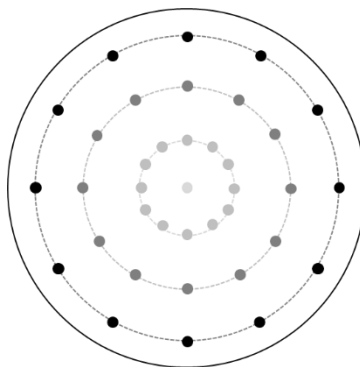


Fig. 3.15 Ideal layout of the circular tactile display (for concept description).

i. clock. One of the most representative displays that transmit information in a circular form is the clock. Typical clocks display hour, minute, and second hands at an angle on a circle. The circular braille display also displays time information with the same concept. Assuming that 12 braille pins are placed in each circle, arranged at intervals of 30 degrees. Then time information can be provided in 1 hour, 5 minutes, and 5 seconds intervals. The upper-left/right, and the bottom-left panel in Fig. 3.16 shows “4h 45m 5s” using a circular braille display. The braille pin is placed in three circles corresponding to the position of the clock hands. The upper-left panel shows time and minutes, and the upper-right panel shows seconds as well. In the lower-left panel, the reference pin is activated at the 12, 3, 6, and 9 o'clock positions on the outermost circle. The bottom-right panel shows “12h 00m” where the clock, minute and second pins are aligned in one line at the 12 o'clock position with the remaining reference pins located at 90-degree positions.

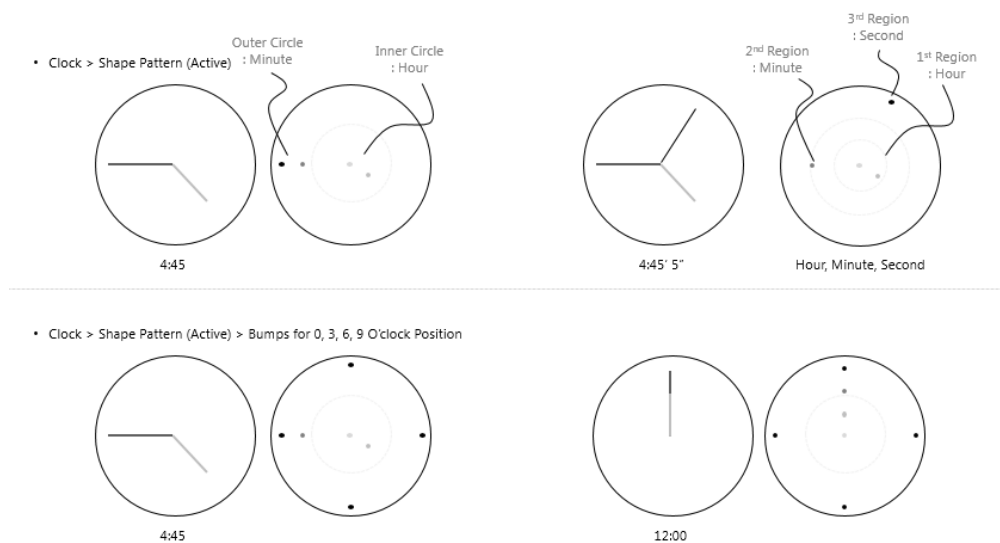


Fig. 3.16 Illustration of 'clock' concept in the circular tactile display.

ii. direction. It can be efficient to express apparent motion varying in a direction through a circular tactile display. Fig. 3.17 shows an example of delivering orientation information through an up-down sequence of braille pins in a circular array. The upper panel in Fig. 3.17 conveys direction through a circular braille sequence of apparent motion in a direction. In the lower panel in Fig. 3.17, the direction information is transmitted using a piece-wise linear braille sequence. In order to transmit a turn-right signal, for example, the two figures on the right in Fig. 3.17 depict sequences that start at the 6 o'clock position and is folded 90 degrees at the center of the display towards the right, the desired turn direction.

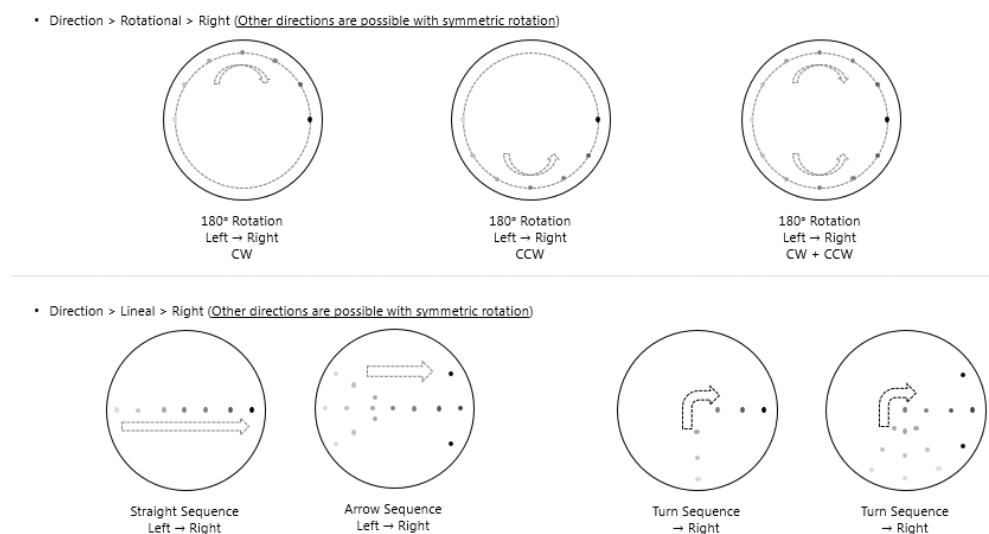


Fig. 3.17 Illustration of ‘direction’ concept in the circular tactile display (the temporal sequence is depicted as the transparency in each black dot: lower transparency stands for an earlier sequence).

iii. metaphors and effects. Fig. 3.18 shows two effects based on two natural phenomena: wave propagation and radar interface. The wave effect expresses the spreading of a wave by activating the pins from the inner circle in the center to outer circles. It is difficult to express the soft feel of a wave through a braille display, but it renders a tactile effect that seems like ‘tickling’ from the innermost to the outermost circle through the movement of small braille pins. The radar effect maps the movement of the scanning indicator, which moves around 360 degrees on the circle, to the sequence of braille pins. It converts the braille pins that form a specific angle to on-state corresponding to the sector-shaped indicator region and sequentially displays the movement of the scanning indicator while switching braille pins to the on and off states over 360 degrees.

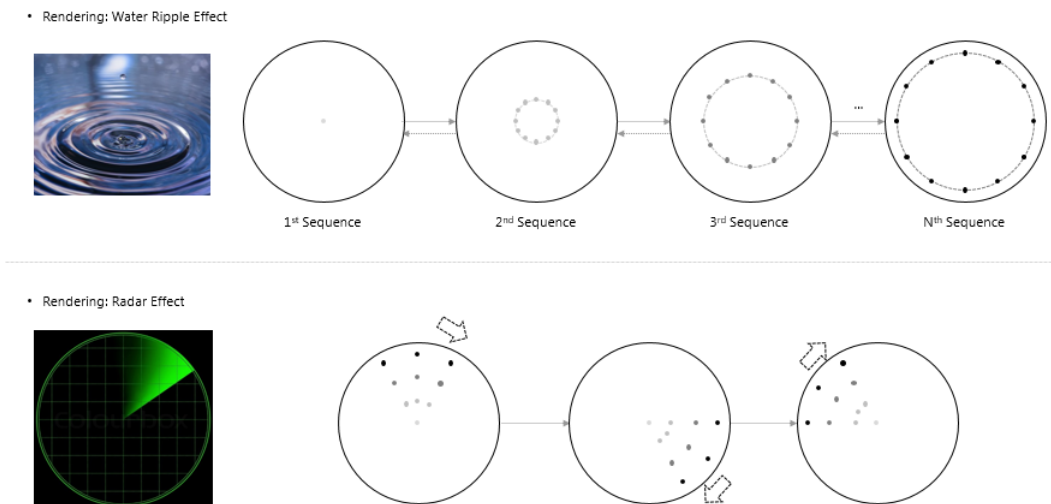


Fig. 3.18 Illustration of ‘metaphor and effects’ concept in the circular tactile display.

3.3 Braille Stick

3.3.1 Design and Layout

In the original configuration of the module board and braille cells, the 16 braille modules cells are driven sequentially according to a serial packet. Accordingly, we devised a stick-type braille display to match the role of the braille display to the original purpose. The Dot braille module has the advantages of low power, below 5 V operating voltage and small size, which is the basis for ensuring mobility. Stick-type form factor can be easily grasped in hand, and it can display more information with all 16 modules at a time. It supports wireless connectivity via Bluetooth. Physical buttons were added to the stick for user interaction such as forward and backward seeking of information. Battery recharging functionality is also added to the prototype. Together, the mobility, connectivity, and informative design are meaningful for the visually impaired people in this internet of things society (Fig. 3.19).

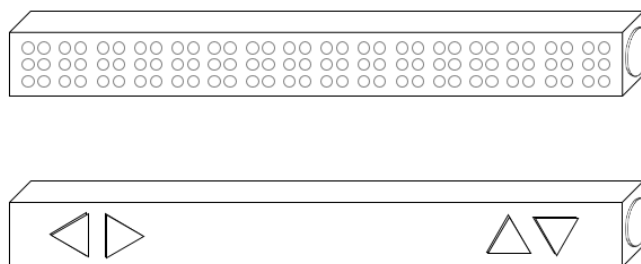


Fig. 3.19 Illustration of braille stick prototype.

3.3.2 Wireless Serial Communication Module

For the mobility and connectivity of the stick-type braille display, we developed a wireless communication module. The control board provided by Dot Incorporation is driven by wired serial communication. It can be controlled wirelessly by connecting a Bluetooth module that supports UART. In addition, an on-off slide switch is placed on the bottom layer of the stick, a lithium-ion battery is mounted on the stick for mobile power supply, and a charging circuit that supports charging through a USB connector is included. The braille module control board and the Bluetooth module are connected for transmitting and receiving information via serial protocols. The battery and the USB power of the charging circuit are used for power supply in common, and the power is supplied or cut off by the on-off switch. Fig. 3.21 shows the setup after mounting and connecting the modules and components mentioned above based on the schematic in Fig. 3.20. The parts including the Bluetooth module are placed on the first layer, the braille control board on the second layer, and the braille module on the third layer. Finally, the three layers are embedded into a rectangular parallelepiped stick.

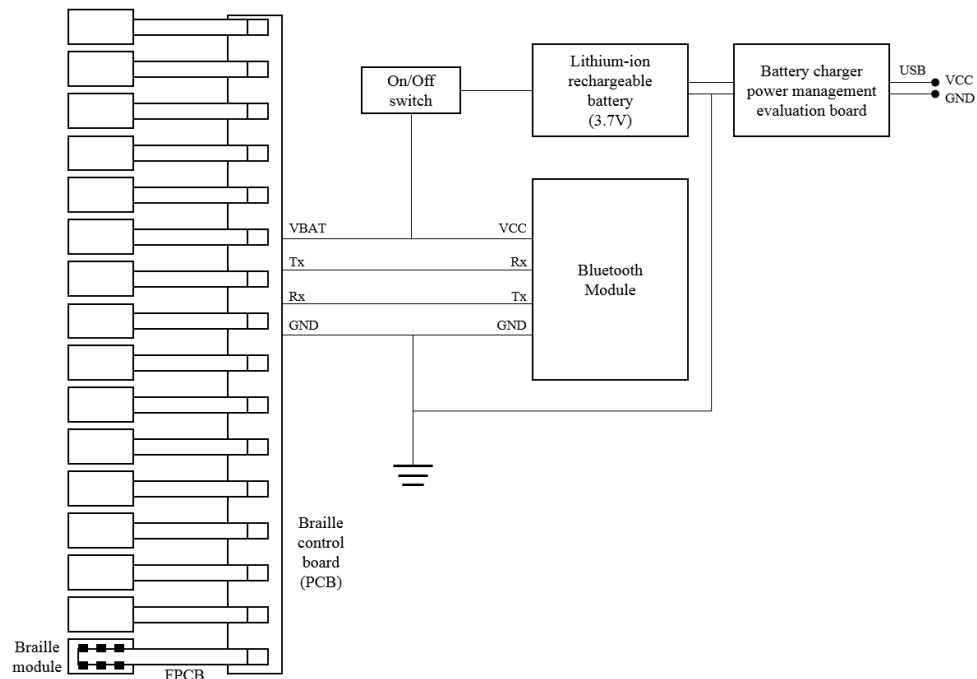


Fig. 3.20 Connection schematic for wireless serial communication module (standalone braille stick).

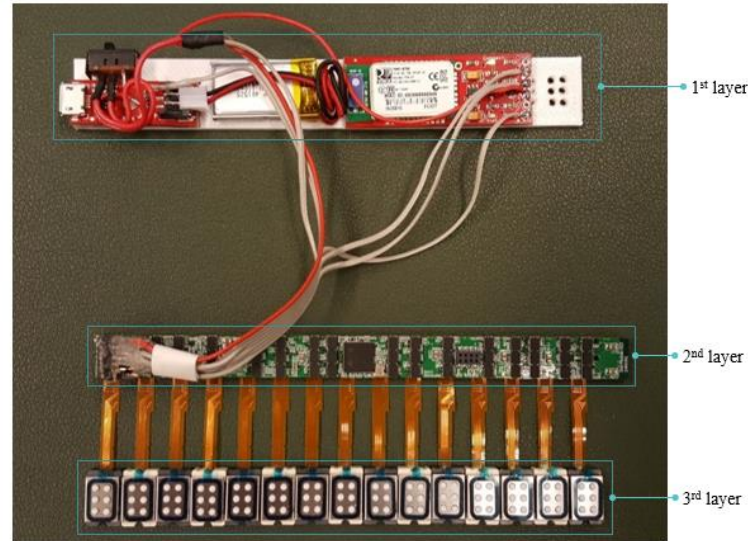


Fig. 3.21 Assembled Bluetooth serial control module.

After all of the hardware was assembled and configured to control the braille module wirelessly, it was tested by sending control signals from a computer to the stick via Bluetooth communication. Fig. 3.22 shows the sequence of hexadecimal codes in a packet that moves all pins to an up-state and all pins to a down-state. It was demonstrated that by transmitting UART signals via Bluetooth, all pins from the 16-braille modules were switched to the up and down states successfully.

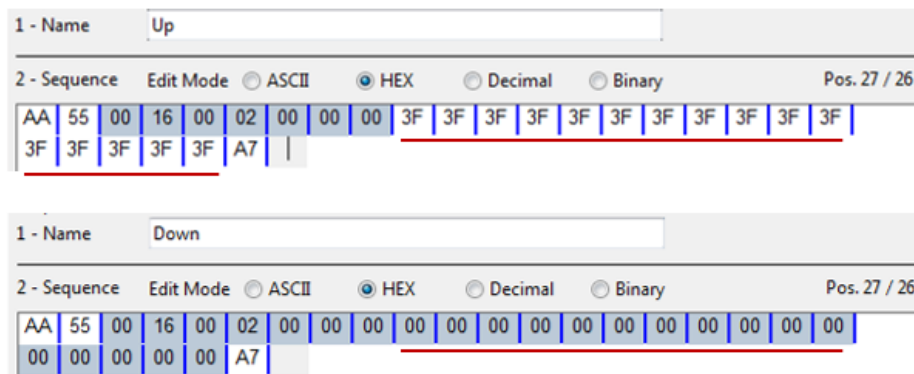


Fig. 3.22 Serial communication packet to control the braille module (underlined 16 hexadecimal values with the red color corresponding to the pin state of 16 braille cells).

3.3.3 Module Ceiling Case

Finally, a top plate was needed to enclose the stick prototype and allow a fingertip to feel the up-down states of all the pins, and it turned out to be a challenging exercise. The top plate contains holes through which the Braille pins can move up and down. When the pin is in the

down-state, the end of the pin should be flat with the top plate, the degree of extrusion between the plate and the braille pin in the up-state should be prominent to allow the braille to be recognized sufficiently. Therefore, the thickness of the plate and the diameter of the hole for each braille pin need to be precise. The measured diameter of the braille pin is 1.3 mm, and accordingly, the diameter of holes needs to be slightly larger than 1.3 mm for the pins to move up and down freely. However, if the diameter of a hole is larger than of the braille pin, the tactile may be felt due to the residual space even a braille pin is in the down-state, and this may be a noise tactile that interferes with the braille recognition of up-state pins. It implies that the down-state pin and plate should be as flat and smooth as possible. We initially chose a plate thickness to 0.65 mm that was the measured height at which the braille pin protrudes from a braille cell in the down state, and the initial diameter of a hole was 1.4 mm which is 0.1 mm larger than the diameter of a braille pin.

The top plate was first created on a 3D printer using the drawing shown in Fig. 3.23 with Autodesk Fusion 360 and Fig. 3.24 shows the 3D printed result. Though there was no significant difference in thickness between the drawing and the printed plate, the hole size tended to be irregular in size and smaller than the predetermined diameter of 1.4 mm and this is because of the tolerance (resolution) of the 3D printer. In addition, when we combined with the braille module with a thickness of 0.65 mm, the down-state braille pin was placed concave downward, then we conclude that the thickness needs to be decreased. Additional attempts at 3D printing with a reduced thickness and increased diameter for holes did not yield an acceptable outcome. As a result, it became clear that a more precise method is needed for creating the holes in the top plate. For example, drilling holes on an iron plate would place the holes at more precise locations and also create a smoother texture. Trial and error also led to the specification of 0.35 mm for a top plate cut from an iron plate.



Fig. 3.23 Drawing of the top plate for the ‘braille stick’ for 3D printing.
(length: 121.50 mm, width: 16.60 mm, height: 0.65 mm, hole diameter: 1.4 mm)

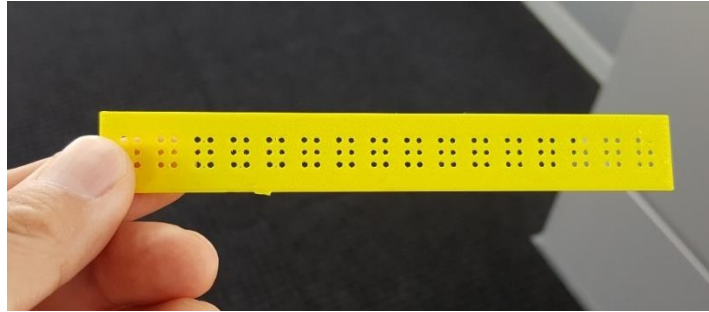


Fig. 3.24 3D printed top plate for ‘braille stick.’

3.4 Electroactive Polymer Tactile Display

3.4.1 Module Structure Analysis

The 3-by-3 tactile display module was supplied by Korea University of Technology and Education (KOREATECH). It utilizes the principle of converting electric energy into mechanical deformation when a high voltage is applied to a polymer elastomer, also called electroactive polymer. VHB 4910 polymer tapes with such properties are widely used, and the polymer tape used in this actuator array plays the role of moving a small plastic cylindrical pin up and down with the stretched tape membrane deformed by electric stimulation [25].



Fig. 3.25 3-by-3 electroactive polymer tactile display.

The electroactive polymer actuator is composed of five layers as shown in Fig. 3.26. The bottom layer is a plate located at the bottom with a ring-shaped conductive terminal. A VHB tape layer with a conductive carbon grease ring allows it to be connected with the conductive material on the bottom plate. In this same configuration, the bottom plate and the middle plate with the VHB tape layers on each plate form electroactive polymer layers which are actuated by high

voltage with a cylindrical plastic pin in between. The last plate at the top protects the upper VHB tape layer and locks the plastic pins between the top and bottom plates.

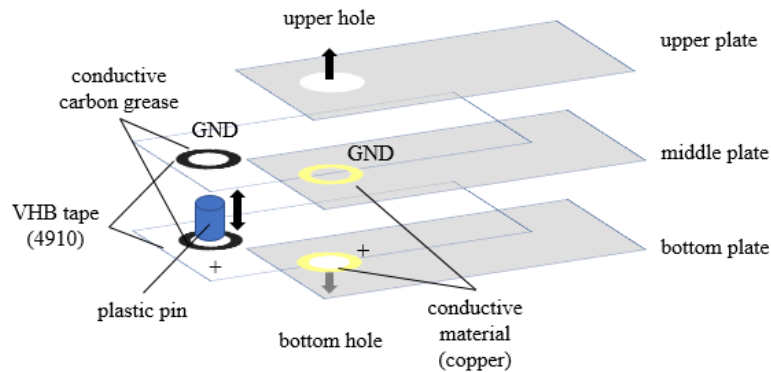


Fig. 3.26 Structure of the electroactive polymer actuator.

3.4.2 Control Circuit

The circuit configuration for controlling the electroactive polymer actuators driven at high voltages is as follows. (Provided by KoreaTech University). The circuit consisting of two transistors as shown in the circuit schematic of Fig. 3.27. The NPN transistor (2N2222A or 2N2222) is located on the left side, and it works as a switching circuit corresponding to an input signal such as PWM or digital signals. The second MOSFET transistor on the right (IXBH12N300 or IXBH12N250) amplifies the low voltage of the input signal to a high voltage above 1 kV. The power required for signal amplification is supplied by a DC-DC converter (EMCO E50) capable of supplying voltages up to 5 kV.

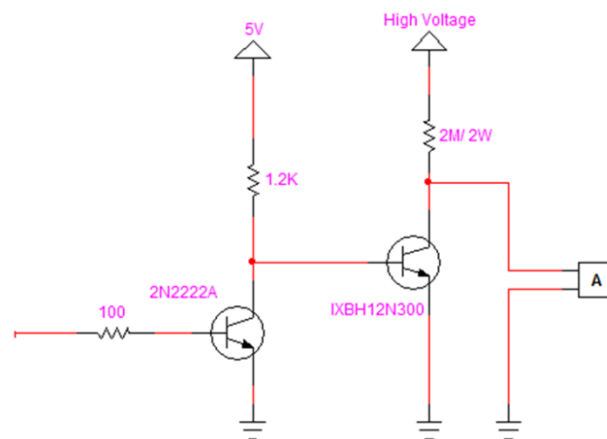


Fig. 3.27 High voltage control circuit of electroactive polymer actuator (from KOREATECH).

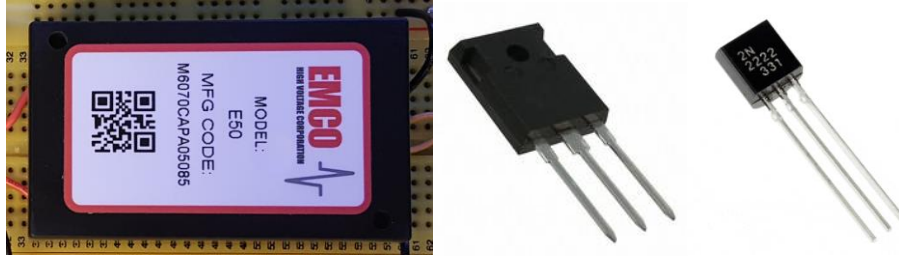


Fig. 3.28 High voltage DC converter (EMCO E50), MOSFET transistor (IXBH2N250-ND), NPN transistor (2N2222) used in the high voltage control circuit.

Oscilloscope and function generator was used to verify that the desired output signal. Since the electroactive polymer membrane (VHB tape) used in this thesis research was stretched and attached to the plate in order to make the electroactive layer thin, therefore, it is prone to damage by continuous input or by a discrete pulse signal which has a rapid cycle. For this reason, the pulse signal with 50% duty cycle and a frequency of less than 100 Hz to ensure the discontinuity of the input signal and increase the period of a pulse signal to reduce on time for actuation. Since the output voltage exceeds the range of the oscilloscope used for measurement, a voltage divider was used to bring the output voltage down to within the range of the oscilloscope. It is possible to calculate the output voltage (V_{out} : actuator input voltage) using Equation 3.1 if the value of input voltage (V_{in} : a measured voltage of oscilloscope) is known, and the input voltage (V_{in}) can be calculated using Equation 3.2 inversely. For example, if we choose the input voltage (V_{in}) as 1 kV, the calculated value of the output voltage (V_{out}) is about 5.65 V (see Equation 3.3).

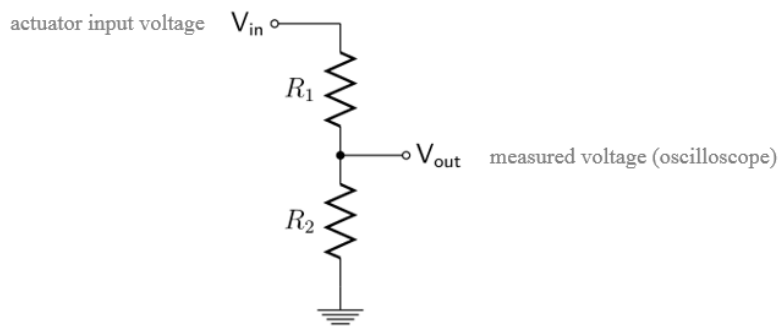


Fig. 3.29 Voltage divider circuit for measuring a high voltage output.

$$V_{out} = \frac{R_2}{R_1 + R_2} \cdot V_{in} \quad (3.1)$$

$$V_{in} = \frac{R_1 + R_2}{R_2} \cdot V_{out} \quad (3.2)$$

$$V_{out} = \frac{10900\Omega}{(1920000 + 10900)\Omega} \cdot 1000V = 5.65V \quad (3.3)$$

$$(R_1 = 1.92M\Omega, R_2 = 10.9K\Omega, V_{in} = 1kV)$$

For testing, a square pulse with a frequency of 10 Hz and a 50% duty cycle was used (left panel of Fig. 3.30). The waveform of the input signal generated by the function generator is as shown in the right panel of Fig. 3.30. The shape of the waveforms confirms that a square pulse input signal (voltage about 5.2 V and frequency about 10 Hz) produced pulses of the same frequency at the output. However, when the circuit is passed through two transistors, the original input signal is slightly changed, and the output pulse is ramping up to a stable voltage state. The measured peak-to-peak voltage of the output signal on the oscilloscope is 2.688 V. Accordingly the calculated input voltage which is the actuator input voltage is 0.48 kV (see Equation 3.4).

$$V_{in} = \frac{(1920000 + 10900)\Omega}{10900\Omega} \cdot 2.688V = 480V \quad (3.4)$$

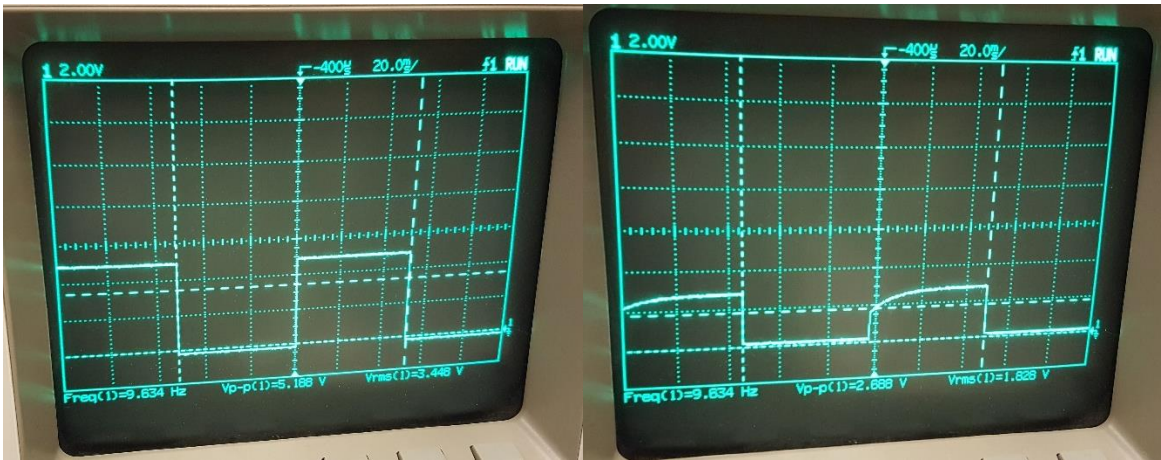


Fig. 3.30 Input and output signals of the control circuit.

Based on the confirmation of the circuit and input-output signals, we tested the operation of connecting one pin of the polymer actuator. The output of the high voltage applied to the actuator rises according to the input of the DC-DC converter, and the actuator operates stably at the DC-DC converter input of about 6.5 - 7 V. When the pulse is applied, the actuator moves instantaneously, causing a slight displacement in the z-direction, and which gives a subtle tapping sensation to a fingertip.

Because the electroactive polymer actuators have thin membranes, operate the actuator pins with a higher voltage or pushing hard with fingers can easily tear the membrane and damage the actuator. Therefore, after confirming the operation of the actuator, we carried out an

endurance test to check whether it can withstand a stable operating voltage for a sufficient amount of time. The 7.0 V signal at 10 Hz with a 50% duty cycle was used as the input to the DC-DC converter, and the output of the high-voltage amplifier was connected to one actuator continuously for 1 hour. The actuator passed the durability test successfully.

The control circuit was miniaturized on a temporary board as shown in the upper-right panel of Fig. 3.31, and its operation was confirmed by connecting it to an actuator. Next, we designed a PCB as shown on the left and middle-right panel of Fig. 3.31, and assembled components such as transistor and resistor as shown in the lower-right panel of Fig. 3.31. By connecting nine channels of Arduino with the 3-by-3 electroactive polymer actuator array and nine control circuit boards, it is possible to operate all nine pins and get the desired pattern sequence through sending PWM signal for each channel. The control circuits receive the input signal from Arduino and deliver the amplified signal at a high voltage to the actuator.

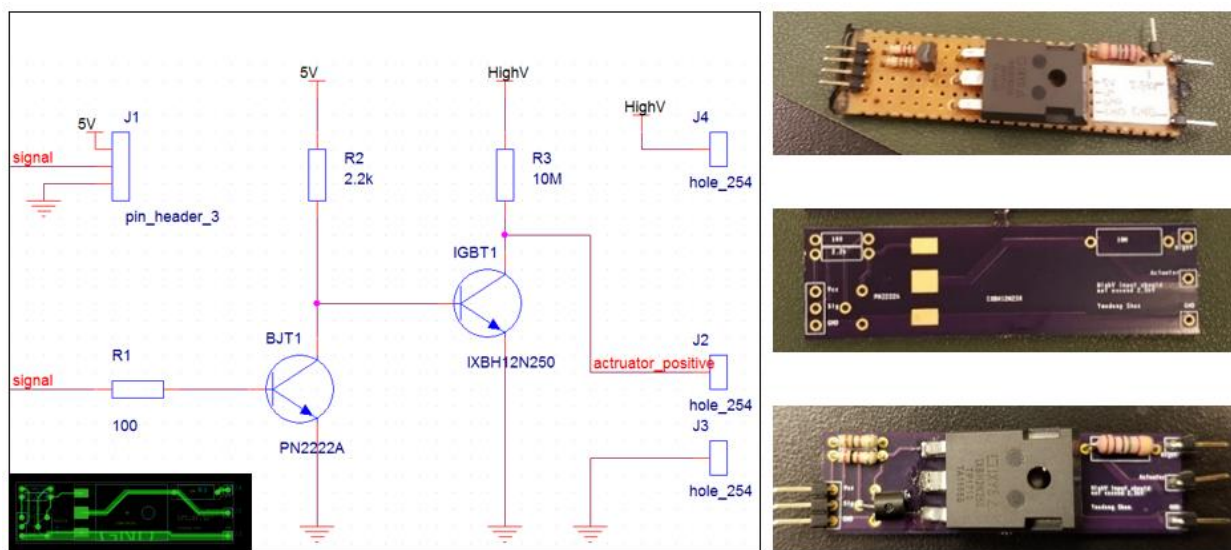


Fig. 3.31 Schematic of PCB for polymer actuator control board (left) and assembled result (right).

3.5 Summary and Discussion

Three types of tactile displays are introduced using a braille module made by Dot Incorporation and a polymer actuator made by Korea University of Technology and Education. It was intended to provide more natural tactile feedback and meaningful information to the user beyond the existing vibrotactile feeling and low information transmission. The braille module used in this thesis is one step beyond the electronic braille technology used in conventional

braille devices. It is useful to use the electromagnetic braille mechanism with tiny size and low operating voltage at a reasonable cost.

Firstly, we tried to create a circular array type braille display that is optimized to provide circular metaphoric information and effects using the Dot braille module. It can be a medium to transmit meaningful information through the tactile sense such as time and direction, and the tactile expression of a relaxing metaphor such as water ripples spreading in a pond. However, the control board provided by Dot Inc drives the 16 module cells sequentially with one packet, leading to a long delay that prevents the creation of arbitrary patterns with the braille array. Therefore, it is necessary to implement a customized control board for actuating pins independently rather than using a serial communication protocol. Even though this is entirely feasible, it nonetheless increases the complexity of the control circuitry significantly as every two braille pins require one driver IC and creating arbitrary movement effects through the braille array requires direct, not serial access, to the braille pins. Another challenge is that whereas it is feasible to recognize the patterns created by the braille array with a fingertip, it is difficult to discern such patterns when they are presented passively on the skin near the wrist. In particular, when the braille pin touches the skin, if the force pushing the pin is too small, the pin may not move up against the skin properly. In addition, the sensations imparted by the braille pins are not always clearly perceivable depending on the body site used, contact force and skin surface curvature. For these reasons, the circular braille array was deemed inappropriate for further exploration in this thesis research.

The braille stick is the second prototype based on the Dot Inc. braille module that makes use of the linear configuration of the 16 modules and the control boards provided by Dot Incorporation. Since it can operate with a 3.7 Vdc lithium-ion battery, it was possible to use a Bluetooth module for wireless communication with a computer. The dimension of the braille stick is about 121.50 (L) × 16.60 (W) × 17.00 (H) mm, which can be comfortably held in hand. It is expected that braille sticks could be an important medium for improving the accessibility of various devices and media if software compatibility with various electronic devices is ensured. However, we decided to discontinue to develop the braille stick further since we encountered some issues in fabricating a top plate that is sufficiently smooth and thin with precisely placed holes for all the braille pins. Thus, although it is meaningful to convey the information of the

brille itself, we found it insufficient to satisfy the direction of this study which is extending the feel and expressiveness through tactile feedback.

Finally, a new prototype using a 3-by-3 array of electroactive polymer actuators is created to explore new sensations that are different from those delivered with mechanical vibrations. We could confirm the operation characteristics of the electroactive polymer by deforming it at a high voltage using a custom-designed high voltage amplifier circuit. Due to the fast response of the polymers to electrical inputs, a realistic-feeling tapping sensation can be delivered to the skin. In addition, the same tapping effect is clearly transmitted even when the cylindrical pin between the polymer layers is pushed. In the end, we abandoned the electrostatic polymer prototype due to the need for very high voltage (about 1 kV), poor durability and the limited range of sensations it can deliver beyond tapping.

4. PALMSCAPE: CALM AND PLEASANT VIBROTACTILE SIGNALS

This chapter presents the main study of this thesis research, including the development of *palmScape* prototype and the design of natural and delightful vibrotactile signals. It is expanded from the following paper draft:

- Sang-Won Shim and Hong Z. Tan, "palmScape: Calm and pleasant vibrotactile signals," in review.

4.1 Introduction

As vibrotactile alert signals become ubiquitous on mobile devices, the question arises as to how to devise alert signals that are rich in meaning, carry natural or intuitive messages and are generally more pleasant than a “buzz.” In the case of smartwatches and phones, it is desirable to provide gentler vibrotactile feedback by designing factors (tactile stimulators) with a lower operating frequency or use wideband factors to optimize the sensation for each usage and context.

Studies on vibrotactile alerts tend to focus on its functional benefits (e.g.,[26, 27]) or its information contents (e.g.,[28, 29]). More recently, many researchers have turned to the study of emotional responses to such signals. For example, vibrotactile stimulation imitating human touch was created and evaluated. While squeeze-like signals were judged to be unpleasant and high in arousal, signals that felt like finger touch were found to be pleasant and relaxing [30]. In general, signals at low intensities tend to lead to neutral valence, and most signals at high intensities feel annoying (low valence). It thus appears difficult to design vibrotactile signals varying in amplitude, frequency, duration, rhythm, envelope, etc., that lead to high valence ratings, especially at low arousal levels (e.g.,[20, 31]). Recently, several studies have investigated stroking-like signals [32, 33], in an attempt to stimulate the C-fibers to evoke pleasant sensations [34] and to create an alarm system for pleasant awakening [22].

Most studies on affective haptics use the circumplex model for subjective ratings of valence and arousal [14]. The higher (or lower) the valence, the more pleasant (or unpleasant) the emotion is. The higher (or lower) the arousal, the more exciting (or calm/relaxing) the signal is perceived to be. While some studies use only positive integers for valence and arousal ratings

(e.g., 1 to 9 [35, 36]), others use a symmetric positive/negative scale (e.g., -4 to 4 [15, 20]). Since affect ratings are relative in nature, ratings along a '1, 9' scale can be converted to a '-4, 4' scale and vice versa. The present study uses the circumplex model for validation of the vibrotactile signals we have designed so that our results can be compared to the findings from published studies.

A common characteristic of tactile alert signals is that they feel like “buzzing” (although Google has made it a priority to remove buzzing from its Pixel 2 and Pixel 3 phones). A major strategy in creating natural and pleasant tactile sensations is to move away from the high-frequency vibrotactile signals typical of the annoying “buzzing” and incorporate lower-frequency signals that can lead to richer sensations such as slow motions, roughness, and flutter. The need for richer haptic displays was well recognized by researchers developing haptic devices for sensory substitution. For example, the artificial mechanical-face built around a plastic skull [37-39], the OMAR system [40], and the multi-finger tactual display [28, 41] were all designed to deliver kinesthetic motions (large-amplitude, low-frequency), tactile (small-amplitude, high-frequency) vibrations, and the sensations associated with the intermediate frequencies and amplitudes, to one or more digits. Along the frequency continuum, signals on the order of a few Hertz are perceived as slow motions, those within 10-70 Hz feel like a flutter (at small amplitude) or rough (at large amplitude), and those above 150 Hz belong to smooth vibrations [42-45]. The dominant frequency of many natural phenomena, such as breathing (12-20 breaths per minute) and heartbeat (60-100 beats per minute), fall into the low-frequency, slow-motion range of 1.67 Hz or lower. Incorporating signals at this very low frequency into our vibrotactile design is an important strategy of the present research.

The present research asks the question of how to *delight* a user with vibrotactile alerts. Our work focuses on vibrotactile stimulation, the most common form of haptic alerts. We use multiple factors in order to expand the spatial contents of the tactile experience. We choose the palm to be the stimulation site due to the relatively large size of the broadband factors used in our research and the ease with which one can simply place the palm on the 2-by-2 factor array (Fig. 4.1). Our goal is to explore the possibility of designing vibrotactile signals that are judged to be in the fourth quadrant of the valence-arousal space – *pleasant and calm*.

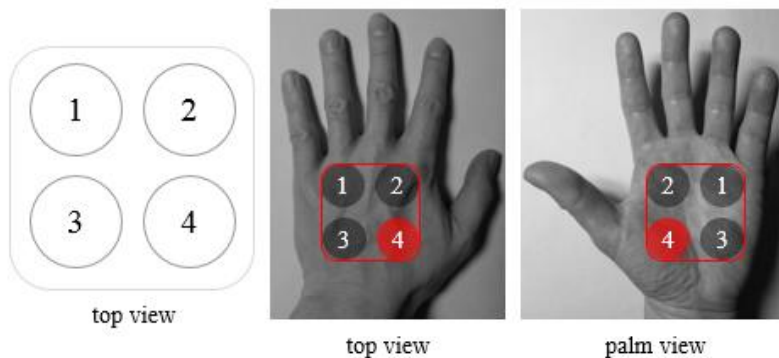


Fig. 4.1 Illustration of *palmScape*.

4.2 A New Tactile Display: *palmScape*

As mentioned above, we have chosen a voice-coil type broadband actuator capable of delivering vibrotactile stimulation over a wide range of frequencies from below 1 Hz to several hundred hertz, to ensure the presentation of low-frequency stimulation or phenomenon resulting in calm and relaxing sensations. Measurements taken with an accelerometer (Kistler 8794A500) indicate that the actuator (Tectonic Elements, Model TEAX13C02-8/RH) is capable of generating a peak-to-peak out-of-plane displacement of 2 mm at 0.8 Hz. The sensation was that of a small creating "breathing" when held in the palm of a hand. To support the design of spatial variations of natural phenomenon (to be explained later in this chapter), we configured four factors in a 2-by-2 array that fits comfortably in a palm. The resulting prototype, called *palmScape*, opens new possibilities for a signal design that will be described in Sec. "4.3 Design Approach" in more details.



Fig. 4.2 *palmScape* (left) and *palmScape-II* (right, wireless prototype).

The first prototype of *palmScape* consists of a 2-by-2 factor array placed on a round plate filled with silicone rubber to isolate the vibrations (left panel of Fig. 4.2). According to the manufacturer’s spec sheet, the tactors have a constant impedance of $8\ \Omega$ in the frequency range of 50 to 2,000 Hz, except for a peak near 600 Hz. Each tactor measures about 30 mm in diameter and 9 mm in thickness. A MATLAB program generated four independent waveforms that were synchronously converted to four analog audio signals by a MOTU 24Ao device. The signals were then amplified and used to drive the four tactors, respectively (see Fig. 4.3). We verified with an accelerometer (Kistler 8794A500) that the tactor responses followed the signal waveforms from about 300 Hz down to < 1 Hz. A second prototype, *palmScape II*, is subsequently built for demo purposes (right panel of Fig. 4.2, by Hatch51 LLC, Lafayette, IN). The demo unit is battery powered and contains eleven demo signals that can be triggered by pressing one of the eleven buttons on the side of the unit, respectively.

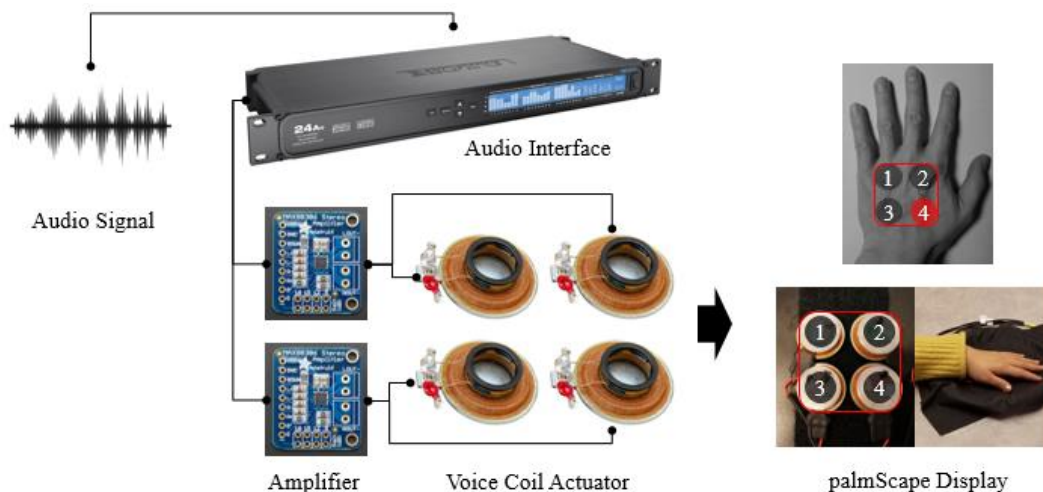


Fig. 4.3 Audio interface and amplifier connected to voice-coil actuators of palmScape display.

4.3 Design Approach

This section outlines the design principles and guidelines that we have followed. Our work draws inspiration from [23, 46, 47] that outline strategies for designing signals that are explicitly paired with linguistic phrases, and/or associated with natural events, in addition to heuristics.

4.3.1 Design Principles

Our signal design follows three principles.

i. Beyond simple vibration. As discussed above, a key strategy of the present research is to introduce low-frequency components into the design of vibrotactile signals to enrich their *expressiveness*. Purely vibrational signals are homogeneous, monotonic, narrow in its expressiveness, and neutral in emotional content. They correspond to a narrow range of sensations we experience in our everyday lives. To overcome the limitations, factors that move at very low frequencies with a sufficient displacement are needed to render soft and gentle kinesthetic motions to express deformations and movements such as breathing and heartbeat.

ii. Be natural and delightful. We are exposed to frequent vibrotactile feedback from smartphones and wearable devices in our daily lives. It is imperative that the vibrotactile feedback on our skin be comfortable, informative and pleasant. To achieve this goal, we take a design approach that is based on natural metaphors to maximize the natural expressiveness of our haptic signals and invite empathy from the users, bringing pleasure and delight to people.

iii. Be simple and distinctive. We want to achieve simple and distinctive signal patterns that are unique, recognizable and easily learned. By distilling the essence of natural phenomena and simplifying our signals to carry the minimum information required of expressing the physical characteristics of natural events, we can maximize the consensus of users' interpretation of our custom-designed vibrotactile icons. The results will be a collection of vibrotactile signals that are easily distinguishable, quickly learned and highly recognizable.

4.3.2 Design Guidelines

Based on these principles, our research has led to the following five design guidelines. The following paragraphs focus on the design considerations for a wide range of natural phenomena. A detailed description of the final sixteen custom-designed signals and their associated metaphors is presented in Sec. 4.6 "Summary and Design Thinking Revisited."

G1. Natural metaphors. We sought to understand the physical characteristics of natural phenomena and designed haptic signals that matched the features. For example, we focused on the *liveliness* of heartbeat, breathing, and pulsation. We applied *randomness* in creating twinkles, bubbles, and raindrops. We incorporated *repeatability* in ripples, cicadas, (horse)

galloping, and frog (croaking). For earthquake and thunder, we used *gradualness* to build up or dissipate energy.

G2. Richness through dimensions. Findings from research on tactile icons [48-50] and tactile speech communication [28, 51] have clearly established the use of multiple signal dimensions to enrich the tactile experience. Fig. 4.4 illustrates the progression from a single-point display to a 2-factor linear display, to a 2-by-2 planar display, and then to our *palmScape* display that incorporates slow motions along the z-axis.

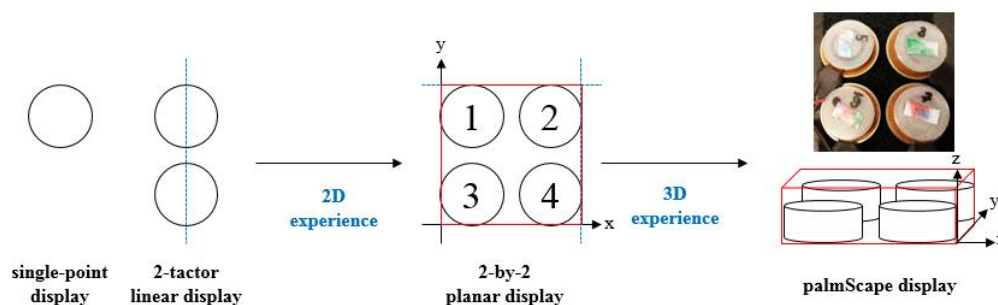


Fig. 4.4 Expanding the spatial richness of a tactile display from a single-point vibration to a truly 3D experience.

In addition to expanding the spatial dimension of a display, we also broadened the use of frequency by (1) lowering the *carrier frequency* (≤ 3 Hz) to create slow kinesthetic motions along the z-axis (e.g., breathing), and (2) lowering the *amplitude-modulation frequency* (≤ 1 Hz) to express a gradual change of intensity (e.g., earthquake). Fig. 4.5 provides some examples.

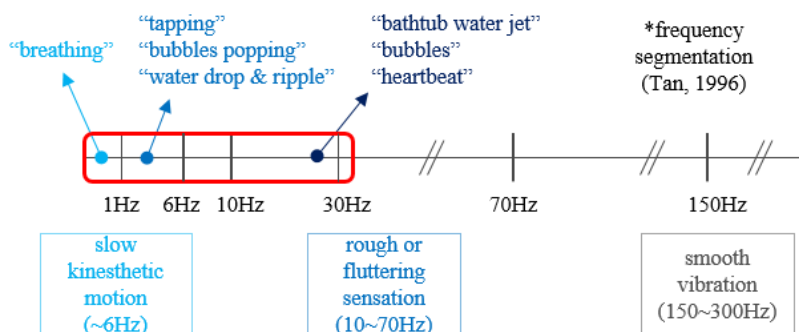
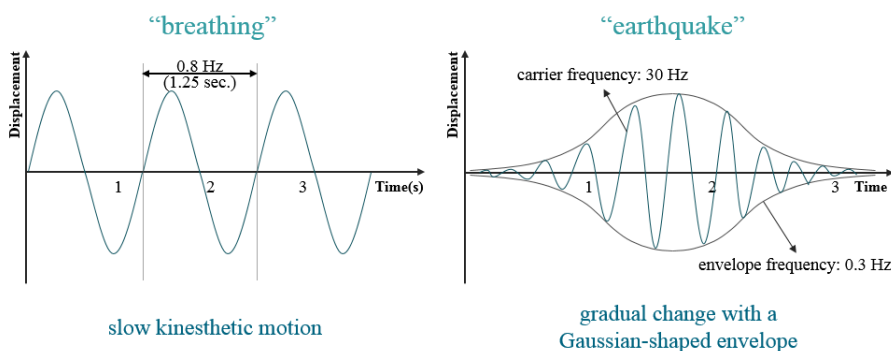


Fig. 4.5 (Top) Illustration of the use of lower frequencies for designing vibrotactile icons in the present research. (Bottom) Waveforms for “breathing” that evokes the sensation of holding a small puppy in the palm (left), and “earthquake” that conveys a gradual build-up and dissipation of rough, rumbling sensation under the skin (right).

Fig. 4.5 continued



G3. Parts and whole. When dealing with a complex physical phenomenon such as heartbeat, we approached the design of vibrotactile icons by first identifying the four main events (e.g., expansion of the left atrium) during one cycle of a heartbeat (Fig. 4.6), found a good representation of each event, and combined them into one composite vibrotactile icon with proper temporal offsets of the four events.

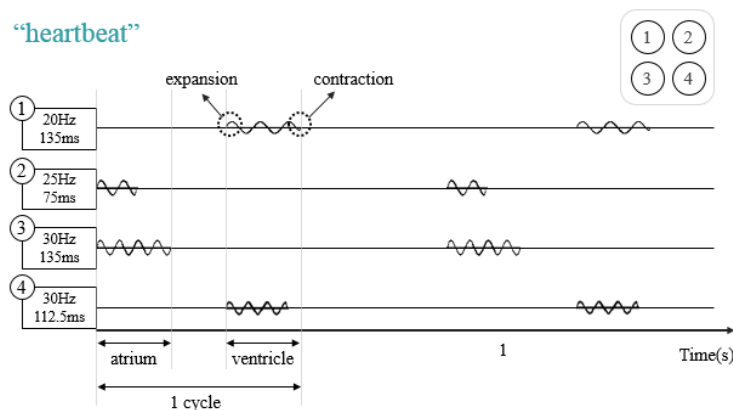


Fig. 4.6 Illustration of the “heartbeat” signal. Shown are the main events making up a heartbeat and the factors used to represent each event. See the upper-right corner for factor numbering.

G4. Simplicity. When it comes to designing distinctive and memorable vibrotactile icons, *less is more*. This is because of factors such as temporal and intensive masking, limited spatial attentional span, poor haptic numerosity judgment, finite temporal-order judgment capability, etc. Therefore, care should be taken to remove signal components that are redundant, can potentially mask other components, or otherwise do not contribute much to the overall perception. Parameters should be judiciously chosen and used sparingly. For example, the “cicadas” signal consists of a high-pitched 120-Hz background noise with a 32-Hz amplitude

modulation for added roughness, and a few bursts of a 60-Hz signal modulated at 2 Hz (Fig. 4.7). The latter cuts in four times and then fades out.

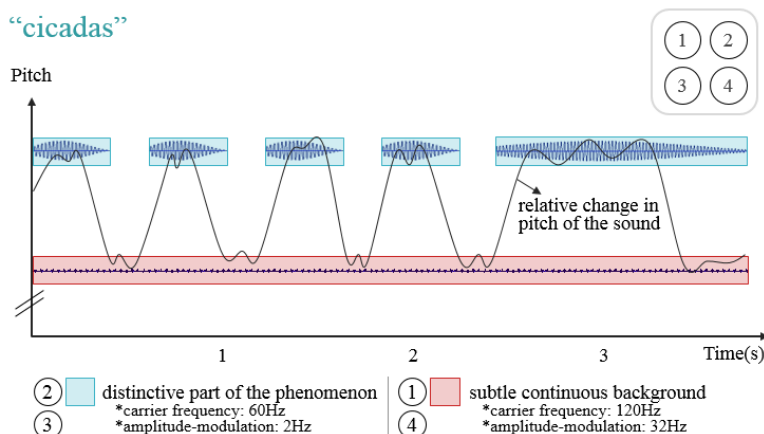


Fig. 4.7 Illustration of the “cicadas” signal.

G5. Randomness. While some natural phenomena such as heartbeat and breathing carry a regular rhythm, others exhibit a less predictable behavior pattern. When designing the vibrotactile icons for the latter, the multiple parameters making up the haptic signal follow a more stochastic process. In the case of “raindrop” (Fig. 4.8), for example, the inter-stimulus interval between two adjacent “raindrops” [47] varied from 70.4 to 316.8 ms, the frequency varied randomly within 80 - 120 Hz, and the stimulation location was randomized among the four factors. Although we kept the signal amplitude constant, the perceived intensity varied due to frequency variations. We found it important to limit the range of frequency variation in order to create a subtle and natural fluctuation in perceived vibrotactile intensity and pitch.

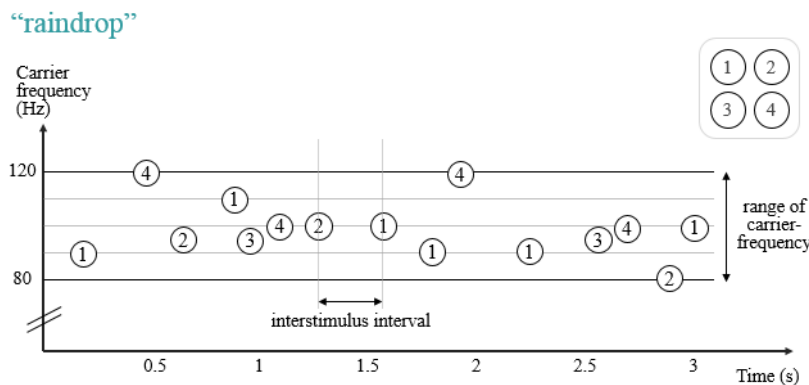


Fig. 4.8 Illustration of the “raindrop” signal.

In addition to the design approaches mentioned above, we also employed other considerations for more natural and diverse expressions. For example, the musical elements of rhythm can promote a sense of familiarity with the user. Starting the design process with a sound analysis is conducive to accessing the expression of the vibrotactile phenomenon in a more straightforward manner. We also focused on barely detectable or low-intensity signals to create subtle sensations (e.g., “twinkle”). In other scenarios such as “thunder,” an intense and short beginning (~10 ms) led to the feeling of a strong impact, and a fast drop (~5 ms) from peak amplitude resulted in a satisfying “knock” sensation.

4.4 Affective Rating Experiment

4.4.1 Participants

Fourteen participants (P01 - P14; 7 males and 7 females; age range 19 - 38 years old, average age 24.4 ± 4.4 years old) took part in the affective rating experiment. All but one (P12) are right handed with no known sensory or motor impairments with their hands. Three of the participants are native English speakers, and the others speak English fluently as a second language. All reported prior haptic experience with devices such as smartphones, game consoles/controllers, smartwatches, electric toothbrushes, and massage devices. By self-report, three participants are extroverts, six are introverts, and five are ambiverts. Each participant signed an IRB-approved informed consent form and was compensated for their time.

4.4.2 Calibration and Equalization of Intensity

Prior to the main experiment, the detection threshold for each participant was estimated, and the perceived intensities of the four tactors were equalized. Individual detection thresholds were measured at 150 Hz with tactor #4 under the left thenar eminence (see Fig. 4.1). The detection thresholds were measured using a three-interval, two-alternative, one-up two-down adaptive forced-choice procedure with trial-by-trial correct-answer feedback, and the perceived intensity of the four tactors was equalized using the method of adjustment [52]. The results were used to ensure that the perceived signal intensities were similar for each participant. The calibration and intensity equalization procedures used in the present study were similar to those reported in [10].

4.4.3 Stimuli

Twenty signals (see Table 4.1) were created to evaluate the design approach outlined in Sec. 4.3. Signals #1-16 were nature-inspired, custom-designed vibrotactile stimulation patterns that felt pleasant, natural and delightful. Four additional signals were included from two earlier studies [20, 22] as “references.” Signal #17 was modified from a type of vibrotactile alarm signal rated as the most pleasant (highest valence) in [22] (in our study, 300-ms, 120-ms overlap, increasing amplitude from 0.25 to 1.25g, co-varying frequency, moving over the four factors). Signals #18-20 were the three signals in [20] that obtained the highest valence ratings at the highest intensity (300-Hz, 1000-ms at 1.4 g), the lowest intensity (60-Hz, 1000-ms at 0.12g) respectively, and a medium intensity (150-Hz, 1000-ms at 0.39g) which is located in a neutral region near the origin inside of the triangular distribution.

Table 4.1 The 20 stimuli used in the present study.

No.	Stimulus Name	No.	Stimulus Name
1	breathing	11	cicadas
2	earthquake	12	bath tub water jet
3	heartbeat	13	frog
4	raindrop	14	(horse) galloping
5	elephant trod	15	knock
6	tapping	16	bubbles popping
7	thunder	17	alarm [22]
8	twinkle	18	notification 1 [20]
9	bubbles	19	notification 2 [20]
10	water drop & ripple	20	notification 3 [20]

The parameters for the sixteen signals designed for the present study vary along many dimensions in ways that depend on the characteristics of the natural phenomena that inspired the vibrotactile icons. The main design parameters for each stimulus are as follows. **Breathing** (#1) is a slow kinesthetic motion at 0.8 Hz. **Earthquake** (#2) is a 30-Hz vibration modulated with a 0.3-Hz Gaussian-shaped envelope to express a gradual change in intensity. They were illustrated in Fig. 4.5. **Heartbeat** (#3) was illustrated in Fig. 4.6, and **raindrop** (#4) in Fig. 4.8. **Elephant trod** (#5) is a 20-Hz carrier frequency vibration delivered to all 4 factors simultaneously to express a deeper pounding effect. **Tapping** (#6) consists of a carrier frequency of 2 Hz with a rapidly-falling envelope. **Thunder** (#7) is a 150-Hz vibration with a high initial amplitude that attenuates gradually following a 0.3-Hz Gaussian-shaped envelope. **Twinkle** (#8) consists of

300-Hz vibrotactile pulses at low intensities at randomized tactor locations. *Bubbles* (#9) is a soft 20-Hz vibration with changing tactor locations. *Water drop & ripple* (#10) starts with a gentle 180-Hz pulse on tactors #1 and 4 for “water drop,” followed by 5-Hz or 10-Hz “ripples” delivered to all four tactors. *Cicadas* (#11) was illustrated in Fig. 4.7. *Bathtub water jet* (#12) is a 10-Hz vibration with a 0.3-Hz amplitude modulation delivered randomly to one of the tactors. *Frog* (#13) uses two superimposed frequencies of 50 and 120 Hz with an amplitude modulation at both 1.7 and 16 Hz. *Horse galloping* (#14) consists of multiple carrier frequencies of 3, 5, 7, 180, and 300 Hz to express rigid tapping on the ground. *Knock* (#15) contains short vibrotactile pulses with superimposed components at 30 and 300 Hz. *Bubbles popping* (#16) uses a 2-Hz vibration with a fast-decaying amplitude to represent slow popping. We reflect on the design process for the sixteen signals and their effectiveness in achieving our design goals after presenting the results of the affective rating experiment (see Sec. 4.6 “Summary and Design Thinking Revisited”).

4.4.4 Procedure

The participants were asked to place their left palm gently on the palmScape display with tactor #4 right under the thenar eminence and the other three tactors covered by the palm (see Fig. 4.9). The participants were asked to maintain a light contact and avoid pressing down too hard on the tactors.

To familiarize the participants with the circumplex model, they felt two signals first: a sawtooth waveform at a high intensity, and 25-ms 30-Hz pulses at a low-intensity. They were told that the two signals were examples near the extremes of the valence and arousal scales. They were then introduced to the graphic icons adopted from [15] and the 9-point integer scale marked under the icons (see Fig. 4.10).

The main task required the participants to rate the valence and arousal of the 20 vibrotactile signals using integers between 1 and 9. Each signal was presented 5 times, and the signal sequence was randomized for each participant. On each trial, the participant saw the text label for the vibrotactile signal presented, felt the corresponding signal, and entered two integers corresponding to the perceived valence and arousal of the signal. The participant completed 4 blocks of 25 trials, with a break between the blocks. The entire experiment lasted around 1.5 hours for each participant.



Fig. 4.9 Experimental setup: (left) noise-reduction headset, the factor array display, elbow support, computer monitor and mouse; (right) the participant in the middle of the affective rating experiment.

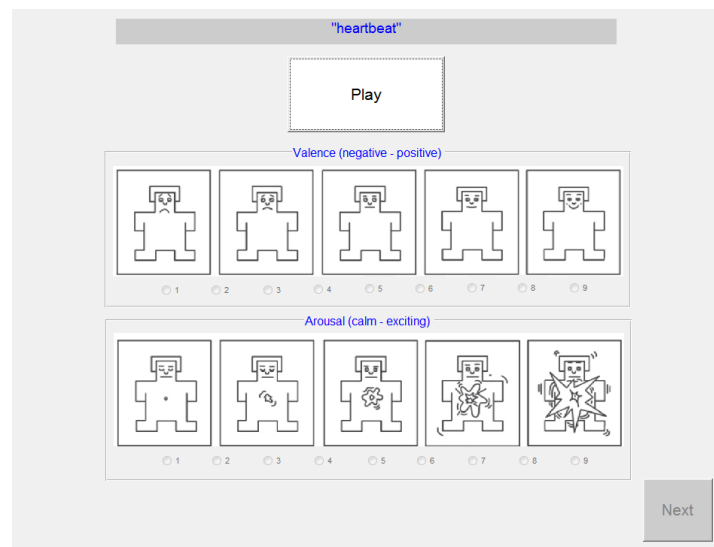


Fig. 4.10 A screenshot of the computer screen for the affective rating experiment.

4.5 Results

The affective ratings for the 20 stimuli are shown in Fig. 4.11 as filled dots (#1-16) and filled squares (#17-20, the references). The position of each filled dot or square corresponds to the (valence, arousal) coordinate averaged over the 70 ratings (14 participants \times 5 ratings per stimulus). The boxed number next to each filled symbol corresponds to the stimulus number listed in Table 4.1. Several patterns can be observed immediately. First, we succeeded in designing vibrotactile patterns that landed in the fourth quadrant, meaning calm and pleasant. Second, the 20 filled symbols cluster around a line with a slope of -1 , indicating a negative correlation of valence and arousal ratings. The “louder” signals tend to be perceived as less pleasant, and the “quieter” signals perceived as more pleasant. Third, given similar arousal

ratings, the four reference signals received the lowest valence ratings. The four colors of the filled symbols encode the four stimulus groups according to the arousal ratings of the four reference signals: purple = low arousal (#19); green = medium arousal (#20); orange = medium-high arousal (#17); and blue = high arousal (#18). Therefore, the 16 stimuli designed in the present study all felt more pleasant than the reference signals.

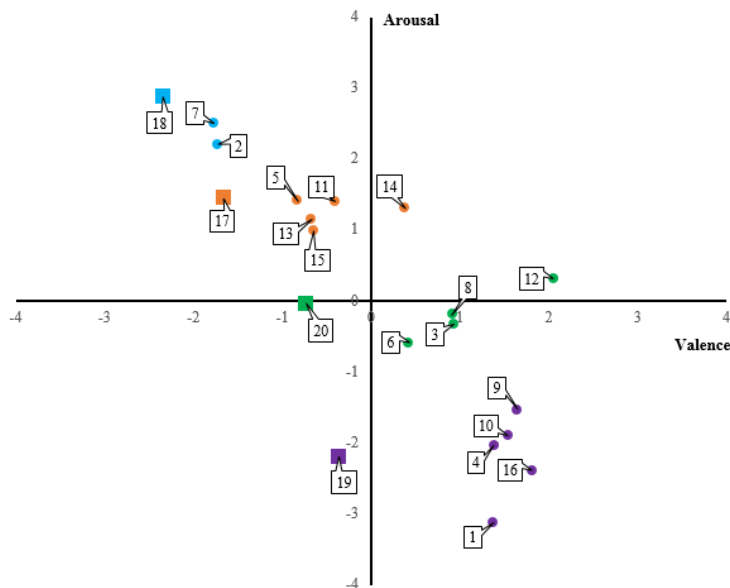


Fig. 4.11 Experimental results. The filled dots and squares show results from the present study. See Table 4.2 for the V-A rating values and standard deviations for each signal.

Across the 14 participants, the standard deviations of valence ratings for the 20 stimuli ranged from 1.14 to 2.35 with a mean of 1.68. The standard deviations of arousal ratings ranged from 1.11 to 1.80 with a mean of 1.40 (see Table 4.2). In addition, inter-personal differences on affective ratings over the 20 vibrotactile signals were compared. There were significant differences in the V-A ratings among the participants as shown in Fig. 4.12. The fourteen participants showed significant differences in the range and the mean values of valence and arousal ratings across the 20 signals. Furthermore, some signals lacked consistent ratings as inferred through the response ranges or their standard deviations listed in Table 4.2. For example, the "breathing" (#1) signal appears to have the largest rating range and the highest standard deviation in valence, and "elephant trod (#5)" has the largest range and standard deviation in arousal. In the valence rating of "breathing" signal, the perceived pleasantness differed among the participants depending on whether the lively, breathing-like slow movements felt like a small puppy in the palm (thereby evoking positive affect) or somewhat creepy. In the

case of arousal, the "elephant trod" signal was supposed to represent the heavy feeling of an elephant's foot hitting the ground. However, it could have been perceived to be gentler and smoother due to the lower frequency. Therefore, individual differences of affective responses to vibrotactile stimuli may exist due to the difference in interpretation over some characteristics of each signal such as the pleasantness of slow motions, and perceived intensity or smoothness. This may make it challenging for the participants to evaluate valence and arousal.

Table 4.2 V-A rating mean values, range and standard deviation for each signal.

No.	Stimulus Name	Over 14 participants								Quad- rant in V-A
		Valence				Arousal				
		Mean Range	Mean StDev.	Sample Mean (N: 70)	Sample StDev. (N: 70)	Mean range	Mean StDev.	Sample Mean (N: 70)	Sample StDev. (N: 70)	
1	breathing	[-2.8, 4]	2.34	1.37	2.35	[-4, 0.2]	1.06	-3.11	1.31	4th
2	earthquake	[-3.6, 2]	1.80	-1.73	1.86	[-1, 3.8]	1.13	2.21	1.27	2nd
3	heartbeat	[-1.2, 4]	1.45	0.93	1.62	[-3.8, 1.4]	1.64	-0.33	1.80	4th
4	raindrop	[-0.8, 3]	1.18	1.39	1.42	[-3.4, 0.4]	1.09	-2.03	1.26	4th
5	elephant trod	[-3.6, 2.2]	1.65	-0.83	1.77	[-1.4, 4]	1.67	1.41	1.77	2nd
6	tapping	[-1.2, 3]	1.02	0.43	1.29	[-2.2, 1]	0.98	-0.59	1.35	4th
7	thunder	[-3.8, 1.4]	1.41	-1.77	1.58	[-0.2, 4]	1.23	2.51	1.38	2nd
8	twinkle	[-2.8, 3]	1.52	0.91	1.74	[-3, 1.8]	1.21	-0.19	1.58	4th
9	bubbles	[-0.4, 3.8]	1.35	1.64	1.55	[-3.2, 0.2]	1.22	-1.53	1.37	4th
10	water drop & ripple	[-1.8, 3.6]	1.74	1.54	1.84	[-4, -0.4]	1.08	-1.90	1.30	4th
11	cicadas	[-3.4, 3.8]	2.04	-0.40	2.21	[-0.6, 3.2]	1.10	1.40	1.46	2nd
12	bath tub water jet	[0.2, 3.2]	1.00	2.06	1.14	[-1, 2.6]	1.07	0.31	1.43	1st
13	frog	[-2.6, 1.2]	1.19	-0.67	1.52	[-0.6, 3.2]	1.14	1.16	1.38	2nd
14	(horse) galloping	[-1.6, 1.8]	1.06	0.39	1.32	[-0.4, 2.8]	0.96	1.31	1.25	1st
15	knock	[-2, 0.6]	0.92	-0.64	1.29	[-1.2, 2.4]	0.99	1.00	1.36	2nd
16	bubbles popping	[-1.6, 3.8]	1.44	1.81	1.55	[-3.4, 0]	1.02	-2.39	1.18	4th
17	alarm	[-3.4, 3]	1.60	-1.66	1.83	[-0.8, 3.2]	1.07	1.46	1.28	2nd
18	notification 1	[-4, 3]	1.77	-2.34	2.03	[1, 4]	1.00	2.89	1.11	2nd
19	notification 2	[-3, 3.4]	1.79	-0.36	1.93	[-4, 1]	1.40	-2.20	1.54	3rd
20	notification 3	[-3.6, 3]	1.64	-0.73	1.80	[-1.8, 2]	1.19	-0.04	1.60	3rd
	Total	[-2.3, 2.1]	1.50	0.07	1.68	[-3.1, 2.9]	1.16	0.07	1.40	-

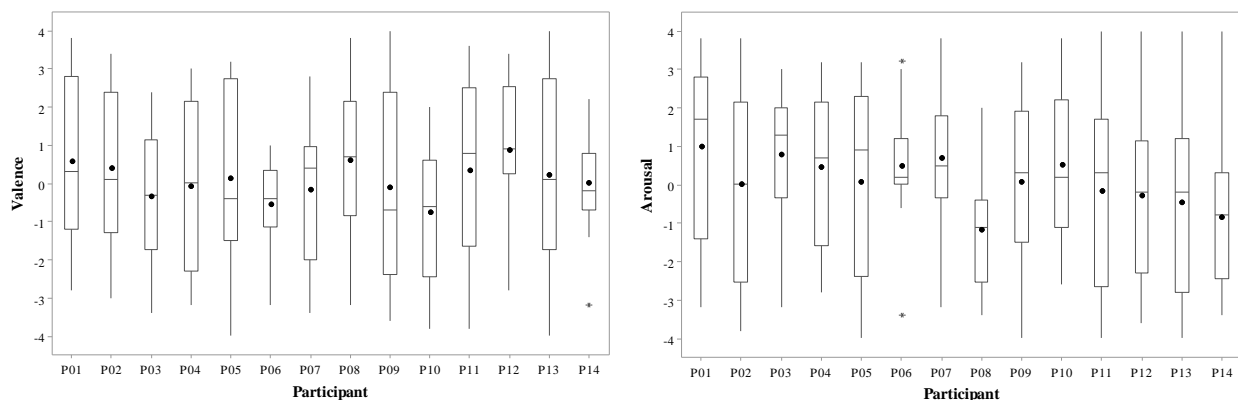


Fig. 4.12 Boxplot of valence (left panel) and arousal (right panel) ratings averaged over the 20 signals for each participant.

A two-way ANOVA with the factors participant and signal was conducted on variance and arousal ratings. The results show that both participant and signal number are significant factors for valence [participant: $F(13,1120) = 25.15$, $p < 0.001$; signal: $F(19,1120) = 151.58$, $p < 0.001$] and arousal [participant: $F(13,1120) = 46.75$, $p < 0.001$; signal: $F(19,1120) = 265.29$, $p < 0.001$] ratings. The interaction between participant and signal is also found to be significant for valence [$F(247,1120) = 13.28$, $p < 0.001$] and arousal [$F(247,1120) = 6.23$, $P < 0.001$].

The valence-arousal rating distribution patterns can be classified into three major types among the 14 participants, as illustrated in Fig. 4.13. The left plot in Fig. 4.13 shows the “general” pattern of data distribution exhibited by 11 of the 14 participants. It looks similar to the pattern shown in Fig. 4.11: the 20 signals cluster around a line with a negative slope in the V-A space. The central plot in Fig. 4.13 shows the “reversed” exhibited by one participant (P01). It shows the 20 signals cluster around a line with a positive slope, indicating that P01 tended to rate valence (pleasantness) higher as arousal (excitedness) increased. The right plot in Fig. 4.13 shows a relatively narrow and “neutral” distribution of valence and arousal for most of the signals. The two participants (P06, P14) tended to respond at the middle of the valence and arousal range except for four signals that are far from the cluster formed by most of the signals.

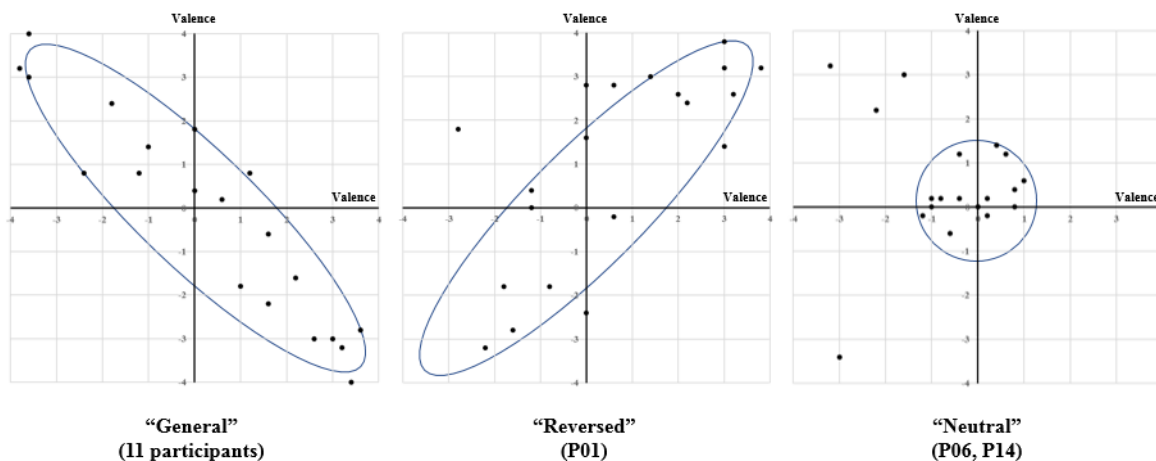


Fig. 4.13 Three types of rating distribution patterns in the V-A space: General, reversed, and neutral.

When all values of valence and arousal ratings for the 20 stimuli and all the participants were averaged (1400 ratings for valence and arousal: 14 participants \times 20 stimuli \times 5 ratings per stimulus), the grand mean values are close to zero (valence: 0.07, arousal: 0.07). This is shown by the red 'x' in Fig. 4.14 next to the origin of the V-A space. When the valence and arousal ratings were averaged across the 20 signals for each participant, the mean values for each participant reside near the origin. The numbers next to the triangles correspond to the 14 participants in Fig. 4.14. This tendency reminds us that affective rating is subjective and relative. It implies that each participant performed the affective ratings relatively within the context of the 20 vibrotactile stimuli.

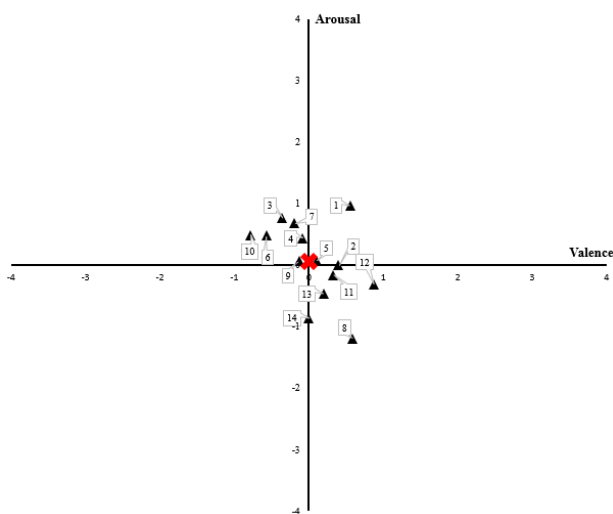


Fig. 4.14 Grand mean for all ratings (red cross) and mean values averaged over the 20 signals for each participant (triangles).

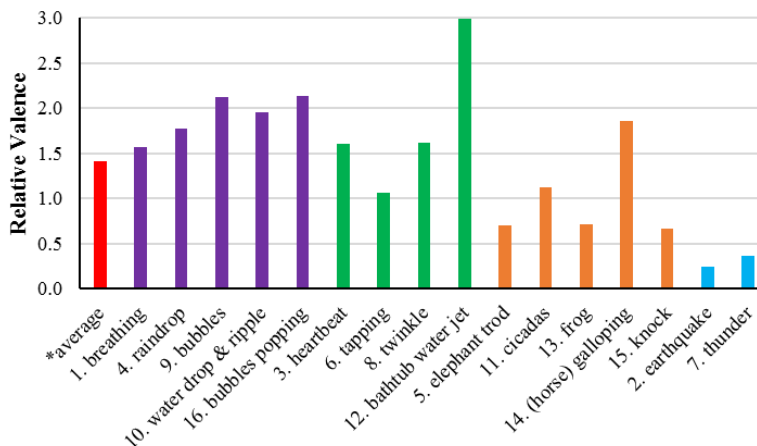


Fig. 4.16 Increase in valence ratings for stimuli #1-16 as compared to the reference stimulus (#17-20) at similar arousal ratings, calculated from the blue line in Fig. 4.15.

In Summary, the signals that are most calm (low arousal) and pleasant (high valence) are the purple filled dots. They consist of signal #1 (breathing), #4 (raindrops), #9 (bubbles), #10 (water drop & ripple) and #16 (bubbles popping). These signals all contain some form of slow motions except for #4, confirming our design approach of using kinesthetic motions to achieve calm and pleasant vibrotactile icons. Among the green-filled dots, #12 (bathtub water jet) has the highest valence rating, followed by #3 (heartbeat) and #8 (twinkle). Again, #3 and #12 contain low-frequency movements. Stimuli #4 (raindrops) and #8 (twinkle) are both light and slightly irregular, another winning combination for a delightful vibrotactile experience.

4.6 Summary and Design Thinking Revisited

The present research set out to broaden the expressive range of vibrotactile icons by creating a more realistic and natural vibrotactile experience. We believe that users of mobile devices can be more receptive to calm and pleasant alerts for an upcoming calendar event or a new social media posting. This can help eliminate “buzzing” from our daily living and reduce the stress and annoyance associated with it. We envision a day when people shop for a mobile phone for its playful and delightful haptic effects, and calm and pleasant haptic alerts become an integral part of our digital life.

The most significant finding of the present study is that we succeeded in creating five vibrotactile stimuli that reside in the fourth quadrant of the valence-arousal space, a region that has hardly been occupied by similar attempts before. These vibrotactile signals often brought a

smile to the person experiencing it for the first time. Some signals such as #12 (bathtub water jet) helped people relax. Others, for example, #1 (breathing), was “controversial:” some people loved the signal because it made them think of their favorite pets, and others found it “creepy” because it felt eerily alive. The anecdotal notes are good indications that the emotional responses to some of our signals were visceral and not abstract.

Our experimental results validated our design approach based on natural and familiar physical phenomena. They show that systematically vary the parameters that make up a vibrotactile waveform is not sufficient for creating pleasant-feeling signals. Note that we used the text labels corresponding to our custom-designed vibrotactile icons during the experiment to set the proper context. This may have influenced the valence-arousal ratings obtained in the present study. In the future, we will expand the range of affect that can be expressed with vibrotactile signals through further design exercises. We will also explore the affective ratings for patterns designed for one or two factors, with the goal of achieving vibrotactile alerts that are compatible with the requirements of mobile devices.

An important contribution of this thesis research is the systematic approach to the design of vibrotactile icons that can express a more realistic feel. While the signals resulting from the design approach and the affective ratings obtained on the signals are important tangible results of this thesis research, sharing the design thinking and insight gained will hopefully inspire and guide other haptic designers to discovering more effective vibrotactile signals. We revisit the use of natural phenomena and metaphors in our signal design and examine the effectiveness of our approach by going through each of the sixteen signals next.

No. 1. “breathing” (G2. Richness through dimensions – slow kinesthetic motion in the z-direction, Fig. 5.15). The design task started from the simple idea that a breathing-like vibrotactile simulated with a slowly changing envelope could deliver a more comfortable and pleasant experience. However, without low-frequency modulation, we confirmed visible movements of the actuators in the z-direction when driven with very low carrier frequencies (< 1 Hz), making it possible to explore the use of low-frequency vibrotactile signals. The breathing signal uses a carrier frequency of 0.8 Hz, which corresponds to roughly 48 breaths per minute. In general, the typical respiratory rate is about 12 to 20 times per minute for adults [53] and 30 to 60 for a baby up to 6 months. Besides, according to the Animal Emergency Center, the normal breathing rate of dogs is 10 to 30 breaths per minute for adults and 15 to 40 for puppies. The

faster respiratory pattern is also true for other newborn mammals [54]. With the *palmScape*, the feeling of a small animal breathing at a slightly faster respiration rate is implemented due to the limit in the lowest frequency of the actuator. However, it still conveys a realistic feeling of a small puppy breathing in the palm.

One thing to consider when implementing slow kinesthetic motion over very low frequencies of less than 1 Hz is that it takes more power due to the very low gain of the actuator at this low frequency. The *palmScape* tactile display system allowed up to 3W and initially tried to drive four factors simultaneously with a carrier frequency of 0.8 Hz to implement a "breathing" signal, but because of the 3W power limitation range, only two factors can be driven with a carrier frequency of 0.8 Hz. Therefore, we have selected 2 factor which are located in the diagonal direction, and factor 2 and 3 were selected to get the maximum spatial effect by movement of two factors. As a result, the slow kinesthetic movement in the z-direction of two factor diagonally placed was enough to create living breathing.

No. 2. "earthquake" (G1. Natural metaphors – gradualness, Fig. 5.16). While most people know what it feels like to feel the breathing of a person or an animal, few have experienced an earthquake in real life. However, we can probably characterize earthquakes a rumbling sensation that increases in intensity as the shock wave reaches a spatial location. In the "earthquake" signal, the rough rumbling sensation is expressed through a carrier frequency of 30 Hz. The gradual build-up and dissipation of energy is achieved with a Gaussian envelope that rises and falls in 3.3 s and modulates the amplitude of the 30-Hz vibration. For the "earthquake" signal, its arousal rating was the highest except for the reference signal (# 18) and "thunder," but the measured amplitude value showed that it was the lowest except for the "breathing" signal which has the lowest arousal score. This demonstrates that the perceived arousal level of a signal is affected by many factors and may not be simply correlated with signal amplitude alone. The destruction of this correlation is due to *palmScape*'s ability to express various metaphors and natural phenomena, and thus this is possible because of the capability to expand and provide a 3D tactile experience.

No. 3. "heartbeat" (G3. Parts and whole - lively feeling, Fig. 5.17). One of the most natural and familiar tactile sensations that can be felt on the palm is "heartbeat." The feelings of living things through heartbeats convey vivacity. There have been many attempts to express "heartbeat," typically conveying the feel of heartbeat using a small linear actuator with a high

resonant frequency. The sensation was not natural or lively, except for the familiar rhythm of "heartbeat." However, Apple Watch used a relatively large linear actuator capable of delivering very low-frequency signals to create a heartbeat pattern for emotional communication between users through touch interaction. The linear actuator transmits in-plane vibrations that feel large in spatial extent and massive in its perceived impact, like a thump. This effect, combined with repeated tapping, created a lively heartbeat effect. However, the vibration shook the whole Apple Watch and lacked the authenticity associated with the chest wall heaved up and down with real heartbeats.

Using the out-of-plane, z-directional slow movement of the *palmScape* actuators, we aimed to recreate the heaving motion of the chest wall. In addition, we used the four tactor locations to mimic the four chambers of a heart: left/right atria and left/right ventricles. We timed the pulses sent to each tactor such that they resembled the movement order of the four chambers. The frequencies of the four pulses were between 20 - 30 Hz to convey the feeling of pumping through muscle contractions. In design, sometimes intuitive thinking and insight have a more significant impact than an analytical approach. We relied on what felt right to the palm rather than taking measurements on a chest wall and attempting to recreate the signals.

No. 4. "raindrop" (G5. Randomness – temporal interval, Fig. 5.18). The "raindrops" signal expresses the feeling of raindrops that fall slowly and sporadically on the palm of your hand. Some natural phenomena have a repetitive pattern, and others appear random. The timing of a discrete sequence of "raindrops," however, may be modeled by a stochastic distribution. Thus, an important factor in expressing "raindrops" is the random timing of each raindrop. In created nature, the strength and spread of each raindrop on the palm also depends on the speed, amount and angle. Therefore, while the most important parameter for "raindrops" is the temporal interval between raindrops, we also varied the intensity, frequency, and duration of each short pulse within a small range so that each raindrop feels subtly variable. We also randomly assigned the tactor location of each raindrop.

The top right of Fig. 5.18 shows the waveform of one raindrop pattern. It consists of about 1.5 cycles of a pulse in a 16-ms duration. Although the amplitude is small, the actuator moves up and down quickly, creating a little pulse-like sensation on the palm. The carrier frequency is randomly selected for each raindrop between 80 and 120 Hz. The relatively higher frequencies as compared to those used in "breathing" and "heartbeat" give a slightly sharper

sensation than a dull thump. This is because although raindrops are tiny and its intensities are weak, we need to consider the amount of impact that is concentrated on a narrow area on the palm. As a result, the "raindrop" has a light intensity, but it could be a feeling of tiny tapping or pulsation in perception level. Besides, we randomly chose the factor for delivering the stimulus to create a more natural feeling. Together, the use of randomized low-intensity levels, carrier frequency, pulse duration, inter-stimulus interval, and factor location have produced a delightful feeling of gentle raindrops.

No. 5. “elephant trod” (G2. Richness through dimensions – shaky illusion, Fig. 5.19). The "elephant trod" signal expresses the feeling of a giant foot hitting the ground such as that of an elephant. This is a shocking/impactful expression using vibrotactile stimulation, similar to the strong rumbling sensation on game controllers such as DualShock of PlayStation and Nintendo Switch. To express a strong impulse using ERM motor, a large eccentric mass is attached to the shaft of a rotating motor that momentarily turns it actively. Sometimes another motor with a relatively small eccentric mass can be used to transmit different shocks. Since the eccentric mass rotates quickly for a short time, low-frequency components are likely to deliver a heavy feeling. However, the sensation delivered by the mechanical force of mass can be somewhat rough and hard, and this tendency is also similar to an LRA. The feel of impact or shock that we intend to express in palmScape is slightly different. Not only does palmScape deliver a substantial impact with smoother feeling on the palm, but it also augments the impact with a spatial perception through the four factors and an illusion of momentary movement of the whole vibrotactile display surface.

The "elephant trod" signal gives the feeling a large object striking on the ground through activating all four factors simultaneously with a 20-Hz pulse of 200 ms. The 200 ms is perceived to be a brief vibrotactile reminder on a mobile device, yet it is long enough time to deliver a sustained vibrotactile effect. Thus, the 20-Hz carrier frequency produces a bumpy and shaky illusion of hitting the ground, and the 200-ms time sustains the feelings. In addition, the four factors give a strong impression of simultaneous shaking over a large area. At 20 Hz, it also produces a strong but soft feeling accompanied by movements on the skin, which almost produces an illusion of compressing the soil on the ground. The vibration amplitude (acceleration) measured from one factor is 0.79 g, which is relatively low compared with the other vibrotactile patterns used in the study. With the spatial summation effect, the simultaneous

activation of all four factors delivers a massive perceived impact, which resulted in relatively high arousal ratings and somewhat negative valence ratings.

No. 6. “tapping” (G2. Richness through dimensions - signal truncation, Fig. 5.20). The "tapping" signal represents a direct tapping on the skin. The Apple Watch utilizes a relatively large linear actuator to create an illusion of tapping the wrist using a horizontal movement for a short time at a low frequency. However, the "tapping" signal on the *palmScape* is not an illusion but a real tapping itself.

It is assumed that the signal has to instantaneously reach the peak amplitude in order to create the feeling of tapping by using a low-frequency movement in the z-direction. However, after confirming the capability of slow motion with lower frequency, “tapping” sensation was enabled by cutting off a 2-Hz input signal to the tactor by resetting the waveform to 0 at 80 ms before the signal reaches the first peak value at 125 ms. As a result, the actuator moves to the z-direction and then instantaneously falls to the average point, and which gives ‘tapping’ sensation.

No. 7. “thunder” (G1. Natural metaphors - metaphor diversity, Fig. 5.21). The "thunder" signal intends to express the phenomenon of thunder and lightning with a tactile sensation. To broaden the expressiveness, we tried to use the *palmScape* to express not only positive and pleasant emotions but also phenomena that could feel somewhat negative. Furthermore, we could achieve a range of signals that span the negative to a positive range of valence values. The pattern can be optimized to smoother feel with a lower frequency and also the intensity can be lowered to ensure a more positive and calm emotion. However, we tried to design the stimulus of the natural metaphor or phenomenon as it is, and as a result, we could get a nearly uniform distribution of positive and negative areas in the V-A space within the 20 vibrotactile stimulus set.

The "thunder" signal has the highest peak acceleration among the 20 stimuli. This is from the initial impact of the signal to mimic the initial explosive sound of the thunder. In order to deliver the impression of large impacts with limited resources such as limited amplitude and available system power, it is necessary to utilize the properties of tactile sensitivity such as higher perceived intensity in the 100-300 Hz range. Therefore, at the beginning of the "thunder" signal, we added a relatively high frequency of 150 Hz (tactor 1) and 135 Hz (tactor 4) compared to the other signals used in this thesis research. In addition, since the phenomenon of "thunder" is accompanied by the electrical phenomenon of lightning, a short, almost instantaneous high-

frequency pulse was used to express it. For factors 1 and 4, a 30-Hz waveform lasts for 1400 and 1550 ms respectively, which represents the shock and rumbling sensation in addition to the 40-ms high-frequency component at the beginning of the pattern. For factors 2 and 3, 30-Hz signals of 200 ms duration are presented in order to enhance the power of initial shock. In order to express the rumbling effect of the gradual build-up and dissipation after the initial shock of the lightning, a 3000-ms long Gaussian envelope is used to modulate the amplitude of the signals mentioned above. In addition, the vibrations on factors 1 and 4 were cut abruptly, leaving the factor to ring a bit before the vibration stops, which gives a subtle stinging-like sensation suggestive of faint residual electric lightning.

No. 8. “twinkle” signal (G5. Randomness – location, Fig. 5.22). The "twinkle" signal is a pattern that expresses the feeling of small and shiny particles spreading in space, like the imagination of twinkle stars. By delivering the same pattern of vibrotactile stimulus repeatedly with subtly randomized perceived intensity, we could recognize the repeated sequence randomly appearing at different regions of the palm.

The duration of the pattern for one raindrop is 20 ms, which corresponds to the most extended duration used for keyclick feedback that still feels crisp as opposed to “buzzy” [55]. The "twinkle" signal uses a high carrier frequency of 300 Hz to express a subtle sharp and tickling impression that is qualitatively similar to numbness in hand. When the signal uses a high carrier frequency of around 250 Hz corresponding to the region of the lowest absolute detection thresholds, their perceived intensity is higher compared to that of a stimulus at the same amplitude but lower carrier frequency. Accordingly, we use lower amplitudes for “twinkle” to achieve a subtler effect.

No. 9. “bubbles” (G2. Richness through dimensions – softness, Fig. 5.23). The "bubbles" signal represents the feel of bubbles rising from a water surface. The feel of water is one of the most familiar sensations we experience in our everyday life. Since water is a liquid, it is not easy to express its feeling using vibrotactile stimuli. The liquid has a soft and fluidic tactile feel because the shape is not fixed. Therefore, it is challenging to deliver the phenomenon of water such as flowing or deformation through the tactile display. However, the expression of water is worth trying because it is not only a universal human experience but also an excellent medium to convey a feeling of softness and flexibility. While a still pool of water is hard to express with vibrotactile patterns, we can think about the more dramatic phenomena such as

water droplets on the surface of the water, rising bubbles in a bathtub, and splashing water droplets in boiling water, to facilitate design and emulation.

We decided to design a soft feel of water bubbles rising above the surface of the water. The "bubbles" signal uses a carrier frequency of 20 Hz to deliver a gentle push on the palm. A duration of 160 ms was used to consider the time it takes for one droplet to rise to the surface. As shown in Fig. 5.23, as soon as the third sinusoidal cycle ends and the fourth cycle begins, the amplitude reaches zero quickly as the signal duration reaches 160 ms, which is intended to represent the phenomenon of droplets disappearing. The same droplet disappearing effect occurs in tactor 4 at 800 ms with the tactor location sequence '3-2-4-1' (tactor numbers in the sequence), creating a natural sensation of bubbles spreading over a broader range of the palm.

No. 10. "water drop & ripple" (G3. Parts and whole - fluids, Fig. 5.24). The "water drop & ripple" signal is a tactile representation of the feeling that a water droplet is falling and waves spreading out on a surface. "Water drop & ripple" signal is divided into at least two natural phenomena: a droplet hitting the surface of the water, and ripples occurring after a droplet falls. When we think about the falling of a water drop, the phenomenon of a water drop hitting the water surface can be simplified by the impact between the water drop and water surface. Furthermore, if we analyze the phenomenon in more detail, the impacted medium (water surface) goes down to the z-direction instantaneously and then rises again to return to its original position, especially in the case of a body of fluid.

To express this phenomenon, the tactile display is able to express the slow motion in the z-direction. At the beginning of the signal waveform for "water drop" in Fig. 5.24, it starts at a low carrier frequency of 7 Hz. A one-period signal is suitable to represent the impacted fluid momentarily moving down and up in the z-direction. The signal ended before the completion of one cycle so that the actuator returns to the neutral position quickly in response to the amplitude dropping to near zero. In addition, a relatively high carrier frequency of 180 Hz was added at the starting point to express the somewhat sharp feeling at the moment of impact. Furthermore, the extremely short duration of 3.2 ms in tactor 2 and 3 with a high carrier frequency of 300 Hz serves to delicately express the feeling of water splashing after the moment of impact.

After a certain time period, waves form and spread calmly on the surface of the water. It is challenging to express the phenomenon through vibrotactile or other haptic techniques. A single, resonance-type of an actuator cannot easily move at a very low frequency or express any

spatial information. However, *palmScape* can express slow movements in the z-direction, and the four factors can be used to express wave propagation. Some strategies are needed on how to express the temporal and spatial characteristics of the waves. We used factor 1 to express the feeling of rough waves that occur in the earliest time after the falling of the water droplet which uses a carrier frequency of 10 Hz and an amplitude modulation at 5 Hz. The ripple effect is expressed with the remaining factors 2, 3, and 4 with a low carrier frequency of 5 or 10 Hz. Gaussian amplitude modulation was used to express the attenuation of the propagating waves. This way, the four factors represent a more realistic wave feeling in the limited palm area by distributing their roles in expressing waves with different timing parameters and different sensations.

No. 11. “cicadas” (G4. Simplicity - design with sound, Fig. 5.25). The "cicadas" signal is a tactile pattern of crying cicadas designed from sound waveforms. Sound and vibration are intricately related in that both are delivered through waves in their respective mediums, and a vibration and vice versa usually accompany a sound. Therefore, starting from a sound from a natural phenomenon or metaphor can be a fruitful way for the design of vibrotactile icon. It is very intuitive and easy to start with the analysis of the crying sound of the cicadas to design the feel of "cicadas" vibrotactile signal.

The "cicadas" signal used in this thesis research consists of four repeated short cries and one long last cry. As the cicadas use their bodies to produce sound, they continue to vibrate and change in intensity and roughness. It is necessary to simplify and express the most dramatic elements from natural phenomena and metaphors to capture the essence of the sensory experience. In cicadas, a continuous change in intensity and roughness can be simplified to 'strong crying' and 'weak crying.'

To express the ‘strong crying’ of a cicada, we used a carrier frequency of 60 Hz with amplitude modulation of 2 Hz. The 60 Hz carrier frequency delivers a rough feeling of 'strong crying' and the magnitude of the amplitude increases and decreases for about half a period of the 2 Hz modulation for a duration of 437.5 ms, representing the changes in intensity. After the fourth strong cry, the fifth 'strong cry' applied with the amplitude modulation of 0.5 Hz to express the attenuation of crying sound for about 3 times amount of duration than the normal crying. We applied a carrier frequency of 120 Hz and amplitude modulation of 32 Hz to express the 'weak crying' of the cicadas in factor 1 and 4. Besides, the signal of "weak crying" was kept

from the beginning to the end while strong crying is present instead of stopping the “weak crying” while “strong crying” signal is present to keep the feeling of crying continuously.

No. 12. “bathtub water jet” (G2. Richness through dimensions - soft pressure, Fig. 5.26). The "bathtub water jet" signal concurrently represented a soft but somewhat strong feel of the water flow with pressure when we move a palm near the water jet. Most importantly, we wanted to draw the user’s pleasant experience on the choice of metaphor and phenomenon. For reference, the "bathtub water jet" signal received the highest valence score (most pleasant) among the 20 vibrotactile patterns in the affective rating experiment.

The vibrotactile representation of “bathtub water jet” signal through *palmScape* was created from the "bubbles" signal by increasing peak acceleration (from 1.14 g to 1.78 g, see Table 5.15) and doubling duration (800 to 1600 ms) to deliver a stronger intensity of the water flow and the feeling of a continuous wave. In addition, the carrier frequency of 20 Hz in "bubbles" was lowered to 10 Hz in order to soften the sensation.

Note that not all four factors are used to represent strong water jets in the “bathtub water jet” signal. We assign a strong water jet signal to factors 1, 2, and 3, and a continuous background stimulus with a relatively low amplitude to factor 4. In particular, two types of sensations are divided into the upper-triangular area occupied by factors 1, 2 and 3 and the remaining corner occupied by factor 4. Due to the strong wave effect of the upper-triangular area and the weak background wave effect of the remaining area, an asymmetric tactile sensation was achieved. This asymmetric sensation corresponds to the phenomenon that the palm is not precisely placed in the center of the jet outlet, and this results in a skewed tactile sense. Therefore, differentiation of the tactile transmission area and mapping different tactile senses asymmetrically can be another approach to designing a more natural tactile sense.

No. 13. “frog” (G4. Simplicity - roughness with dissonance, Fig. 5.27). The "frog" signal is a tactile pattern which represents the croaking sound of the frog and the movement of the vocal sac. The design approach is similar to that for "cicadas" signal which is a tactile representation of the sound. However, for the "frog" signal, the strong croaking is expressed using a somewhat lower carrier frequency of 50 or 32 Hz for factors 2 and 3, respectively (as opposed to the 60 Hz used for “cicadas”). In other words, different frequencies are used at the same time for the two different locations, possibly leading to a dissonant sensation. According to a study on the consonance of vibrotactile chords, the vibrations of a consonance relation can give

an ‘even,’ ‘smooth,’ and ‘pleasant’ feel, and the vibration of dissonance can be somewhat ‘jagged,’ ‘bumpy’ and ‘rough’ [56]. In this "frog" signal, the 32-Hz carrier frequency used in factor 2 is dissonant with the 50-Hz used in factor 3. We intended to create a roughness sensation by using two dissonant frequencies in two adjacent locations at the same time. It is based on the observation that the croaking of a frog and the movement of its vocal sac can be somewhat irregular, and it needs to be expressed with a rough feel.

For ‘weak croaking,’ the signals sent to factors 1 and 4 use a 120-Hz, 200-ms vibration modulated at 16 Hz with a smaller amplitude to express a sharp and rough feeling. The sequence of ‘weak and strong croaking’ is repeated three times to complete the “frog” signal pattern.

No. 14. “(horse) galloping” (G3. Parts and whole - rhythm expression, Fig. 5.28). The "(horse) galloping" signal is a tactile representation of the sound and feel of horseshoes when the horse gallops on a hard path. The phenomenon is similar to "tapping," but it is slightly different in signal representation. The "tapping" signal is a slow movement due to the low carrier frequency of 2 Hz. The “(horse) galloping” signal uses a method that is similar to overdrive for a faster actuator response. In mobile devices equipped with linear actuators, the overdriving function delivers a higher amplitude initially in order to realize a quick response and crisper vibration. Similarly, the “galloping” signal expresses a quick thump by mixing two 16-ms carrier frequencies at 180 and 300 Hz to ‘overdrive’ the factor initially, followed by the 64-ms signals at the lower carrier frequencies of 5 and 7 Hz.

Another notable aspect in the "(horse) galloping" signal is its rhythm. The use of rhythm as a highly familiar phenomenon can lead to a high degree of consensus in its interpretation and bring a common experience among users. When designing for vibrotactile rhythm, we need to consider the temporal masking and temporal-order judgment capabilities of touch [2]. Particular attention should be paid to rhythmic expressions with a fast tempo, and more rhythmic representations are needed for more patterns. Thus, when rhythmic patterns are translated from sound to touch, not all patterns may be properly perceived. In particular, when a pattern located at a mid-point in time has a relatively low intensity, we may miss its presence. In the "(horse) galloping" signal, the intensity of the pattern located in the middle of the rhythm is relatively low, and it may not be perceived as a clear pattern and rhythm as a whole. In addition to rhythm, the “galloping” signal also introduces variations in the intensity, and the amplitude follows a ‘medium-weak-strong’ sequence

No. 15. “knock” (G3. Parts and whole - hitting sensation, Fig. 5.29). The "knock" signal expresses the phenomenon associated with someone knocking on the door with the knuckles. The differences between "tapping" and "knock" lie in the differences in intensity. In addition to the hitting action for the “knock” signal, the feeling of the door shaking is also expressed. To express the stronger and harder ‘knock’ sensation as compared to ‘tapping,’ a high carrier frequency of 280, 300 Hz and a short duration of 12 ms are delivered to factors 1 and 4 at the beginning to create a sense of sharp impact. The feeling of the shaking door is expressed with a 30-Hz 60-ms signal delivered to all four factors, resulting in the feeling of the whole door shaking being transmitted over a broader range of contacted areas.

No. 16. “bubbles popping” (G2. Richness through dimensions - pushing, Fig. 5.30). The "bubbles popping" signal represents the tactile sense of bubbles bursting slowly and finely popping, like soap bubbles. Using a 312.5 ms duration that is slightly longer than 250 ms which corresponds to a half cycle of the carrier frequency of 2 Hz, the factor moves slowly up during the half cycle and gives a smooth pushing sensation to the z-direction. Afterward, the factor goes down and returns to its original position at 250 ms, generating a subtle and somewhat sharp tapping sensation that feels like a bubble bursting in the palm.

5. CONCLUSIONS AND FUTURE WORK

The present research set out to broaden the expressive range of vibrotactile icons by creating a more realistic and natural vibrotactile experience. We believe that users of mobile devices will be more receptive to calm and pleasant alerts for an upcoming calendar event or a new social media posting. This will help eliminate “buzzing” from our daily living and reduce the stress and annoyance associated with it. We envision a day when people shop for a mobile phone for its playful and delightful haptic effects, and calm and pleasant haptic alerts become an integral part of our digital life.

Three types of prototypes that aimed to provide a more natural haptic experience in human-computer interactions were developed and evaluated. After ascertaining their limited expressiveness, a new vibrotactile display, *palmScape*, was developed. A set of signals inspired by natural phenomena were developed for the *palmScape* and their expressiveness evaluated with an affective rating experiment. The most significant finding of the present study is that we succeeded in creating five vibrotactile stimuli that reside in the fourth quadrant of the valence-arousal space, a region that has hardly been occupied by similar attempts before. These vibrotactile signals often brought a smile to the person experiencing it for the first time. Some signals such as #12 (bathtub water jet) helped people relax. Others, for example, #1 (breathing), was “controversial:” some people loved the signal because it made them think of their favorite pets, and others found it “creepy” because it felt eerily alive. The anecdotal notes are good indications that the emotional responses to some of our signals were visceral and not abstract.

Our experimental results validated our design approach based on natural and familiar physical phenomena. They show that systematically vary the parameters that make up a vibrotactile waveform is not sufficient for creating pleasant-feeling signals. Note that we used the text labels corresponding to our custom-designed vibrotactile icons during the experiment to set the proper context. This may have influenced the valence-arousal ratings obtained in the present study. In the future, we will expand the range of affect that can be expressed with vibrotactile signals through further design exercises.

In the future, we will expand the range of affect that can be expressed with vibrotactile signals through further design exercises. We will also explore the affective ratings for patterns designed for one or two factors, with the goal of achieving vibrotactile alerts that are compatible

with the requirements of mobile devices. Other interesting research directions include allowing participants to come up with their own labels for a broad range of vibrotactile signals and checking the consistency of perceived meanings and assessing the memory aspect of affective vibrotactile icons by estimating the retention rates of our signals vs. other types of vibrotactile signals after one exposure.

REFERENCES

- [1] J. M. Wolfe, *Sensation and Perception*. Sinauer Associates, 2006.
- [2] I. R. Summers, *Tactile Aids for the Hearing Impaired*. Wiley, 1992.
- [3] A. B. Vallbo and R. S. Johansson, "Properties of cutaneous mechanoreceptors in the human hand related to touch sensation," *Hum Neurobiol*, vol. 3, no. 1, pp. 3-14, 1984.
- [4] G. A. Gescheider, *Psychophysics: method, theory, and application*. L. Erlbaum Associates, 1985.
- [5] R. T. Verrillo, "Effect of contactor area on the vibrotactile threshold," *The Journal of the Acoustical Society of America*, vol. 35, no. 12, pp. 1962-1966, 1963.
- [6] H. Levitt, "Transformed up-down methods in psychoacoustics," *J Acoust Soc Am*, vol. 49, no. 2, p. Suppl 2:467+, Feb 1971.
- [7] V. Yem, R. Okazaki, and H. Kajimoto, "Vibrotactile and pseudo force presentation using motor rotational acceleration," in *Haptics Symposium (HAPTICS), 2016 IEEE*, 2016, pp. 47-51: IEEE.
- [8] W. McMahan and K. J. Kuchenbecker, "Dynamic modeling and control of voice-coil actuators for high-fidelity display of haptic vibrations," in *2014 IEEE Haptics Symposium (HAPTICS)*, 2014, pp. 115-122: IEEE.
- [9] M. Kaufmann, C. Adelman, and H. Sohmer, "Mapping sites on bone and soft tissue of the head, neck and thorax at which a bone vibrator elicits auditory sensation," *Audiology and Neurotology Extra*, vol. 2, no. 1, pp. 9-15, 2012.
- [10] Charlotte M. Reed, Hong Z. Tan, Zachary D. Perez, E. Courtenay Wilson, Frederico M. Severgnini, Jaehong Jung, Juan S. Martinez, Yang Jiao, Ali Israr, Frances Lau, Keith Klumb, Robert Turcott, and Freddy Abnoui, "A phonemic-based haptic display for speech communication," *IEEE Transactions on Haptics*, Vol. 12, No. 1, pp. 2-17, 2019. (DOI: 10.1109/TOH.2018.2861010)
- [11] D. J. Meyer, M. A. Peshkin, and J. E. Colgate, "Fingertip friction modulation due to electrostatic attraction," in *2013 world haptics conference (WHC)*, 2013, pp. 43-48: IEEE.
- [12] E. L.-C. Law, V. Roto, M. Hassenzahl, A. P. Vermeeren, and J. Kort, "Understanding, scoping and defining user experience: a survey approach," in *Proceedings of the SIGCHI conference on human factors in computing systems*, 2009, pp. 719-728: ACM.
- [13] P. Hekkert, "Design aesthetics: principles of pleasure in design," *Psychology science*, vol. 48, no. 2, p. 157, 2006.
- [14] J. A. Russell, "A circumplex model of affect," *Journal of personality and social psychology*, vol. 39, no. 6, p. 1161, 1980.
- [15] M. M. Bradley and P. J. Lang, "Measuring emotion: the self-assessment manikin and the semantic differential," *Journal of behavior therapy and experimental psychiatry*, vol. 25, no. 1, pp. 49-59, 1994.
- [16] A. Mehrabian and J. A. Russell, "The basic emotional impact of environments," *Perceptual and motor skills*, vol. 38, no. 1, pp. 283-301, 1974.
- [17] I. Bakker, T. van der Voordt, P. Vink, and J. de Boon, "Pleasure, arousal, dominance: Mehrabian and Russell revisited," *Current Psychology*, vol. 33, no. 3, pp. 405-421, 2014.

- [18] P. Lang, M. Greenwald, and M. Bradley, "The International Affective Picture System (IAPS) standardization procedure and initial group results for affective judgments: Technical reports 1A-1D," *Center for the Study of Emotion and Attention*, 1988.
- [19] M. Jeon, "Emotions and Affect in Human Factors and Human–Computer Interaction: Taxonomy, Theories, Approaches, and Methods," in *Emotions and Affect in Human Factors and Human-Computer Interaction*: Elsevier, 2017, pp. 3-26.
- [20] Y. Yoo, T. Yoo, J. Kong, and S. Choi, "Emotional responses of tactile icons: Effects of amplitude, frequency, duration, and envelope," in *2015 IEEE World Haptics Conference (WHC)*, 2015, pp. 235-240: IEEE.
- [21] J. T. Cacioppo, L. G. Tassinary, and G. Berntson, *Handbook of psychophysiology*. Cambridge University Press, 2007.
- [22] G. Korres, C. B. F. Jensen, W. Park, C. Bartsch, and M. Eid, "A vibrotactile alarm system for pleasant awakening," *IEEE transactions on haptics*, vol. 11, no. 3, pp. 357-366, 2018.
- [23] D. J. Cohen, K. A. Barker, and M. R. White, "A standardized list of affect-related life events," *Behavior research methods*, vol. 50, no. 5, pp. 1806-1815, 2018.
- [24] A. T. Beck, R. A. Steer, and G. K. Brown, "Beck depression inventory-II," *San Antonio*, vol. 78, no. 2, pp. 490-498, 1996.
- [25] S. Thylander, A. Menzel, and M. Ristinmaa, "A non-affine electro-viscoelastic microsphere model for dielectric elastomers: Application to VHB 4910 based actuators," *Journal of Intelligent Material Systems and Structures*, vol. 28, no. 5, pp. 627-639, 2017.
- [26] M. Fukumoto and T. Sugimura, "Active click: tactile feedback for touch panels," in *CHI'01 Extended Abstracts on Human Factors in Computing Systems*, 2001, pp. 121-122: ACM.
- [27] M. L. G. a. S. Zhai, "Touchscreen haptic augmentation effects on tapping, drag and drop, and path following," *Proceedings of CHI 2019, to appear*, 2019.
- [28] H. Z. Tan, N. I. Durlach, C. M. Reed, and W. M. Rabinowitz, "Information transmission with a multifinger tactual display," *Perception & Psychophysics*, vol. 61, no. 6, pp. 993-1008, 1999.
- [29] L. M. Brown, S. A. Brewster, and H. C. Purchase, "Tactile crescendos and sforzandos: applying musical techniques to tactile icon design," in *CHI'06 extended abstracts on Human factors in computing systems*, 2006, pp. 610-615: ACM.
- [30] J. Rantala, K. Salminen, R. Raisamo, and V. Surakka, "Touch gestures in communicating emotional intention via vibrotactile stimulation," *International Journal of Human-Computer Studies*, vol. 71, no. 6, pp. 679-690, 2013.
- [31] H. Seifi and K. E. Maclean, "A first look at individuals' affective ratings of vibrations," in *2013 World Haptics Conference (WHC)*, 2013, pp. 605-610: IEEE.
- [32] G. Huisman, A. D. Frederiks, J. B. van Erp, and D. K. Heylen, "Simulating affective touch: Using a vibrotactile array to generate pleasant stroking sensations," in *International Conference on Human Haptic Sensing and Touch Enabled Computer Applications*, 2016, pp. 240-250: Springer.
- [33] H. Culbertson, C. M. Nunez, A. Israr, F. Lau, F. Abnoui, and A. M. Okamura, "A social haptic device to create continuous lateral motion using sequential normal indentation," in *2018 IEEE Haptics Symposium (HAPTICS)*, 2018, pp. 32-39: IEEE.
- [34] J. Liljencrantz and H. Olausson, "Tactile C fibers and their contributions to pleasant sensations and to tactile allodynia," *Frontiers in behavioral neuroscience*, vol. 8, p. 37, 2014.

- [35] M. M. Bradley and P. J. Lang, "The International Affective Digitized Sounds (; IADS-2): Affective ratings of sounds and instruction manual," *University of Florida, Gainesville, FL, Tech. Rep. B-3*, 2007.
- [36] P. J. Lang, M. M. Bradley, and B. N. Cuthbert, "International affective picture system (IAPS): affective ratings of pictures and instruction manual. University of Florida, Gainesville," FL, Technical Report A-82008.
- [37] C. M. Reed, W. M. Rabinowitz, N. I. Durlach, L. D. Braida, S. Conway-Fithian, and M. C. Schultz, "Research on the Tadoma method of speech communication," *The Journal of the Acoustical society of America*, vol. 77, no. 1, pp. 247-257, 1985.
- [38] D. Leotta, W. Rabinowitz, C. Reed, and N. Durlach, "Preliminary results of speech-reception tests obtained with the synthetic Tadoma system," *Journal of rehabilitation research and development*, vol. 25, no. 4, pp. 45-52, 1988.
- [39] W. Rabinowitz, D. Henderson, C. Reed, L. Delhorne, and N. Durlach, "Continuing evaluation of a synthetic Tadoma system," *The Journal of the Acoustical Society of America*, vol. 87, no. S1, pp. S88-S88, 1990.
- [40] S. P. Eberhardt, L. E. Bernstein, D. Barac-Cikoja, D. C. Coulter, and J. Jordan, "Inducing dynamic haptic perception by the hand: System description and some results," *Proceedings of ASME Dynamic Systems and Control*, vol. 55, no. 1, pp. 345-351, 1994.
- [41] H. Z. Tan and W. M. Rabinowitz, "A new multi-finger tactual display," in *Proceedings of the ASME Dynamic Systems and Control Division*, 1996, vol. 58.
- [42] V. B. Mountcastle, W. H. Talbot, I. Darian-Smith, and H. H. Kornhuber, "Neural basis of the sense of flutter-vibration," *Science*, vol. 155, no. 3762, pp. 597-600, 1967.
- [43] V. B. Mountcastle, W. H. Talbot, H. Sakata, and J. Hyvärinen, "Cortical neuronal mechanisms in flutter-vibration studied in unanesthetized monkeys. Neuronal periodicity and frequency discrimination," *Journal of neurophysiology*, vol. 32, no. 3, pp. 452-484, 1969.
- [44] S. J. Bolanowski Jr, G. A. Gescheider, R. T. Verrillo, and C. M. Checkosky, "Four channels mediate the mechanical aspects of touch," *The Journal of the Acoustical society of America*, vol. 84, no. 5, pp. 1680-1694, 1988.
- [45] H. Z. Tan, Nathaniel, I. Durlach, "Information transmission with a multi-finger tactual display," Doctoral Dissertation, Department of Electrical Engineering and Computer Science, Massachusetts Institute of Technology, 1996.
- [46] K. E. MacLean, "Foundations of transparency in tactile information design," *IEEE Transactions on Haptics*, vol. 1, no. 2, pp. 84-95, 2008.
- [47] A. Israr, S. Zhao, K. Schwalje, R. Klatzky, and J. Lehman, "Feel effects: enriching storytelling with haptic feedback," *ACM Transactions on Applied Perception (TAP)*, vol. 11, no. 3, p. 11, 2014.
- [48] K. MacLean and M. Enriquez, "Perceptual design of haptic icons," in *Proc. of EuroHaptics*, 2003, pp. 351-363.
- [49] L. M. Brown, S. A. Brewster, and H. C. Purchase, "Multidimensional tactons for non-visual information presentation in mobile devices," in *Proceedings of the 8th conference on Human-computer interaction with mobile devices and services*, 2006, pp. 231-238: ACM.

- [50] P. Barralon, G. Ng, G. Dumont, S. K. Schwarz, and M. Ansermino, "Development and evaluation of multidimensional tactons for a wearable tactile display," in *Proceedings of the 9th international conference on Human computer interaction with mobile devices and services*, 2007, pp. 186-189: ACM.
- [51] W. Rabinowitz, A. Houtsma, N. Durlach, and L. Delhorne, "Multidimensional tactile displays: Identification of vibratory intensity, frequency, and contactor area," *The Journal of the Acoustical Society of America*, vol. 82, no. 4, pp. 1243-1252, 1987.
- [52] L. A. Jones and H. Z. Tan, "Application of psychophysical techniques to haptic research," *IEEE transactions on haptics*, vol. 6, no. 3, pp. 268-284, 2013.
- [53] K. E. Barrett, S. M. Barman, S. Boitano, and H. Brooks, *Ganong's Review of Medical Physiology, 24th Edition*. Mcgraw-hill, 2012.
- [54] J. P. Mortola, "Breathing pattern in newborns," *Journal of Applied Physiology*, vol. 56, no. 6, pp. 1533-1540, 1984.
- [55] Q. Liu, H. Z. Tan, L. Jiang, and Y. Zhang, "Perceptual dimensionality of manual key clicks," in *2018 IEEE Haptics Symposium (HAPTICS)*, 2018, pp. 112-118: IEEE.
- [56] Y. Yoo, I. Hwang, and S. Choi, "Consonance of vibrotactile chords," *IEEE transactions on haptics*, vol. 7, no. 1, pp. 3-13, 2014.

APPENDIX A: INDIVIDUAL RESULT OF THE AFFECTIVE RATINGS STUDY

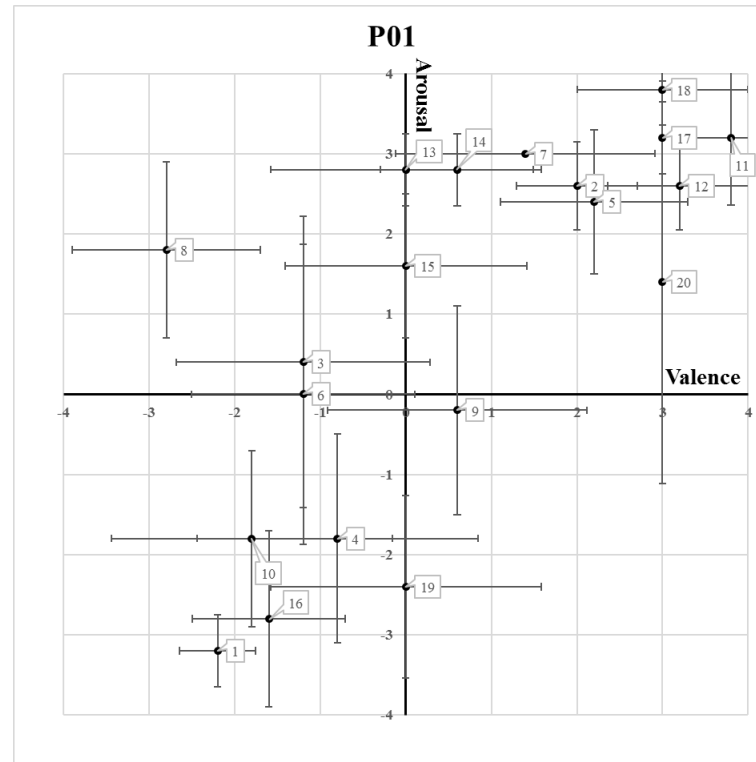


Fig. 5.1 Individual result of affective rating study: P01.

Table 5.1 Individual result of affective rating study: P01.

Signal #	1	2	3	4	5	6	7	8	9	10	11	12	13	14	15	16	17	18	19	20	Avg.
Valence	-2.2	2	-1.2	-0.8	2.2	-1.2	1.4	-2.8	0.6	-1.8	3.8	3.2	0	0.6	0	-1.6	3	3	0	3	0.56
Var-V	0.2	0.5	2.2	2.7	1.2	1.7	2.3	1.2	2.3	2.7	0.2	0.7	2.5	0.8	2	0.8	0	1	2.5	0	1.38
Std-V	0.45	0.71	1.48	1.64	1.10	1.30	1.52	1.10	1.52	1.64	0.45	0.84	1.58	0.89	1.41	0.89	0	1	1.58	0	1.06
Arousal	-3.2	2.6	0.4	-1.8	2.4	0	3	1.8	-0.2	-1.8	3.2	2.6	2.8	2.8	1.6	-2.8	3.2	3.8	-2.4	1.4	0.97
Var-A	0.2	0.3	3.3	1.7	0.8	3.5	0	1.2	1.7	1.2	0.7	0.3	0.2	0.2	0.8	1.2	0.2	0.2	1.3	6.3	1.27
Std-A	0.45	0.55	1.82	1.30	0.89	1.87	0	1.10	1.30	1.10	0.84	0.55	0.45	0.45	0.89	1.10	0.45	0.45	1.14	2.51	0.96

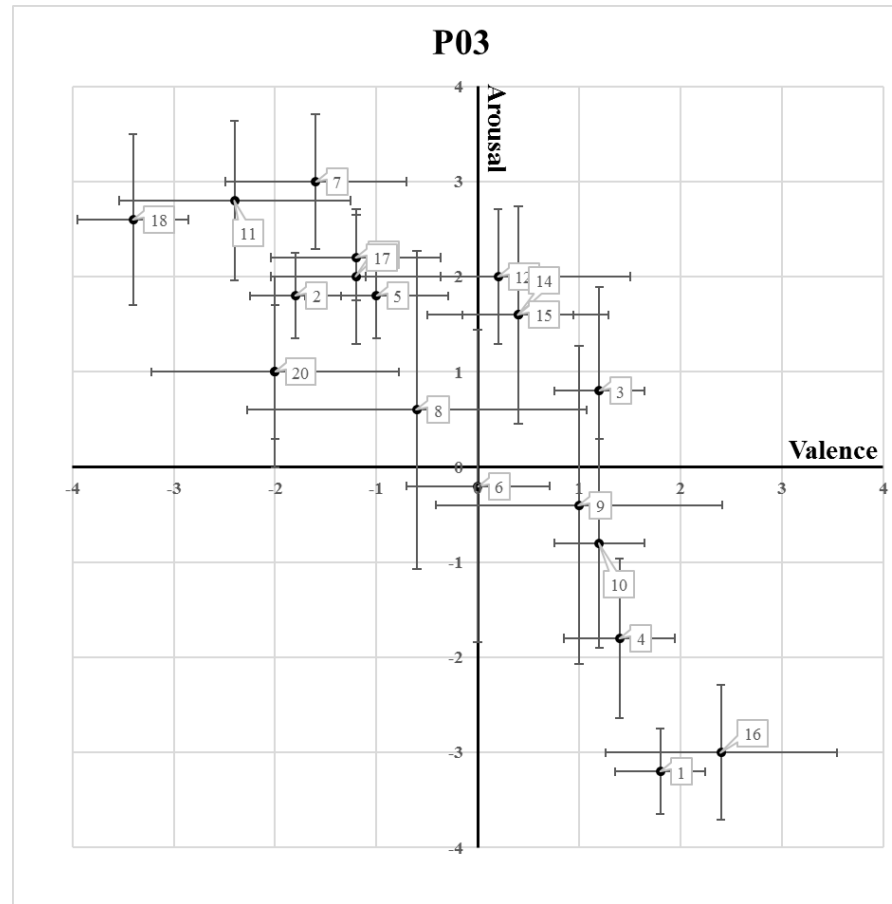


Fig. 5.3 Individual result of affective rating study: P03.

Table 5.3 Individual result of affective rating study: P03.

Signal #	1	2	3	4	5	6	7	8	9	10	11	12	13	14	15	16	17	18	19	20	Avg.
Valence	1.8	-1.8	1.2	1.4	-1	0	-1.6	-0.6	1	1.2	-2.4	0.2	-1.2	0.4	0.4	2.4	-1.2	-3.4	-2	-2	-0.36
Var-V	0.2	0.2	0.2	0.3	0.5	0.5	0.8	2.8	2	0.2	1.3	1.7	0.7	0.8	0.3	1.3	0.7	0.3	1.5	0	0.82
Std-V	0.45	0.45	0.45	0.55	0.71	0.71	0.89	1.67	1.41	0.45	1.14	1.30	0.84	0.89	0.55	1.14	0.84	0.55	1.22	0	0.81
Arousal	-3.2	1.8	0.8	-1.8	1.8	-0.2	3	0.6	-0.4	-0.8	2.8	2	2	1.6	1.6	-3	2.2	2.6	1	1	0.77
Var-A	0.2	0.2	1.2	0.7	0.2	2.7	0.5	2.8	2.8	1.2	0.7	0.5	0.5	1.3	1.3	0.5	0.2	0.8	0.5	1	0.99
Std-A	0.45	0.45	1.10	0.84	0.45	1.64	0.71	1.67	1.67	1.10	0.84	0.71	0.71	1.14	1.14	0.71	0.45	0.89	0.71	1	0.92

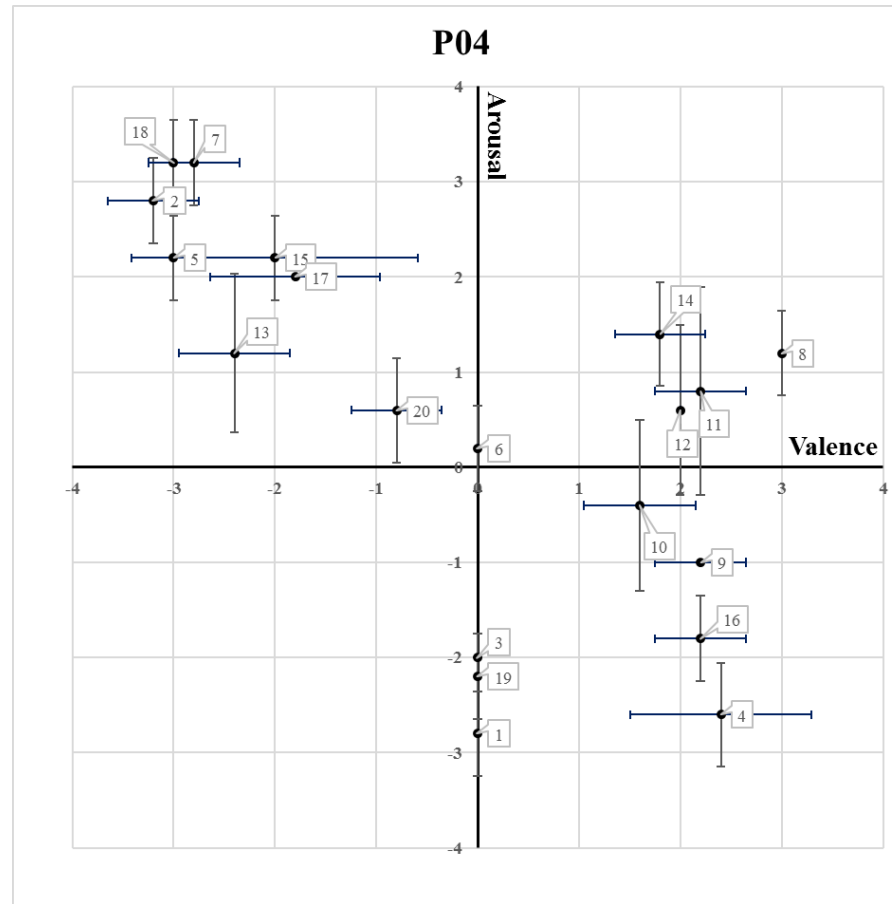


Fig. 5.4 Individual result of affective rating study: P04.

Table 5.4 Individual result of affective rating study: P04.

Signal #	1	2	3	4	5	6	7	8	9	10	11	12	13	14	15	16	17	18	19	20	Avg.
Valence	0	-3.2	0	2.4	-3	0	-2.8	3	2.2	1.6	2.2	2	-2.4	1.8	-2	2.2	-1.8	-3	0	-0.8	-0.08
Var-V	0	0.2	0	0.8	0	0	0.2	0	0.2	0.3	0.2	0	0.3	0.2	2	0.2	0.7	0	0	0.2	0.28
Std-V	0	0.45	0	0.89	0	0	0.45	0	0.45	0.55	0.45	0	0.55	0.45	1.41	0.45	0.84	0	0	0.45	0.37
Arousal	-2.8	2.8	-2	-2.6	2.2	0.2	3.2	1.2	-1	-0.4	0.8	0.6	1.2	1.4	2.2	-1.8	2	3.2	-2.2	0.6	0.44
Var-A	0.2	0.2	0	0.3	0.2	0.2	0.2	0.2	0	0.8	1.2	0.8	0.7	0.3	0.2	0.2	0	0.2	0.2	0.3	0.32
Std-A	0.45	0.45	0	0.55	0.45	0.45	0.45	0.45	0	0.89	1.10	0.89	0.84	0.55	0.45	0.45	0	0.45	0.45	0.55	0.49

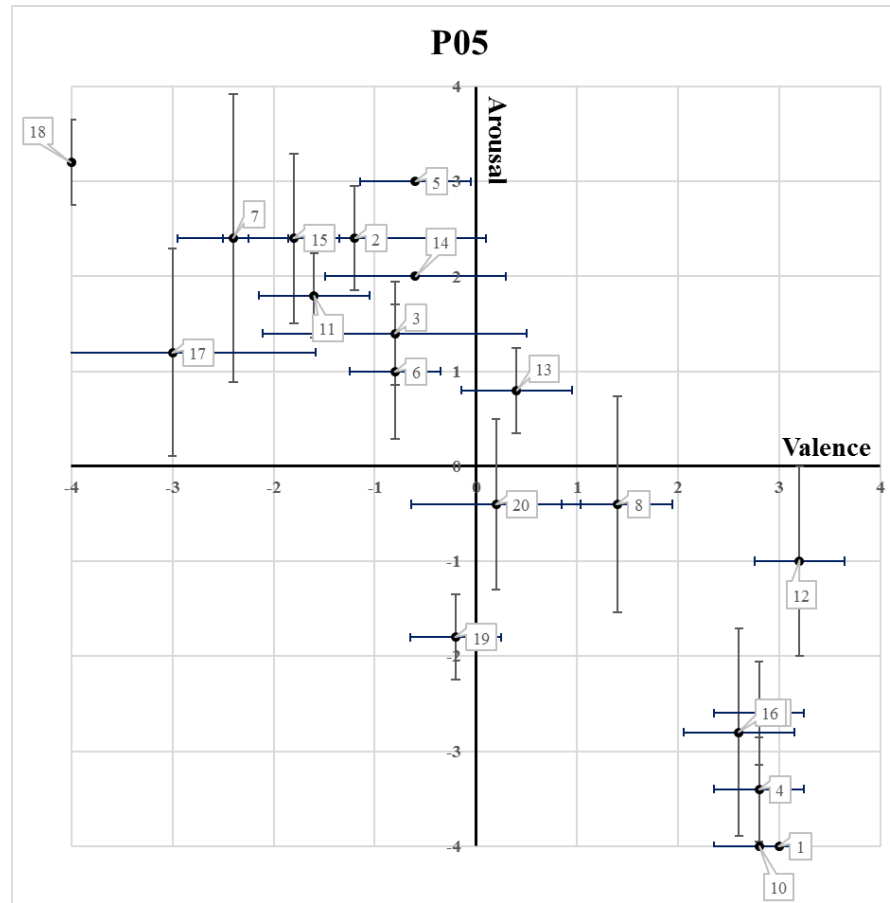


Fig. 5.5 Individual result of affective rating study: P05.

Table 5.5 Individual result of affective rating study: P05.

Signal #	1	2	3	4	5	6	7	8	9	10	11	12	13	14	15	16	17	18	19	20	Avg.
Valence	3	-1.2	-0.8	2.8	-0.6	-0.8	-2.4	1.4	2.8	2.8	-1.6	3.2	0.4	-0.6	-1.8	2.6	-3	-4	-0.2	0.2	0.11
Var-V	0	1.7	1.7	0.2	0.3	0.2	0.3	0.3	0.2	0.2	0.3	0.2	0.3	0.8	0.2	0.3	2	0	0.2	0.7	0.51
Std-V	0	1.30	1.30	0.45	0.55	0.45	0.55	0.55	0.45	0.45	0.55	0.45	0.55	0.89	0.45	0.55	1.41	0	0.45	0.84	0.61
Arousal	-4	2.4	1.4	-3.4	3	1	2.4	-0.4	-2.6	-4	1.8	-1	0.8	2	2.4	-2.8	1.2	3.2	-1.8	-0.4	0.06
Var-A	0	0.3	0.3	0.3	0	0.5	2.3	1.3	0.3	0	0.2	1	0.2	0	0.8	1.2	1.2	0.2	0.2	0.8	0.56
Std-A	0	0.55	0.55	0.55	0	0.71	1.52	1.14	0.55	0	0.45	1	0.45	0	0.89	1.10	1.10	0.45	0.45	0.89	0.62

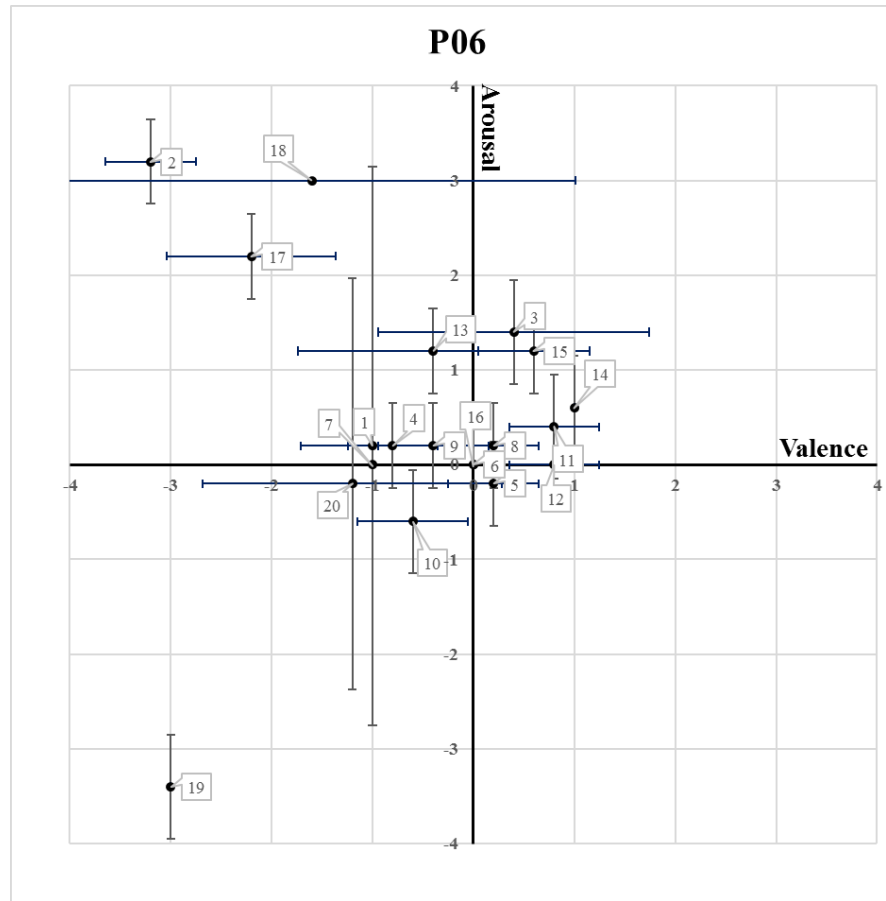


Fig. 5.6 Individual result of affective rating study: P06.

Table 5.6 Individual result of affective rating study: P06.

Signal #	1	2	3	4	5	6	7	8	9	10	11	12	13	14	15	16	17	18	19	20	Avg.
Valence	-1	-3.2	0.4	-0.8	0.2	0	-1	0.2	-0.4	-0.6	0.8	0.8	-0.4	1	0.6	0	-2.2	-1.6	-3	-1.2	-0.57
Var-V	0.5	0.2	1.8	0.2	0.2	0	0	0.2	0.3	0.3	0.2	0.2	1.8	0	0.3	0	0.7	6.8	0	2.2	0.80
Std-V	0.71	0.45	1.34	0.45	0.45	0	0	0.45	0.55	0.55	0.45	0.45	1.34	0	0.55	0	0.84	2.61	0	1.48	0.63
Arousal	0.2	3.2	1.4	0.2	-0.2	0	0	0.2	0.2	-0.6	0.4	0	1.2	0.6	1.2	0	2.2	3	-3.4	-0.2	0.48
Var-A	8.7	0.2	0.3	0.2	0.2	0	0	0.2	0.2	0.3	0.3	0	0.2	0.3	0.2	0	0.2	0	0.3	4.7	0.83
Std-A	2.95	0.45	0.55	0.45	0.45	0	0	0.45	0.45	0.55	0.55	0	0.45	0.55	0.45	0	0.45	0	0.55	2.17	0.57

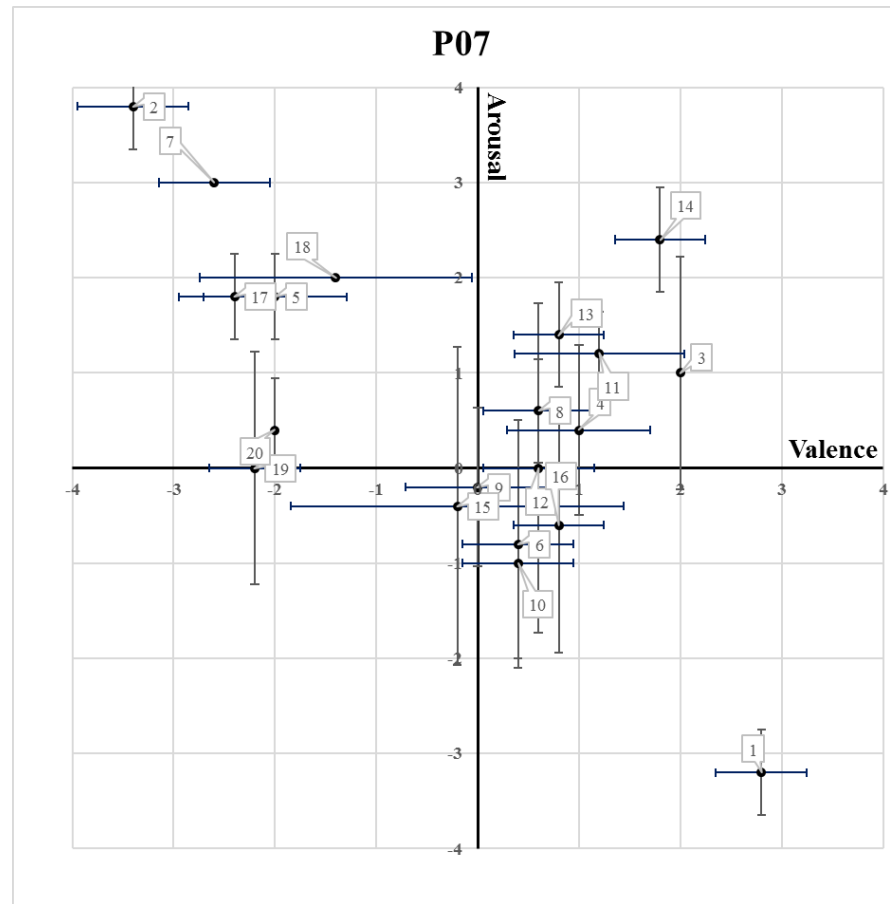


Fig. 5.7 Individual result of affective rating study: P07.

Table 5.7 Individual result of affective rating study: P07.

Signal #	1	2	3	4	5	6	7	8	9	10	11	12	13	14	15	16	17	18	19	20	Avg.
Valence	2.8	-3.4	2	1	-2	0.4	-2.6	0.6	0	0.4	1.2	0.6	0.8	1.8	-0.2	0.8	-2.4	-1.4	-2.2	-2	-0.19
Var-V	0.2	0.3	0	0.5	0.5	0.3	0.3	0.3	0.5	0.3	0.7	0.3	0.2	0.2	2.7	0.2	0.3	1.8	0.2	0	0.49
Std-V	0.45	0.55	0	0.71	0.71	0.55	0.55	0.55	0.71	0.55	0.84	0.55	0.45	0.45	1.64	0.45	0.55	1.34	0.45	0	0.60
Arousal	-3.2	3.8	1	0.4	1.8	-0.8	3	0.6	-0.2	-1	1.2	0	1.4	2.4	-0.4	-0.6	1.8	2	0	0.4	0.68
Var-A	0.2	0.2	1.5	0.8	0.2	1.7	0	0.3	0.7	1	0.2	3	0.3	0.3	2.8	1.8	0.2	0	1.5	0.3	0.85
Std-A	0.45	0.45	1.22	0.89	0.45	1.30	0	0.55	0.84	1	0.45	1.73	0.55	0.55	1.67	1.34	0.45	0	1.22	0.55	0.78

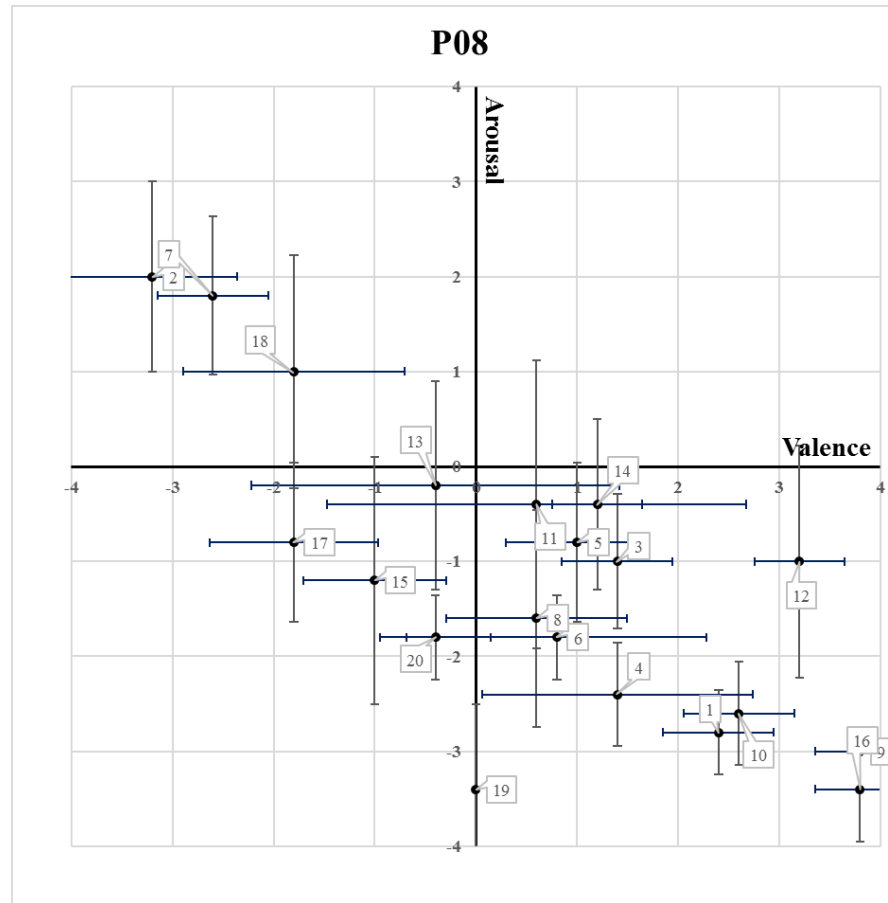


Fig. 5.8 Individual result of affective rating study: P08.

Table 5.8 Individual result of affective rating study: P08.

Signal #	1	2	3	4	5	6	7	8	9	10	11	12	13	14	15	16	17	18	19	20	Avg.
Valence	2.4	-3.2	1.4	1.4	1	0.8	-2.6	0.6	3.8	2.6	0.6	3.2	-0.4	1.2	-1	3.8	-1.8	-1.8	0	-0.4	0.58
Var-V	0.3	0.7	0.3	1.8	0.5	2.2	0.3	0.8	0.2	0.3	4.3	0.2	3.3	0.2	0.5	0.2	0.7	1.2	0	0.3	0.92
Std-V	0.55	0.84	0.55	1.34	0.71	1.48	0.55	0.89	0.45	0.55	2.07	0.45	1.82	0.45	0.71	0.45	0.84	1.10	0	0.55	0.82
Arousal	-2.8	2	-1	-2.4	-0.8	-1.8	1.8	-1.6	-3	-2.6	-0.4	-1	-0.2	-0.4	-1.2	-3.4	-0.8	1	-3.4	-1.8	-1.19
Var-A	0.2	1	0.5	0.3	0.7	0.2	0.7	1.3	0	0.3	2.3	1.5	1.2	0.8	1.7	0.3	0.7	1.5	0.8	0.2	0.81
Std-A	0.45	1	0.71	0.55	0.84	0.45	0.84	1.14	0	0.55	1.52	1.22	1.10	0.89	1.30	0.55	0.84	1.22	0.89	0.45	0.82

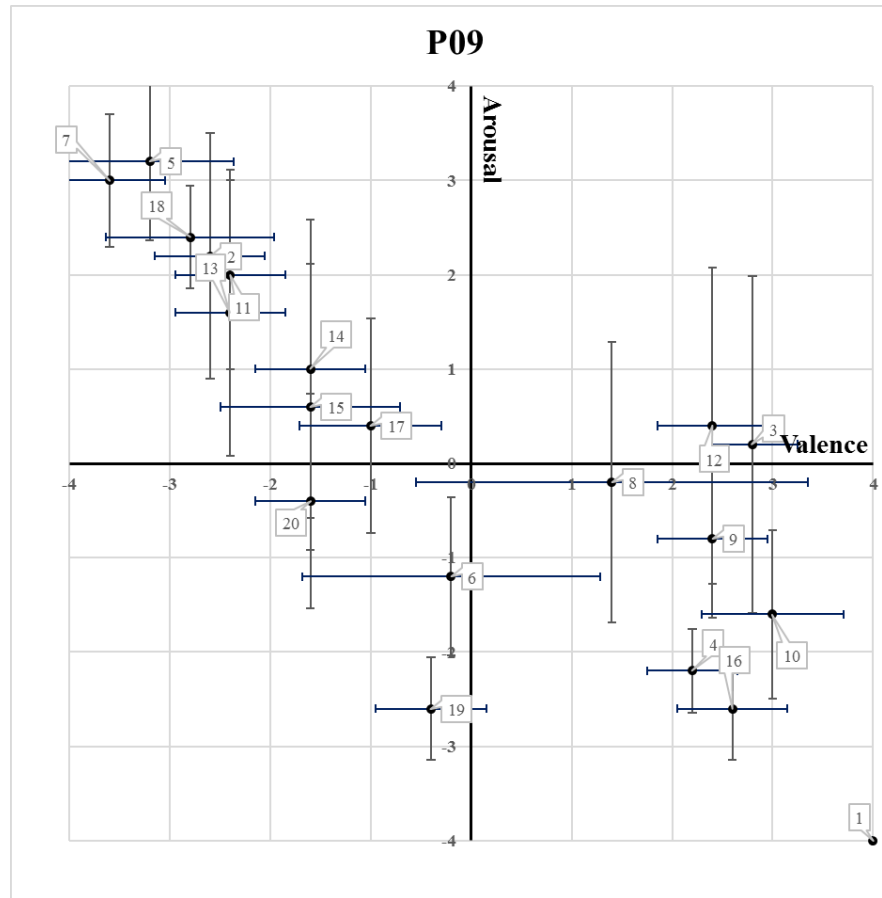


Fig. 5.9 Individual result of affective rating study: P09.

Table 5.9 Individual result of affective rating study: P09.

Signal #	1	2	3	4	5	6	7	8	9	10	11	12	13	14	15	16	17	18	19	20	Avg.
Valence	4	-2.6	2.8	2.2	-3.2	-0.2	-3.6	1.4	2.4	3	-2.4	2.4	-2.4	-1.6	-1.6	2.6	-1	-2.8	-0.4	-1.6	-0.13
Var-V	0	0.3	0.2	0.2	0.7	2.2	0.3	3.8	0.3	0.5	0.3	0.3	0.3	0.3	0.8	0.3	0.5	0.7	0.3	0.3	0.63
Std-V	0	0.55	0.45	0.45	0.84	1.48	0.55	1.95	0.55	0.71	0.55	0.55	0.55	0.55	0.89	0.55	0.71	0.84	0.55	0.55	0.69
Arousal	-4	2.2	0.2	-2.2	3.2	-1.2	3	-0.2	-0.8	-1.6	2	0.4	1.6	1	0.6	-2.6	0.4	2.4	-2.6	-0.4	0.07
Var-A	0	1.7	3.2	0.2	0.7	0.7	0.5	2.2	0.7	0.8	1	2.8	2.3	2.5	2.3	0.3	1.3	0.3	0.3	1.3	1.26
Std-A	0	1.30	1.79	0.45	0.84	0.84	0.71	1.48	0.84	0.89	1	1.67	1.52	1.58	1.52	0.55	1.14	0.55	0.55	1.14	1.02

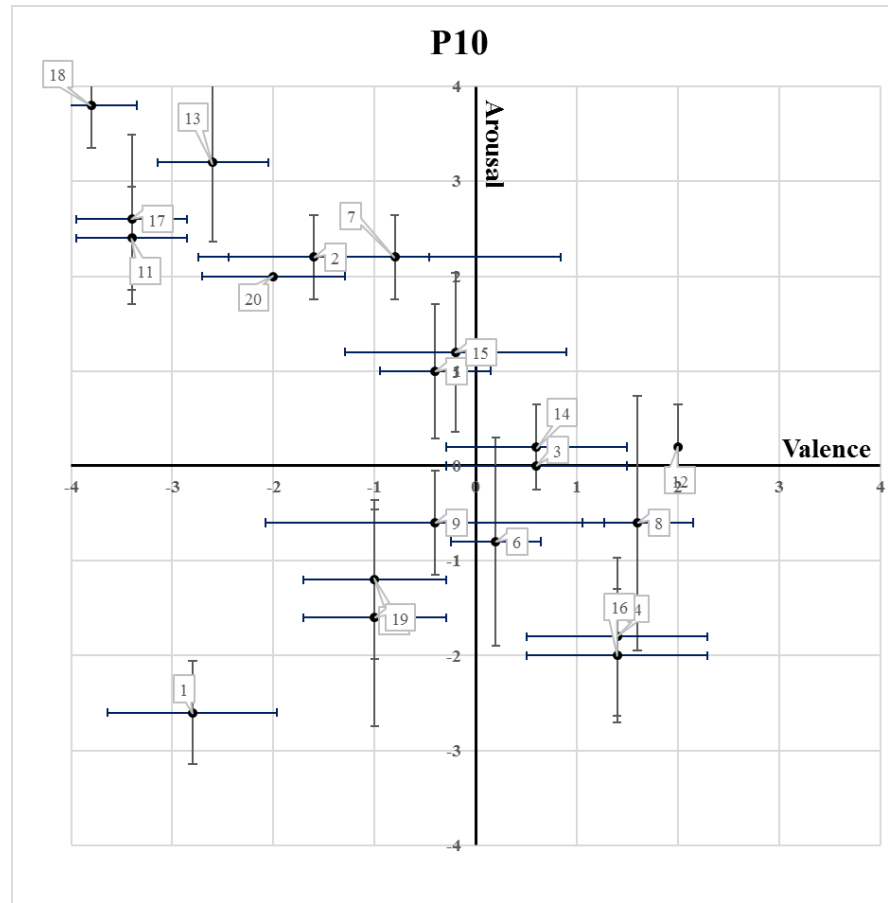


Fig. 5.10 Individual result of affective rating study: P10.

Table 5.10 Individual result of affective rating study: P10.

Signal #	1	2	3	4	5	6	7	8	9	10	11	12	13	14	15	16	17	18	19	20	Avg.
Valence	-2.8	-1.6	0.6	1.4	-0.4	0.2	-0.8	1.6	-0.4	-1	-3.4	2	-2.6	0.6	-0.2	1.4	-3.4	-3.8	-1	-2	-0.78
Var-V	0.7	1.3	0.8	0.8	0.3	0.2	2.7	0.3	2.8	0.5	0.3	0	0.3	0.8	1.2	0.8	0.3	0.2	0.5	0.5	0.76
Std-V	0.84	1.14	0.89	0.89	0.55	0.45	1.64	0.55	1.67	0.71	0.55	0	0.55	0.89	1.10	0.89	0.55	0.45	0.71	0.71	0.79
Arousal	-2.6	2.2	0	-1.8	1	-0.8	2.2	-0.6	-0.6	-1.2	2.4	0.2	3.2	0.2	1.2	-2	2.6	3.8	-1.6	2	0.49
Var-A	0.3	0.2	0	0.7	0.5	1.2	0.2	1.8	0.3	0.7	0.3	0.2	0.7	0.2	0.7	0.5	0.8	0.2	1.3	0	0.54
Std-A	0.55	0.45	0	0.84	0.71	1.10	0.45	1.34	0.55	0.84	0.55	0.45	0.84	0.45	0.84	0.71	0.89	0.45	1.14	0	0.66

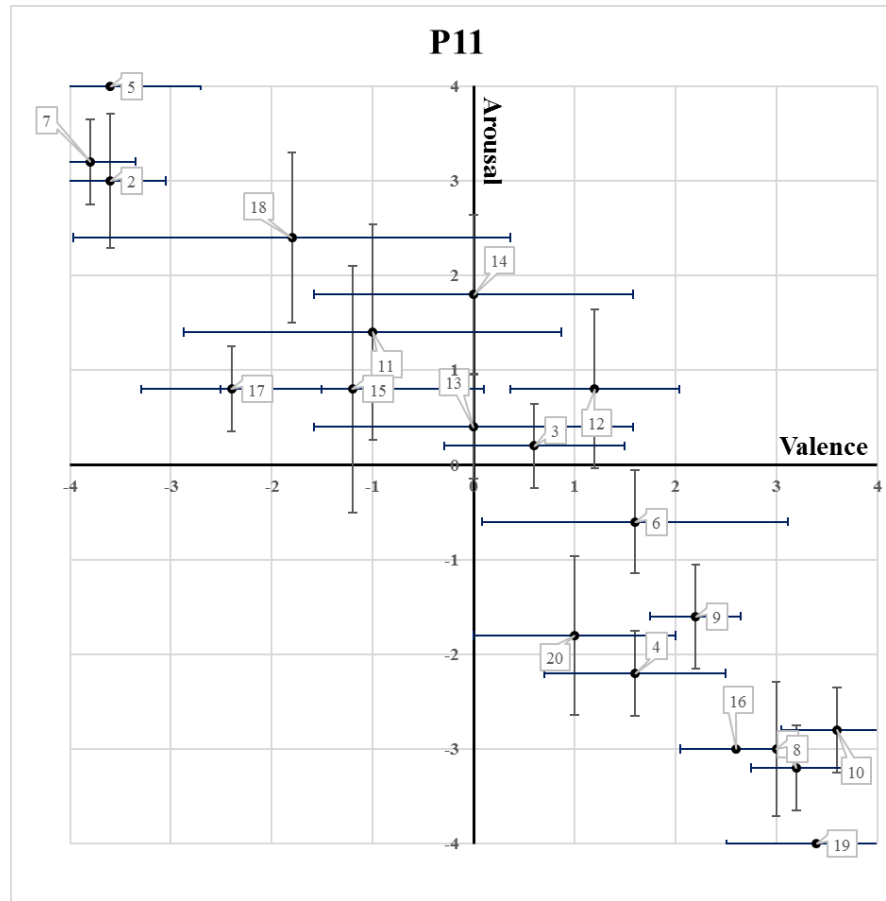


Fig. 5.11 Individual result of affective rating study: P11.

Table 5.11 Individual result of affective rating study: P11.

Signal #	1	2	3	4	5	6	7	8	9	10	11	12	13	14	15	16	17	18	19	20	Avg.
Valence	3.2	-3.6	0.6	1.6	-3.6	1.6	-3.8	3	2.2	3.6	-1	1.2	0	0	-1.2	2.6	-2.4	-1.8	3.4	1	0.33
Var-V	0.2	0.3	0.8	0.8	0.8	2.3	0.2	0	0.2	0.3	3.5	0.7	2.5	2.5	1.7	0.3	0.8	4.7	0.8	1	1.22
Std-V	0.45	0.55	0.89	0.89	0.89	1.52	0.45	0	0.45	0.55	1.87	0.84	1.58	1.58	1.30	0.55	0.89	2.17	0.89	1	0.97
Arousal	-3.2	3	0.2	-2.2	4	-0.6	3.2	-3	-1.6	-2.8	1.4	0.8	0.4	1.8	0.8	-3	0.8	2.4	-4	-1.8	-0.17
Var-A	0.2	0.5	0.2	0.2	0	0.3	0.2	0.5	0.3	0.2	1.3	0.7	0.3	0.7	1.7	0	0.2	0.8	0	0.7	0.45
Std-A	0.45	0.71	0.45	0.45	0	0.55	0.45	0.71	0.55	0.45	1.14	0.84	0.55	0.84	1.30	0	0.45	0.89	0	0.84	0.58

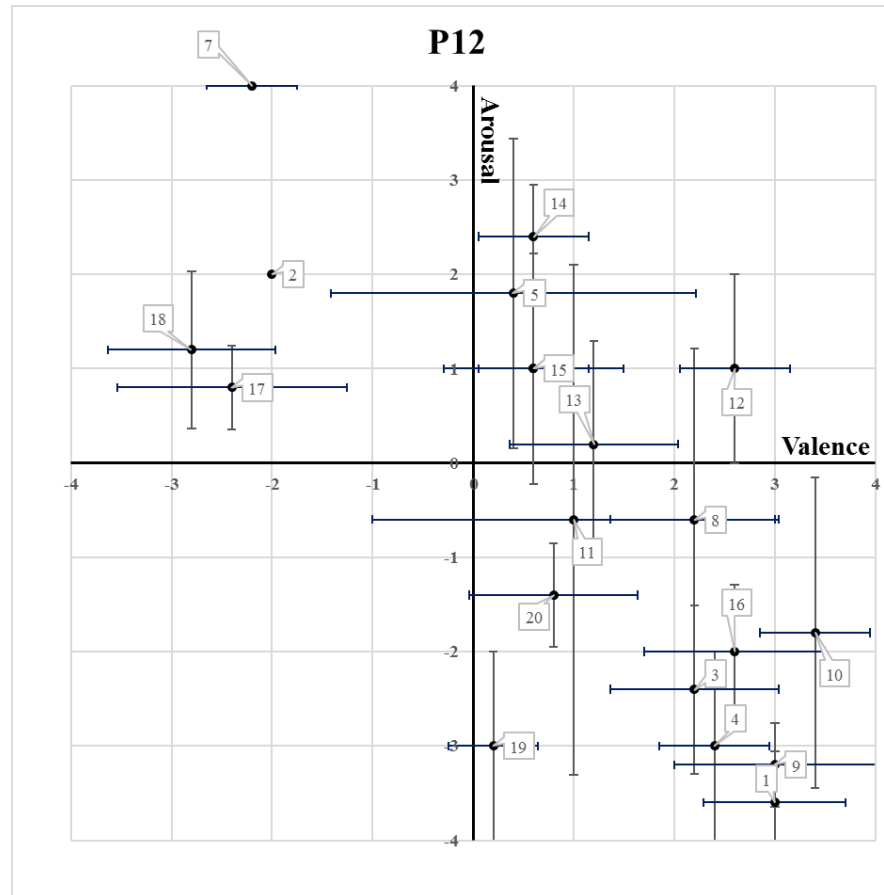


Fig. 5.12 Individual result of affective rating study: P12.

Table 5.12 Individual result of affective rating study: P12.

Signal #	1	2	3	4	5	6	7	8	9	10	11	12	13	14	15	16	17	18	19	20	Avg.
Valence	3	-2	2.2	2.4	0.4	0.6	-2.2	2.2	3	3.4	1	2.6	1.2	0.6	0.6	2.6	-2.4	-2.8	0.2	0.8	0.87
Var-V	0.5	0	0.7	0.3	3.3	0.3	0.2	0.7	1	0.3	4	0.3	0.7	0.3	0.8	0.8	1.3	0.7	0.2	0.7	0.86
Std-V	0.71	0	0.84	0.55	1.82	0.55	0.45	0.84	1	0.55	2	0.55	0.84	0.55	0.89	0.89	1.14	0.84	0.45	0.84	0.81
Arousal	-3.6	2	-2.4	-3	1.8	1	4	-0.6	-3.2	-1.8	-0.6	1	0.2	2.4	1	-2	0.8	1.2	-3	-1.4	-0.31
Var-A	0.3	0	0.8	1	2.7	1.5	0	3.3	0.2	2.7	7.3	1	1.2	0.3	0	0.5	0.2	0.7	1	0.3	1.25
Std-A	0.55	0	0.89	1	1.64	1.22	0	1.82	0.45	1.64	2.70	1	1.10	0.55	0	0.71	0.45	0.84	1	0.55	0.91

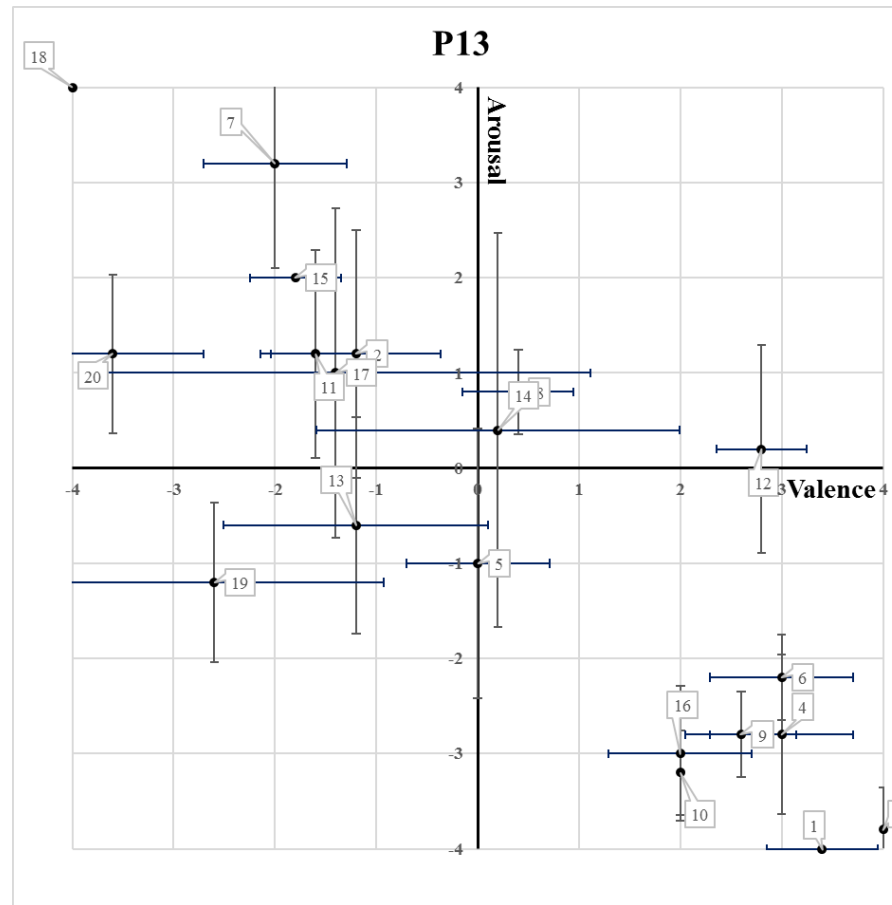


Fig. 5.13 Individual result of affective rating study: P13.

Table 5.13 Individual result of affective rating study: P13.

Signal #	1	2	3	4	5	6	7	8	9	10	11	12	13	14	15	16	17	18	19	20	Avg.
Valence	3.4	-1.2	4	3	0	3	-2	0.4	2.6	2	-1.6	2.8	-1.2	0.2	-1.8	2	-1.4	-4	-2.6	-3.6	0.20
Var-V	0.3	0.7	0	0.5	0.5	0.5	0.5	0.3	0.3	0	0.3	0.2	1.7	3.2	0.2	0.5	6.3	0	2.8	0.8	0.98
Std-V	0.55	0.84	0	0.71	0.71	0.71	0.71	0.55	0.55	0	0.55	0.45	1.30	1.79	0.45	0.71	2.51	0	1.67	0.89	0.78
Arousal	-4	1.2	-3.8	-2.8	-1	-2.2	3.2	0.8	-2.8	-3.2	1.2	0.2	-0.6	0.4	2	-3	1	4	-1.2	1.2	-0.47
Var-A	0	1.7	0.2	0.7	2	0.2	1.2	0.2	0.2	0.2	1.2	1.2	1.3	4.3	0	0.5	3	0	0.7	0.7	0.98
Std-A	0	1.30	0.45	0.84	1.41	0.45	1.10	0.45	0.45	0.45	1.10	1.10	1.14	2.07	0	0.71	1.73	0	0.84	0.84	0.82

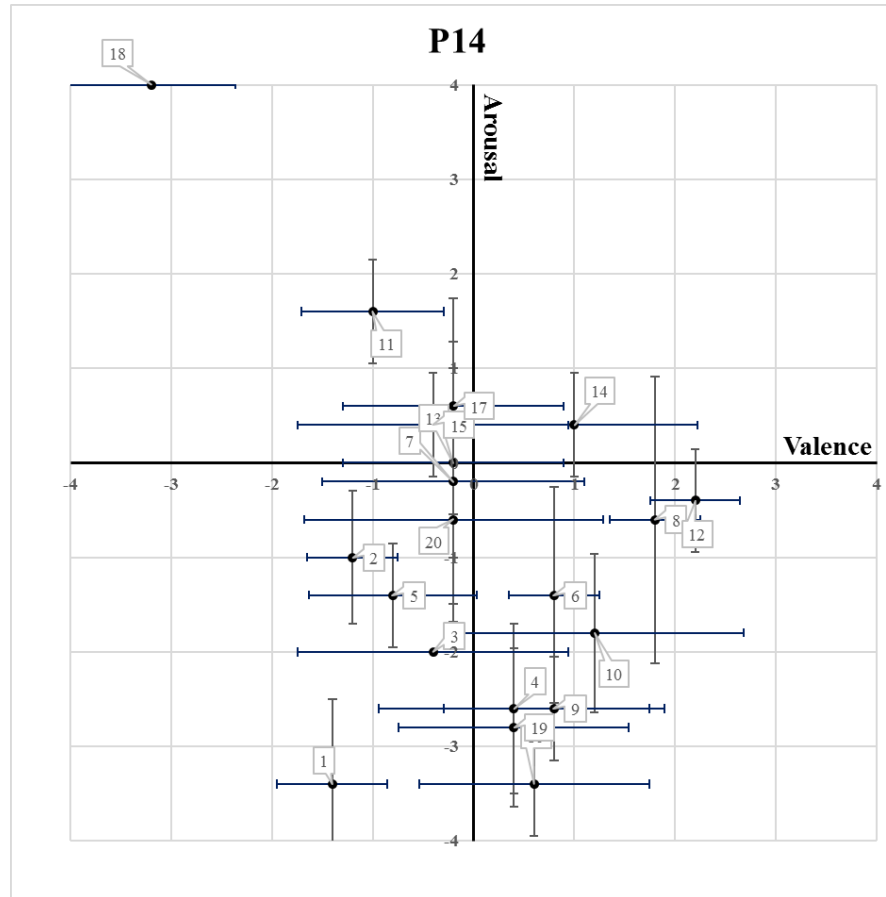


Fig. 5.14 Individual result of affective rating study: P14.

Table 5.14 Individual result of affective rating study: P14.

Signal #	1	2	3	4	5	6	7	8	9	10	11	12	13	14	15	16	17	18	19	20	Avg.
Valence	-1.4	-1.2	-0.4	0.4	-0.8	0.8	-0.2	1.8	0.8	1.2	-1	2.2	-0.2	1	-0.4	0.6	-0.2	-3.2	0.4	-0.2	0.00
Var-V	0.3	0.2	1.8	1.8	0.7	0.2	1.7	0.2	1.2	2.2	0.5	0.2	1.2	1.5	1.8	1.3	1.2	0.7	1.3	2.2	1.11
Std-V	0.55	0.45	1.34	1.34	0.84	0.45	1.30	0.45	1.10	1.48	0.71	0.45	1.10	1.22	1.34	1.14	1.10	0.84	1.14	1.48	0.99
Arousal	-3.4	-1	-2	-2.6	-1.4	-1.4	-0.2	-0.6	-2.6	-1.8	1.6	-0.4	0	0.4	0.4	-3.4	0.6	4	-2.8	-0.6	-0.86
Var-A	0.8	0.5	0	0.8	0.3	1.3	2.2	2.3	0.3	0.7	0.3	0.3	1	0.3	0.3	0.3	1.3	0	0.7	0.8	0.73
Std-A	0.89	0.71	0	0.89	0.55	1.14	1.48	1.52	0.55	0.84	0.55	0.55	1	0.55	0.55	0.55	1.14	0	0.84	0.89	0.76

APPENDIX B: 4-CHANNEL SIGNAL WAVEFORM

Table 5.15 Signal parameter details and applied design approaches.

#	1	2	3	4	5	6	7	8	9	10
<i>Metaphor (label)</i>	<i>breathing</i>	<i>earth-quake</i>	<i>heartbeat</i>	<i>rain drop</i>	<i>elephant trod</i>	<i>tapping</i>	<i>thunder</i>	<i>twinkle</i>	<i>bubbles</i>	<i>water drop & ripple</i>
<i>Carrier Frequency (Hz)</i>	0.8	30	20-30	80-120	20	2	30, 135/150	300	20	5, 7, 10 180, 300
<i>Modulation (Hz)</i> <i>(Amplitude/*Gaussian)</i>	-	*0.3	-	-	-	-	*0.3	-	-	*10/10
<i>Amplitude (Max, g)</i>	0.2	0.43	1.88	2.48	0.79	4.38	15.39	0.82	1.14	3.04
<i>Duration (ms)</i> <i>(Total/*Unit pattern)</i>	5004	3300	2790 *75-135	3200 *16	3000 *200	400 *80	3200	1000 *20	800 *160	2320
<i>Design Approach</i>	ii-1	ii-2, vi-2	ii-1, iii, vi- 1/2/5	v-1/2/3, vi- 3/5	ii-1, vi-2/4	ii-1, vi- 4/6d	ii-1, ii-2, iii, vi-2/4/5	iv, v-3, vi- 3	ii-1, vi-6d	ii-1, ii-2, iii, v-2/3, vi-2/4/5/6d

#	11	12	13	14	15	16	17	18	19	20
<i>Metaphor (label)</i>	<i>cicadas</i>	<i>bathtub water jet</i>	<i>frog</i>	<i>(horse) galloping</i>	<i>knock</i>	<i>bubbles popping</i>	<i>alarm</i>	<i>notifi-cation 1</i>	<i>notifi-cation 2</i>	<i>notifi-cation 3</i>
<i>Carrier Frequency (Hz)</i>	60, 120	10	50, 120	3, 5, 7, 180, 300	30, 300	2	60-200	300	60	150
<i>Modulation (Hz)</i> <i>(Amplitude/*Gaussian)</i>	0.5, 2, 32	0.3	1.7, 16	-	-	-	-	-	-	-
<i>Amplitude (Max, g)</i>	1.37	1.78	2.69	5.71	3.79	1.57	0.99	1.4	0.12	0.39
<i>Duration (ms)</i> <i>(Total/*Unit pattern)</i>	4250	1600 *200	1800	1590 *64	630 *60	1250 *312.5	1200 *300	1000	1000	1000
<i>Design Approach</i>	ii-1, iii, iv vi- 1/2/5	ii-1, iv	ii-1, iii, iv vi-1/2/5	ii-1, iii, vi- 1/2/4/5	ii-1, vi- 1/2/4/5	ii-1, iii, vi- 4/6d	vi-6d/i/f	-	-	-

i. Nature metaphors
(#1 to 16)

v. Randomness
1. Interval
2. Frequency
3. Location

ii. Richness through dimensions
1. Slow Kinesthetic Motion
2. Gradual Change (mod.)

vi. Other considerations
1. Familiar rhythm
2. Inspired from sound
3. Subtle intensity

iii. Parts and whole
iv. Simplicity

4. Clipping intensity
5. Multi-frequency
6. Varying: direction (d), intensity (i), frequency (f)

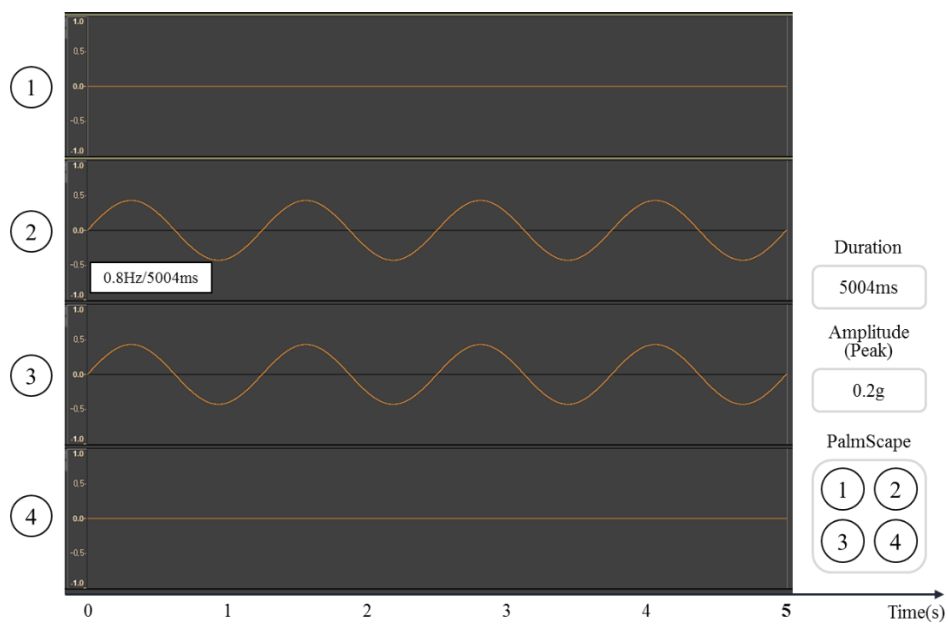


Fig. 5.15 "Breathing" signal (#1).

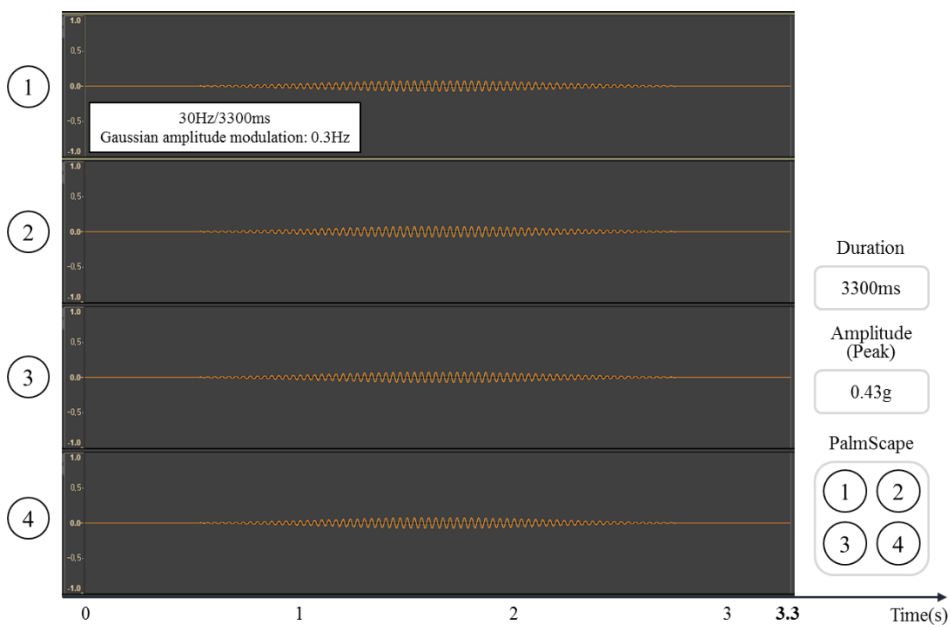


Fig. 5.16 "Earthquake" signal (#2).

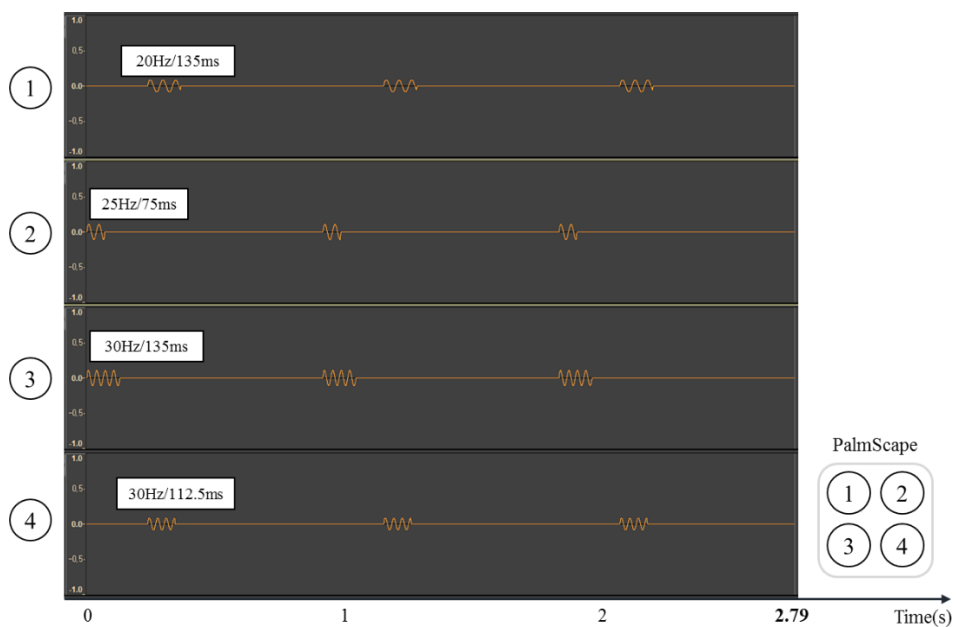


Fig. 5.17 "Heartbeat" signal (#3).

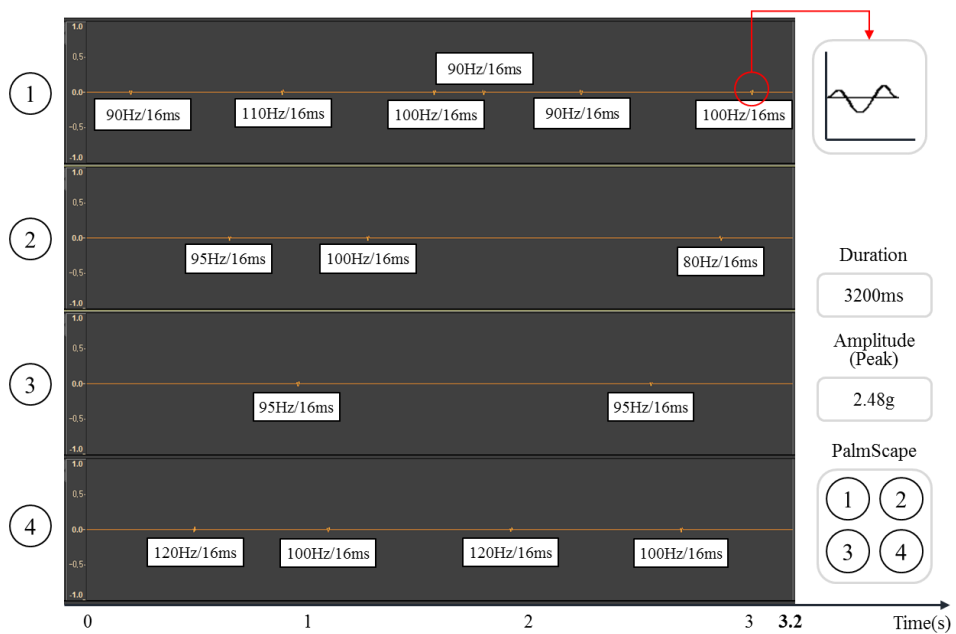


Fig. 5.18 "Raindrop" signal (#4).

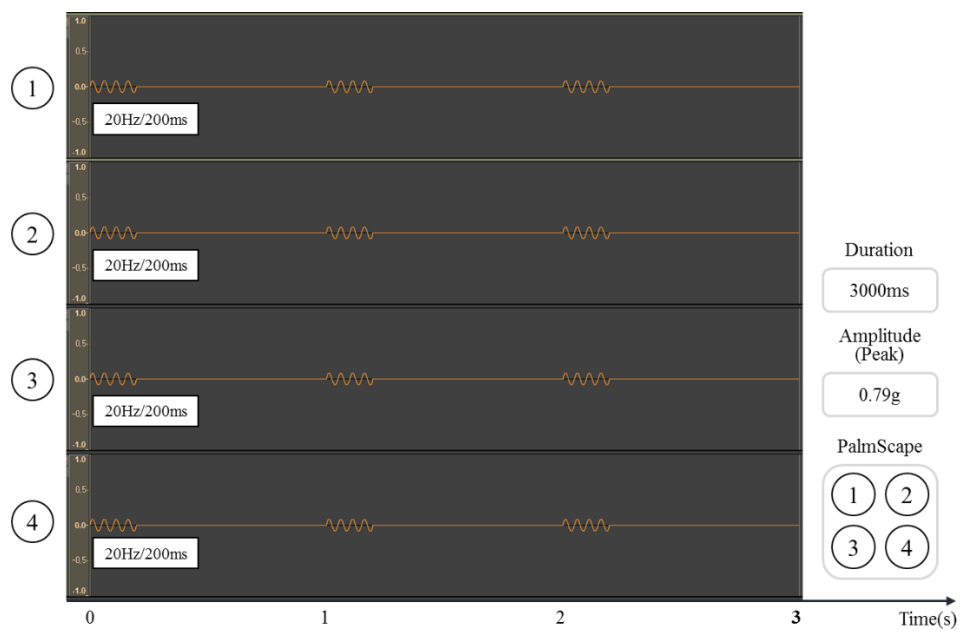


Fig. 5.19 "Elephant trod" signal (#5).

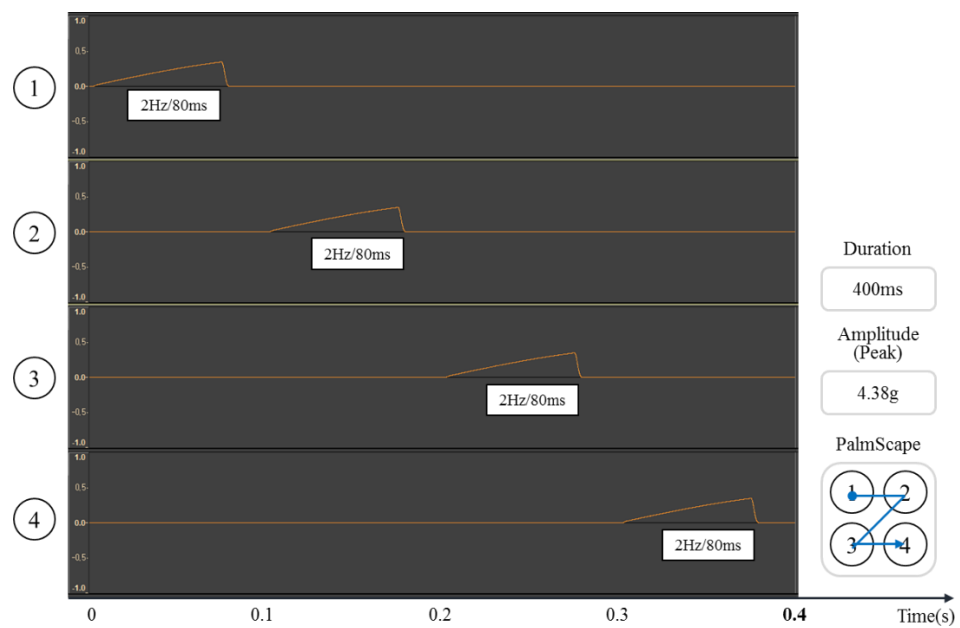


Fig. 5.20 "Tapping" signal (#6).

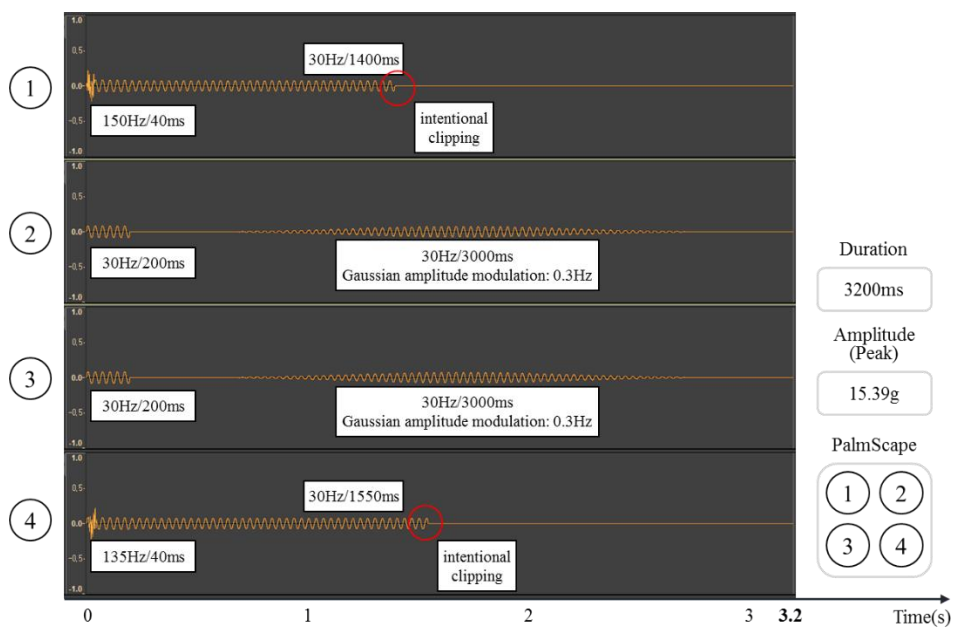


Fig. 5.21 “Thunder” signal (#7).

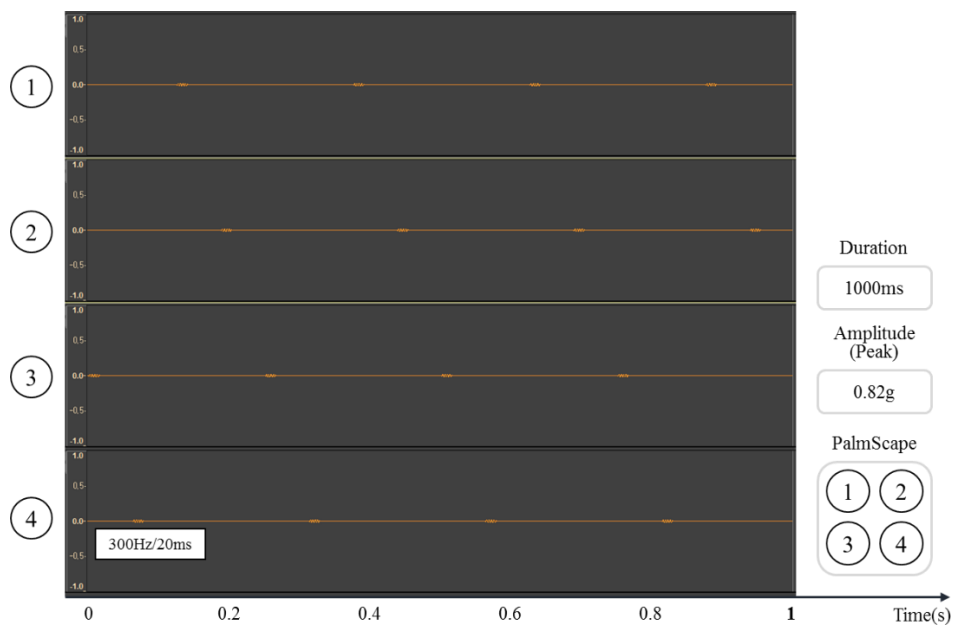


Fig. 5.22 “Twinkle” signal (#8).

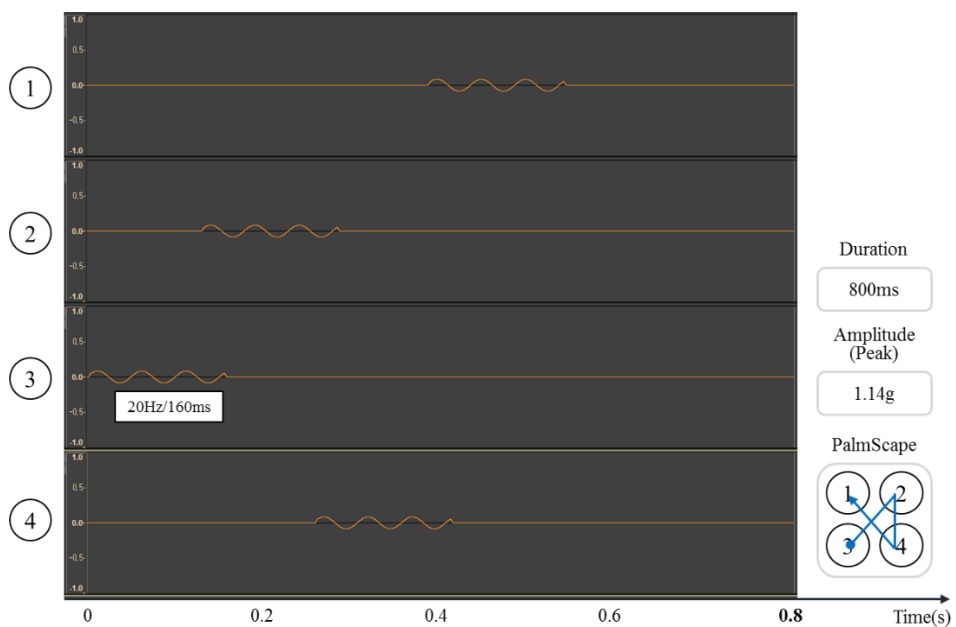


Fig. 5.23 “Bubbles” signal (#9).

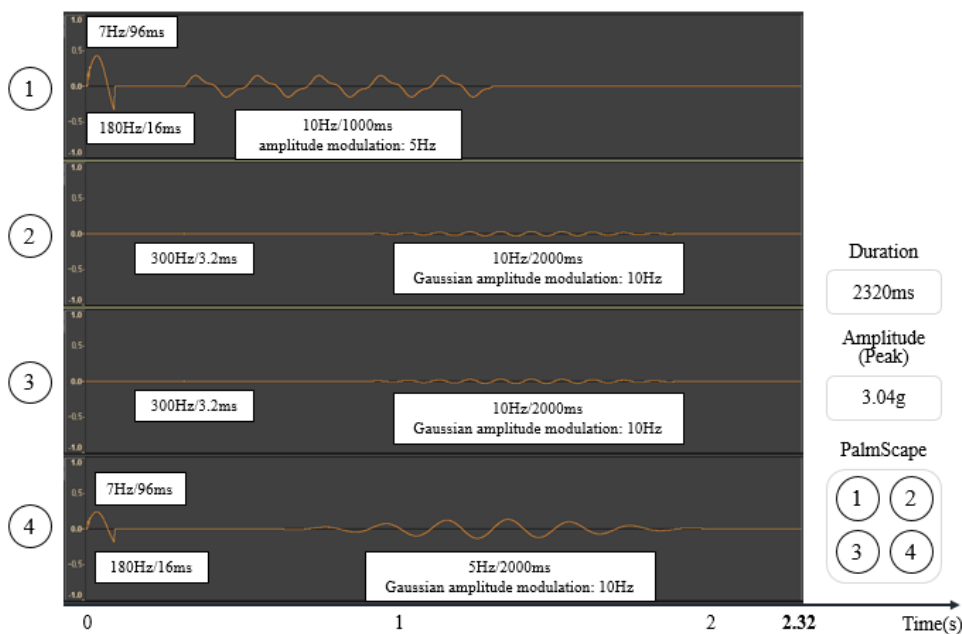


Fig. 5.24 “Water drop & ripple” signal (#10).

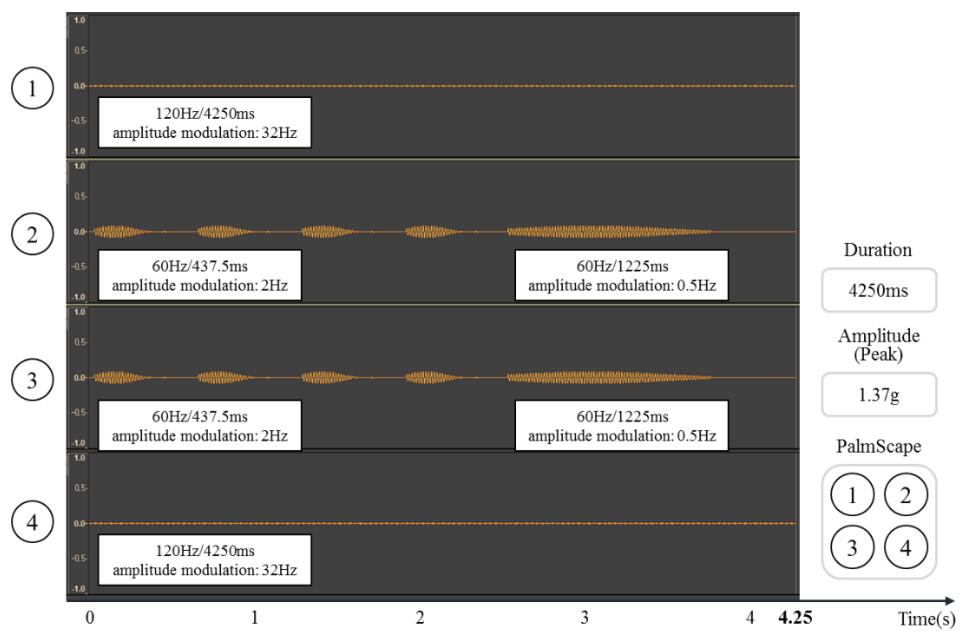


Fig. 5.25 "Cicadas" signal (#11).

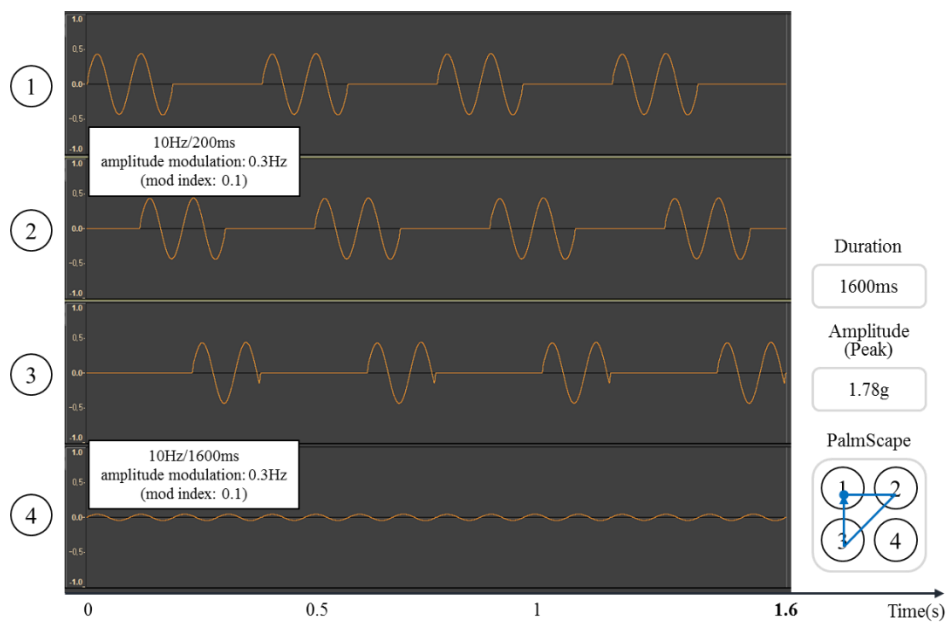


Fig. 5.26 "Bathtub water jet" signal (#12).

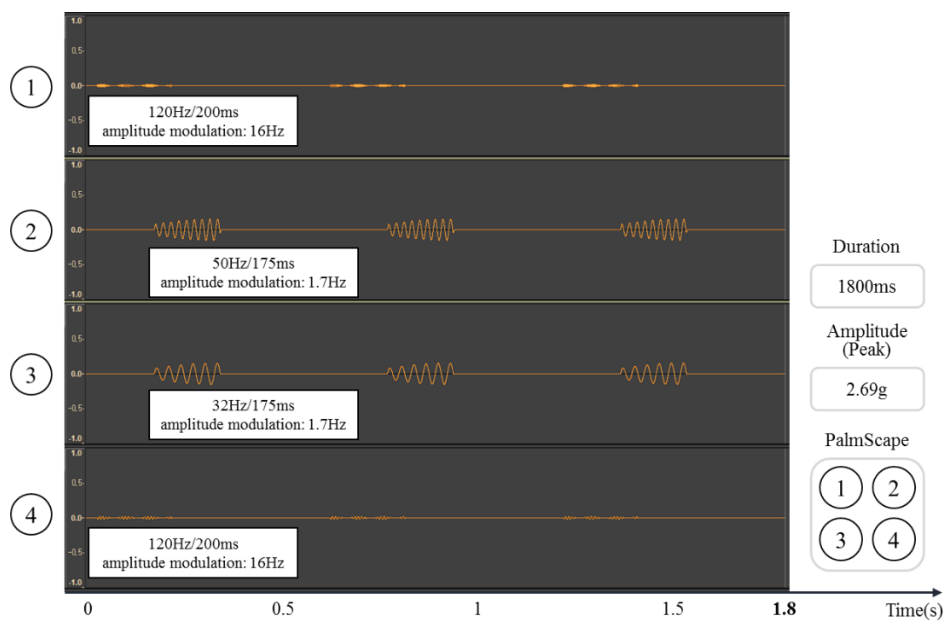


Fig. 5.27 "Frog" signal (#13).

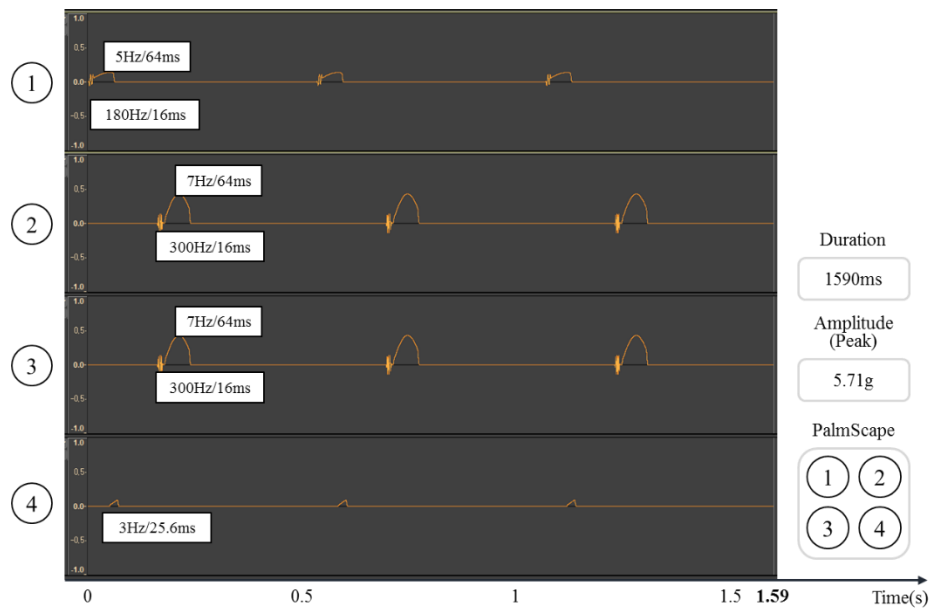


Fig. 5.28 "(Horse) galloping" signal (#14).

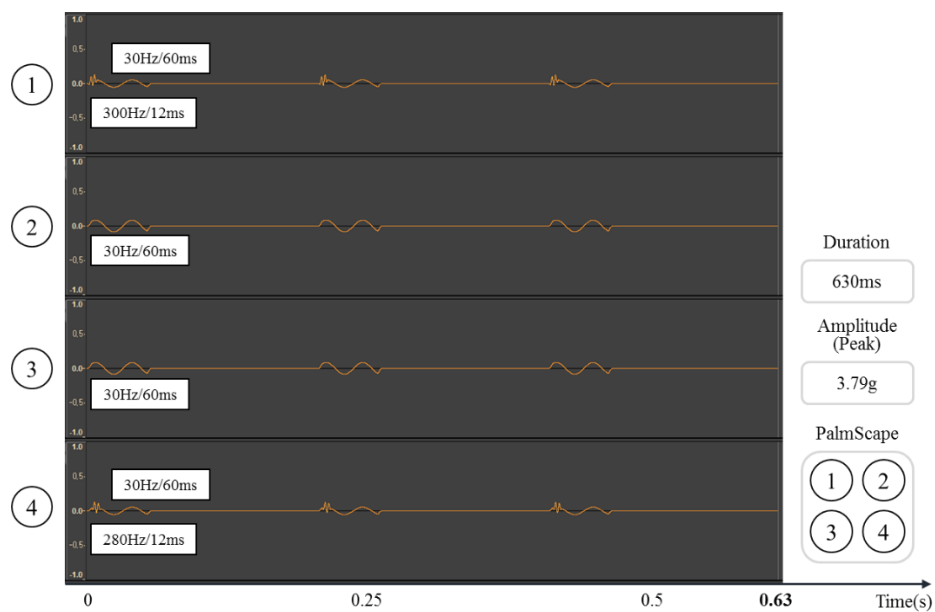


Fig. 5.29 "Knock" signal (#15).

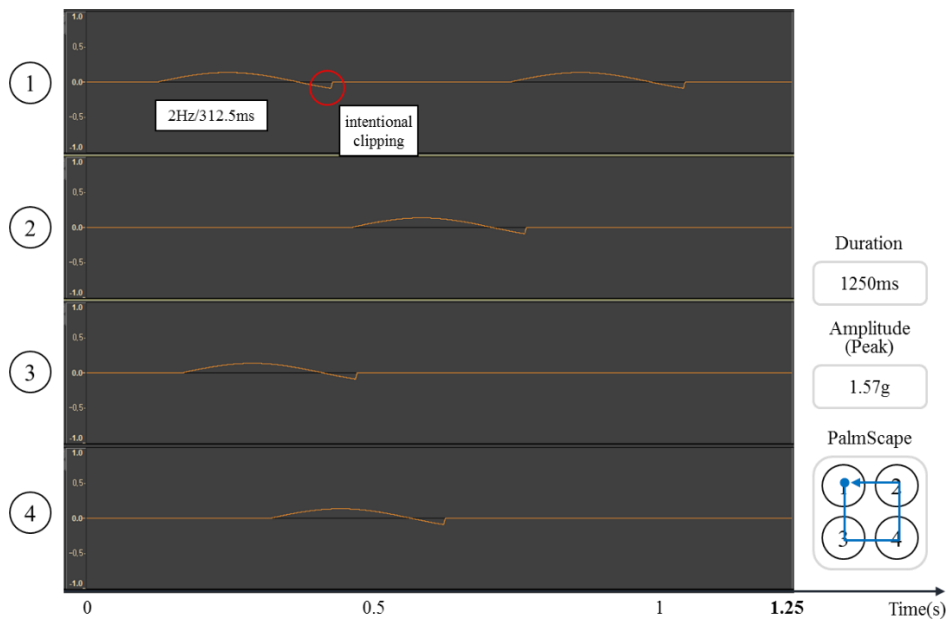


Fig. 5.30 "Bubbles popping" signal (#16).

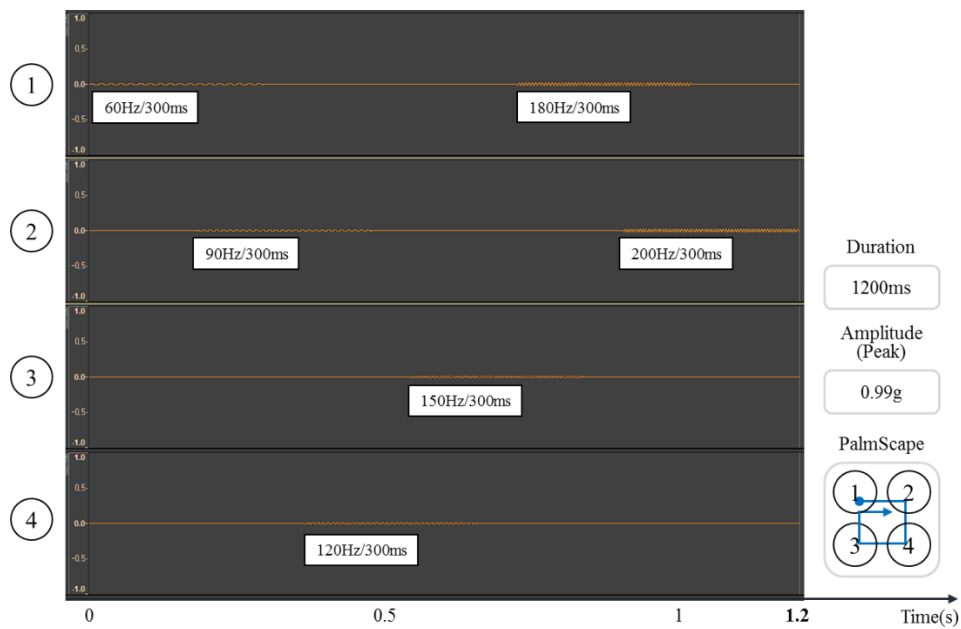


Fig. 5.31 Reference signal - "alarm" (#17).

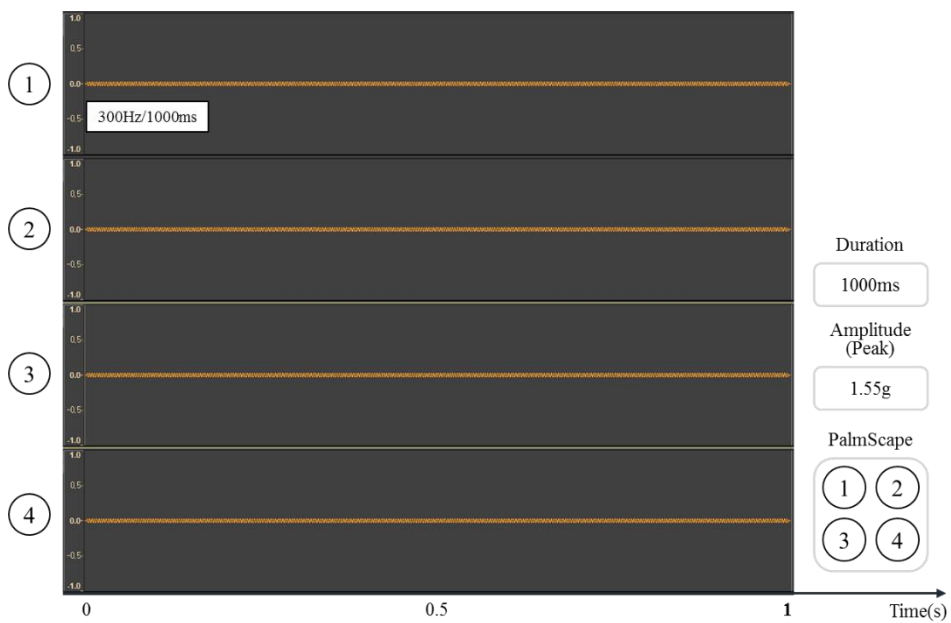


Fig. 5.32 Reference signal - "notification 1" (#18).

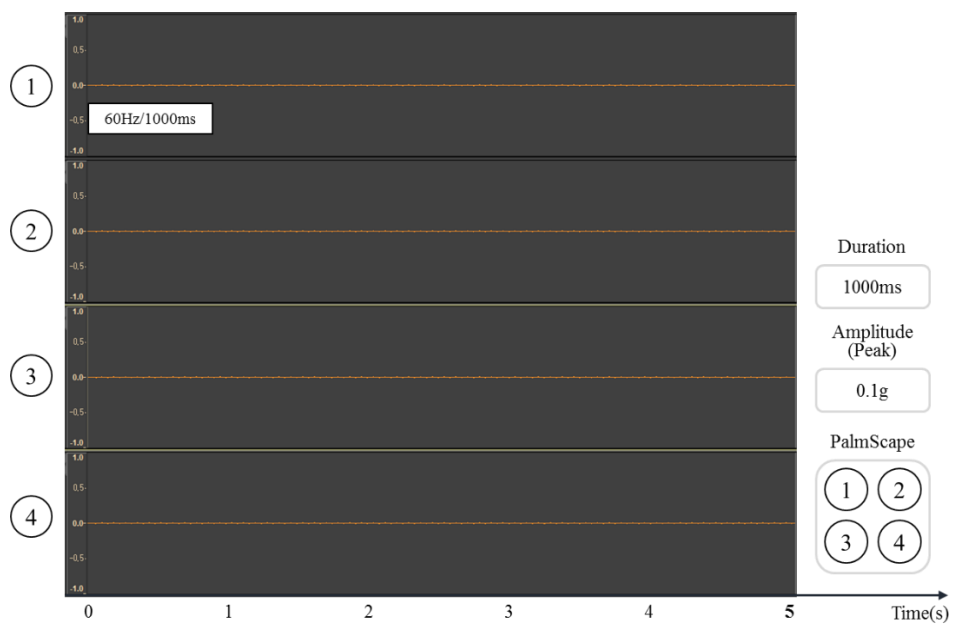


Fig. 5.33 Reference signal - “notification 2” (#19).

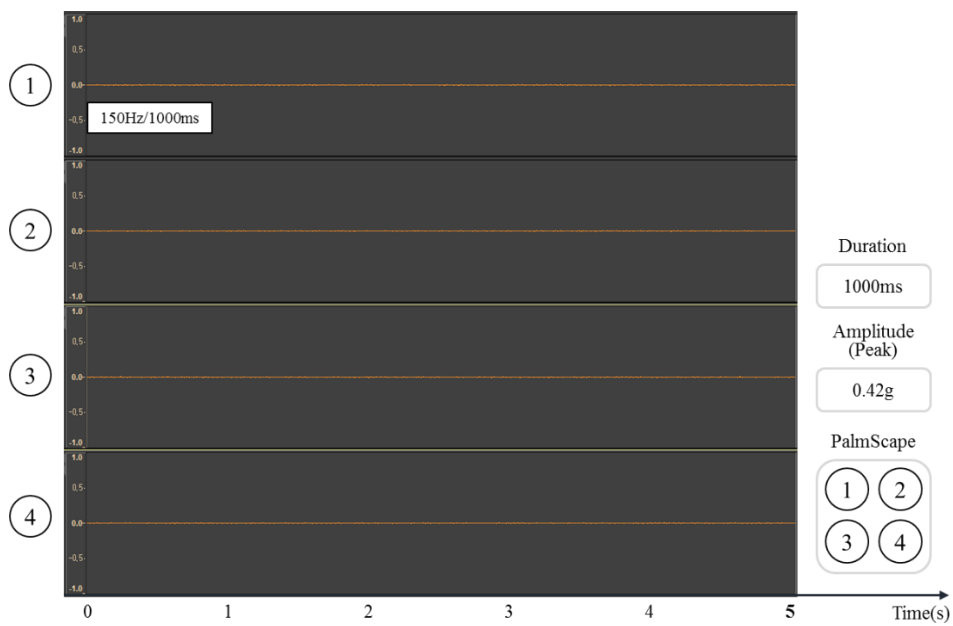


Fig. 5.34 Reference signal - “notification 3” (#20).

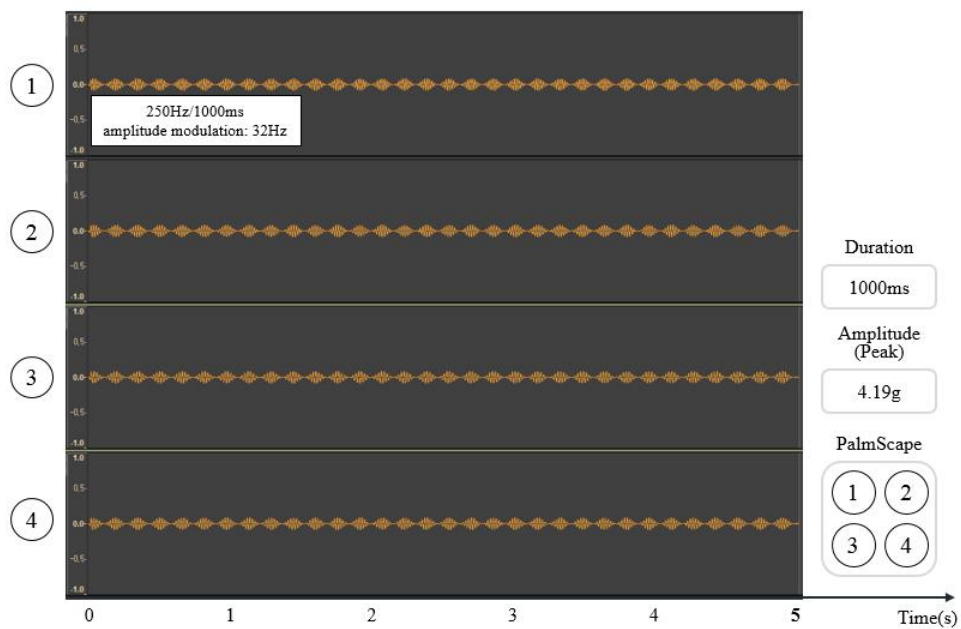


Fig. 5.35 Example signal - "sawtooth."

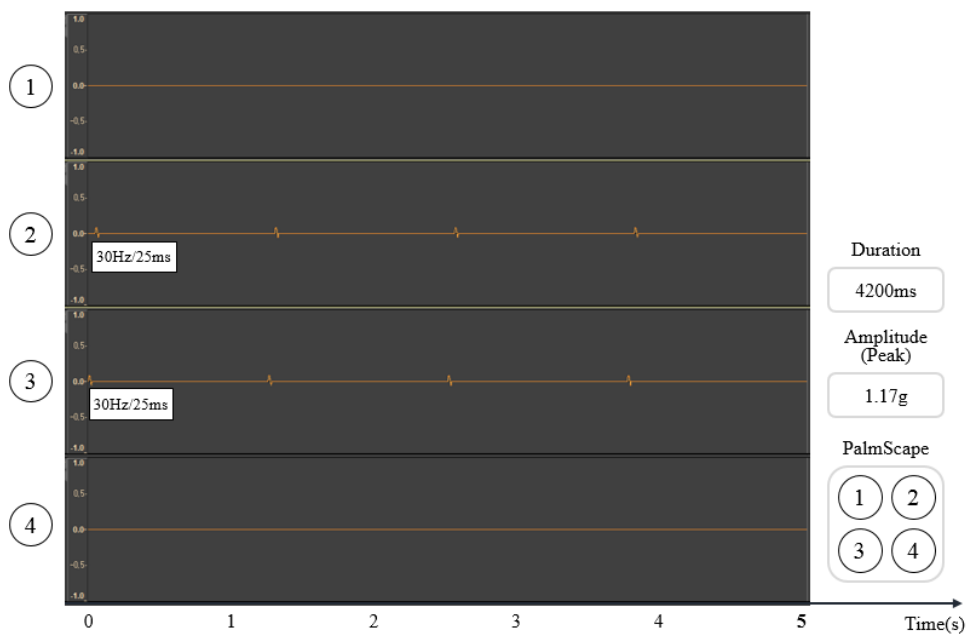


Fig. 5.36 Example signal - "pulsation."

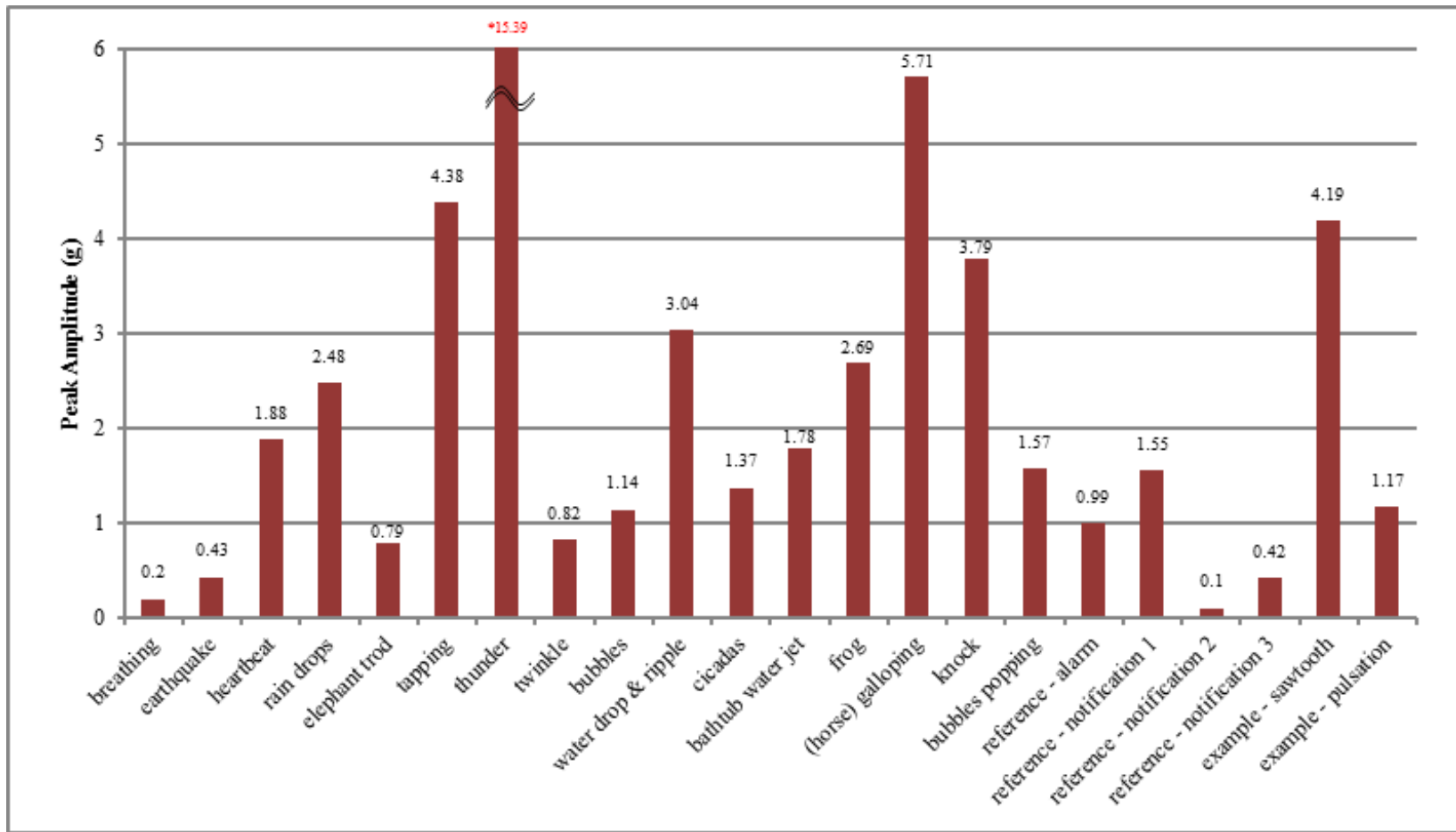


Fig. 5.37 Peak amplitude of each signal used in the affective rating experiment.

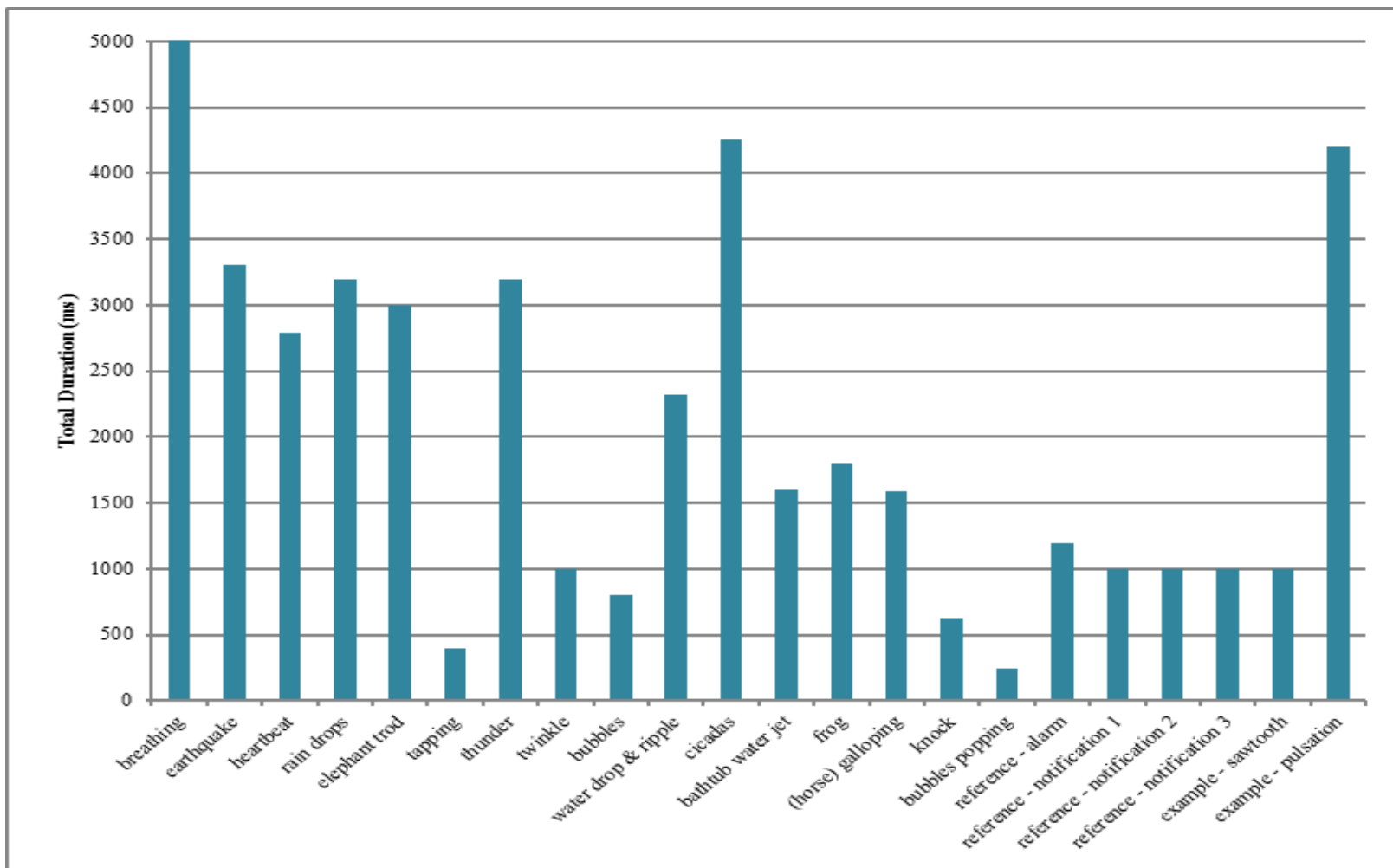


Fig. 5.38 Total duration of each signal used in the affective rating experiment.

VITA

Sang-Won Shim is an auditory and haptic user experience designer at Samsung Electronics mobile division. His goal is to become a user experience designer and a research scientist of human-computer interaction, especially on the auditory and haptic interface to give users authentic, immersive and multimodal experience and accessibility when users meet media, products, and services. He was born in 1981, Incheon, Korea, and he graduated Electrical and Electronic Engineering at Yonsei University, Korea in 2007 and received B.S degree. Since 2006, he has been working at Samsung Electronics as a software engineer for mobile devices, and he moved to the Sound Lab. in mobile design team in 2009. He was chosen for a master's program in Samsung design team, and since 2017, he had been conducting his master's research in School of Electrical and Computer Engineering at Purdue University under Prof. Hong Z. Tan. His research in haptics focuses on the next private notification method by exploring new haptic technology and an advanced vibrotactile display including the signal design which broaden expressiveness and range of affection.